

INFORMATION TO USERS

This manuscript has been reproduced from the microfilm master. UMI films the text directly from the original or copy submitted. Thus, some thesis and dissertation copies are in typewriter face, while others may be from any type of computer printer.

The quality of this reproduction is dependent upon the quality of the copy submitted. Broken or indistinct print, colored or poor quality illustrations and photographs, print bleedthrough, substandard margins, and improper alignment can adversely affect reproduction.

In the unlikely event that the author did not send UMI a complete manuscript and there are missing pages, these will be noted. Also, if unauthorized copyright material had to be removed, a note will indicate the deletion.

Oversize materials (e.g., maps, drawings, charts) are reproduced by sectioning the original, beginning at the upper left-hand corner and continuing from left to right in equal sections with small overlaps.

Photographs included in the original manuscript have been reproduced xerographically in this copy. Higher quality 6" x 9" black and white photographic prints are available for any photographs or illustrations appearing in this copy for an additional charge. Contact UMI directly to order.

**Bell & Howell Information and Learning
300 North Zeeb Road, Ann Arbor, MI 48106-1346 USA
800-521-0600**

UMI[®]

THE UNIVERSITY OF CALGARY

Cellular Base Station Antenna and Diversity Study

by

Lee Patricia Ager

A THESIS

**SUBMITTED TO THE FACULTY OF GRADUATE STUDIES
IN PARTIAL FULFILMENT OF THE REQUIREMENTS FOR THE
DEGREE OF MASTER OF SCIENCE**

DEPARTMENT OF ELECTRICAL AND COMPUTER ENGINEERING

CALGARY, ALBERTA

FEBRUARY, 1997

© Lee Patricia Ager 1997



National Library
of Canada

Acquisitions and
Bibliographic Services

395 Wellington Street
Ottawa ON K1A 0N4
Canada

Bibliothèque nationale
du Canada

Acquisitions et
services bibliographiques

395, rue Wellington
Ottawa ON K1A 0N4
Canada

Your file Votre référence

Our file Notre référence

The author has granted a non-exclusive licence allowing the National Library of Canada to reproduce, loan, distribute or sell copies of this thesis in microform, paper or electronic formats.

The author retains ownership of the copyright in this thesis. Neither the thesis nor substantial extracts from it may be printed or otherwise reproduced without the author's permission.

L'auteur a accordé une licence non exclusive permettant à la Bibliothèque nationale du Canada de reproduire, prêter, distribuer ou vendre des copies de cette thèse sous la forme de microfiche/film, de reproduction sur papier ou sur format électronique.

L'auteur conserve la propriété du droit d'auteur qui protège cette thèse. Ni la thèse ni des extraits substantiels de celle-ci ne doivent être imprimés ou autrement reproduits sans son autorisation.

0-612-48079-8

Canada

Abstract

This thesis investigates a new cellular base station antenna design and a unique pattern diversity scheme. These two projects have been developed to improve the reliability of the received signal in a multipath environment.

The antenna, named the Cylindrical Slot Antenna, has been designed to operate as typical cellular base station antennas with an emphasis on overall size and cost. To evaluate the design, a prototype antenna has been developed and evaluated in a mini-anechoic chamber test set-up.

The pattern diversity scheme incorporates a space diversity configuration and a passive combiner to create two interleaving radiation patterns. The radiation patterns are used to receive the uncorrelated multipath signals, resulting in diversity improvement. A continuous wave uplink test system with a mobile transmitter, operating in the ISM band, has been developed to evaluate the diversity performance.

Acknowledgments

I would like to acknowledge Dr. R. Johnston for his support and guidance throughout this thesis. I would, also, like to thank TRILabs for its support in form of the lab resources, additional funding and especially the friendly staff.

Further appreciation is due to Robert Davies, Grant McGibney, and John McRory for all their valuable input and advice.

Dedication

I would like to dedicate this thesis to my parents, Bob and Sharon, and to my husband, Ron. Without their support and understanding this work would never have been completed.

Table of Contents

Abstract.....	iii
Acknowledgments	iv
Dedication.....	v
Table of Contents.....	vi
List of Figures	ix
List of Tables.....	xii
List of Symbols and Abbreviations	xiii
1.0 Introduction	1
2.0 Problem Statement.....	3
2.1 General Cell Systems.....	5
2.1.1 Current Cellular Systems.....	12
2.2 Multipath.....	14
2.3 Diversity Techniques.....	15
3.0 Measurement Methods.....	20
3.1 Cellular Base Station Antenna.....	20
3.1.1 Efficiency	21
3.1.1.1 Losses.....	22
3.1.2 Radiation Pattern	24
3.1.2.1 S21 Measurements With Probe.....	29
3.1.3 Impedance	30
3.1.3.1 S11 Parameter.....	32
3.1.4 Polarization.....	33
3.1.5 Gain.....	36
3.2 Diversity Scheme.....	38
3.2.1 Transmitter Section	39
3.2.2 Receiver Section.....	44
3.2.3 Data Retrieval.....	48
4.0 Cylindrical Slot Antenna.....	59
4.1 Copper Cylinder - Support Structure.....	60
4.2 Slots - Radiating Element.....	61
4.2.1 Individual Slot.....	61
4.2.2 Resonant Slot.....	64

4.2.3	Slot Array.....	66
4.3	Feed Network	67
4.4	Cylindrical Slot Antenna Measurement Results	78
4.4.1	Radiation Measurement	78
4.4.2	Input Impedance and S11 Parameter.....	80
4.4.3	Electric Field Measurements	82
5.0	Diversity Scheme.....	86
5.1	Magic T	86
5.2	Radiation Pattern	89
5.3	Diversity at the Base Station.....	93
5.4	Diversity Scheme Measurement Results	93
5.4.1	Mean Value.....	94
5.4.2	Probability Distribution.....	100
5.4.3	Cumulative Probability Distribution.....	105
5.4.4	Test Accuracy	108
6.0	Conclusion.....	110
6.1	Cylindrical Slot Antenna.....	111
6.1.1	Radiation Pattern	111
6.1.2	Input Impedance and Return Loss.....	112
6.1.4	Final Observation and Future Work.....	113
6.2	Magic T Experiment.....	114
6.2.1	Ideal Cumulative Distribution Curves	114
6.2.2	Comparing Results and Ideal Curves.....	118
6.2.2.1	Space Diversity.....	119
6.2.2.2	Pattern Diversity.....	119
6.2.2.3	Space and Pattern Combination Diversity	121
6.2.3	Measured Curves	122
6.2.4	Final Observation.....	123
References	124
Appendix A	129
Appendix B	132
Appendix C	145

Appendix D	146
Appendix E.....	148
Appendix F.....	156
Appendix G	157

List of Figures

Figure 2.1	Reflectors, Scatterers and Diffractors.....	4
Figure 2.2	Cluster.....	9
Figure 2.3	Antenna Positioning.....	11
Figure 2.4	TEM Wave.....	13
Figure 2.5	Sample of Multipath Fading Signal.....	15
Figure 2.6	Example of Angular Sectors at the Base and Mobile Sites.....	16
Figure 3.1	Transmission Line.....	23
Figure 3.2	Anechoic System Block Diagram.....	25
Figure 3.3	Separation Distance of Antennas in Far Field.....	26
Figure 3.4	Verification Results for Anechoic Chamber.....	28
Figure 3.5	S parameters.....	30
Figure 3.6	XY Graph to Smith Chart Translation.....	32
Figure 3.9	Channel.....	39
Figure 3.10	Map of Path Traveled.....	41
Figure 3.11	Discone Antenna.....	43
Figure 3.12	S11 of Discone Antenna.....	43
Figure 3.13	Transmitter Section Block Diagram.....	44
Figure 3.14	Path Attenuation Profiles.....	46
Figure 3.14	Path Phase Profiles.....	47
Figure 3.15	Path Delay Profiles.....	47
Figure 3.17	Receiver Section Block Diagram.....	48
Figure 3.18	Measurement Times.....	49
Figure 3.19	Dynamic Range of Receiver and Data Retrieval Sections.....	51
Figure 3.20	Switch Control for 4-to-1 Switch.....	52
Figure 3.21	Data Retrieval Section Block Diagram.....	55
Figure 4.1	Cylindrical Slot Antenna.....	60
Figure 4.2	Slot Orientation for Equations. 4.1 through 4.8.....	63
Figure 4.3	Set-up to Measure Resonant Slot (Not to Scale).....	65
Figure 4.4	Special Feed network and Slot Model.....	66
Figure 4.5	Horizontal Radiation Pattern of Planar Array.....	67

Figure 4.6	Vertical Radiation Pattern of Planar Array.....	67
Figure 4.7	Current in Feed and about Slot.....	68
Figure 4.8	Feed network Mounted on Cylinder.....	69
Figure 4.9	Basic Feed Component (Not to Scale).....	70
Figure 4.10	Basic Feed Network Model.....	71
Figure 4.11	Overall Feed Network (Not to Scale)	73
Figure 4.12	Response at Point A for Slot One	74
Figure 4.13	Response at Point A for Slot Two	74
Figure 4.14	Response at Point B for Slot Three	75
Figure 4.15	Response at Point B for Slot Four.....	75
Figure 4.16	Response at Point A for Slots One and Two.....	76
Figure 4.17	Response at Point B for Slots Three and Four.....	76
Figure 4.18	Response at Point C due to Point A	77
Figure 4.19	Response at Point C due to Point B	77
Figure 4.20	Horizontal, Vertical Polarization Radiation Pattern of Prototype and Planar Array @ 1.275 GHz	80
Figure 4.21	Prototype Antenna Input Impedance and Return Loss.....	81
Figure 4.22	Normalized S21 Parameter of Slot Two.....	82
Figure 4.23	Normalized S21 Parameter of Slot Three.....	83
Figure 4.24	Normalized S21 Parameter of Slot Four.....	84
Figure 5.1	Magic T	87
Figure 5.2	Magic T Phase Characteristics.....	89
Figure 5.3	Radiation Patterns of Different Separations	91
Figure 5.4	Radiation Pattern Development.....	92
Figure 5.5	Received Signals with 5λ Separation between Antennas	97
Figure 5.6	Received Signals with 40λ Separation between Antennas	98
Figure 5.7	Switch 1 with Mean Removed at a 5λ Separation	99
Figure 5.8	Switch 1 with Mean Removed at a 40λ Separation.....	100
Figure 5.9	PDF of the 5λ Separation Inputs.....	103
Figure 5.10	PDF of the 40λ Separation Inputs	104
Figure 5.11	CDF Graph for 5λ Separation	107
Figure 5.12	CDF Graph for 40λ Separation.....	108

Figure 5.13	Effect of Noise on System Accuracy.....	109
Figure 6.1	Ideal M Branch Selection Combining Curves [1].....	116
Figure 6.2	Two Branch Correlated Selection Combining [2].....	118
Figure A.1	Switch Control Layout.....	129
Figure A.2	I/O Computer Plug	130
Figure A.3	4-to-1 Switch Configurations.....	131
Figure F.1	MDS Test Set-up	156

List of Tables

Table 3.1	Minimum Input Signal to Receiver Antennas	57
Table 3.2	Maximum Input Signal to Receive Antennas.....	58
Table C.1	Noise Figure and Gain Specifications.....	145

List of Symbols and Abbreviations

\hat{r}_o	resultant output
'	feet
"	inches
2D	two dimensional
3D	three dimensional
@	at
α	attenuation constant
A/D	analog to digital
A_i	amplitude of i th signal
$a_i(t)$	time-varying amplitude of i th path
AM	amplitude modulation
AMPS	advanced mobile phone standard
A_{pe}	plane earth attenuation
AUT	antenna under test
β	phase constant
BW	bandwidth
CDF	cumulative distribution function
CDMA	code division multiple access
C_{line}	feed line capacitance
cm	centimeters
cos	cosine function
C_s	series capacitance

C_{slot}	slot capacitance
D	antenna maximum overall antenna dimension
$D(\theta, \phi)$	directivity in spherical coordinate system
$\delta(t)$	delta dirac function
Δa	bin width
dB	decibels
dBm	dB referenced to milliwatts
DC	direct current
d_{km}	distance between receiving and transmitting antennas measured in kilometers
E	electric field
ε	permittivity
E_{ϕ}	electric field in phi direction
EIRP	effective isotropic radiated power
E_{θ}	electric field in theta direction
E_r	electric field in radial direction
E_{x0}	electric field amplitude factor
ϕ	phase
$F(\theta, \phi)$	array pattern in spherical coordinate system
$f(\theta, \phi)$	isotropic array pattern in spherical coordinate system
FDMA	frequency division multiple access
F_i	noise figure of ith block

$\phi_i(t)$	time-varying phase of i th path
FM	frequency modulation
G	maximum gain
$G(\theta, \phi)$	gain in spherical coordinate system
$g(\theta, \phi)$	antenna pattern in spherical coordinate system
G_{ai}	gain of i th block
GHz	gigahertz
G_r	receiving antenna gain
Γ_p	reflected power coefficient
G_t	transmitting antenna gain
H	magnetic field
η	efficiency
$h(t, \tau)$	low pass channel characteristics
H_ϕ	magnetic field in ϕ direction
H_θ	magnetic field in θ direction
H_r	magnetic field in radial direction
h_r	receiving antenna height
h_t	transmitting antenna height
Hz	hertz
η_z	intrinsic impedance
I	in-phase
I/O	input output

inf	infinity
IRIS	impulse response identification system
IS	interim standard
ISM	industrial, scientific, and medical
J₀	Bessel function first kind zero order
jX	reactance
K	Boltzmann's constant
kHz	kilohertz
km	kilometers
km/hr	kilometers per hour
L	length
λ	lambda
l	length
ll	two
L_{line}	feed line inductance
log	logarithm to the base 10
L_{slot}	slot inductance
m	meters
μ	permeability
Mag	magnitude
MDS	microwave and RF design system
MHz	megahertz
mm	millimeters

ms	milliseconds
N	number of sources
NF	noise figure
nH	nanohenries
n_i	number of elements in ith bin
NW	northwest
P	power
π	pi
P_+	power from sum output of Magic T
P_-	power from difference output of Magic T
p-p	peak to peak
PCS	personal communications system
PDF	probability distribution function
pF	picofarads
P_i	cumulative distribution function
p_i	probability distribution function
P_{in}	input power
P_r	received power
P_t	transmitted power
Q	quadrature
θ	phase
R	distance from base station to mobile station
r	radius surrounding mobile transceiver

$r(t)$	time-varying received low pass signal
R_d	resistance of dipole
RF	radio frequency
R_i	resistance of i th element
R_{line}	feed line resistance
rms	root mean square
ρ_r	correlation coefficient
R_s	source resistance
R_{slot}	resistance of slot
R_x	receiver
Σ	summing symbol
S/I	signal to interference ratio
S/N	signal to noise ratio
σ^2	variance
sin	sine function
SNR	signal to noise ratio
T	temperature in Kelvin
t	time
TDMA	time division multiple access
TEM	transverse electric and magnetic wave
$\tau_i(t)$	time-varying time delay of i th path
τ_s	time delay required for time diversity scheme
TTL	transistor to transistor logic

T_x	transmitter
v	velocity
U(θ,φ)	radiation intensity in θ and φ coordinates
u(t)	time-varying input low pass signal
UHF	ultrahigh frequency
u_m(t)	mean value
û_m(t)	estimated mean value
V	voltage
VLSI	very large scale integration
V_{TW1}	forward travelling voltage wave
V_{TW2}	reflected travelling voltage wave
Ω	ohms
ω	angular frequency
x	direction along x axis
y	direction along y axis
z	direction along z axis
Z_{in}	input impedance
Z_L	load impedance
Z₀	characteristic impedance of transmission line
°	degree

1.0 Introduction

Cellular radio is the first generation of the ultimate goal - a personal communication system (PCS). The thrust of the PCS network is to provide telephony service as well as all types of data transfer to each individual, with a specific identification number, everywhere and anytime. The cellular radio industry is rapidly growing both in the developed and developing parts of the world by providing a relatively flexible and reliable telephone service to its users. In Canada, the AMPS cellular technology (see Section 2.1.1) was implemented in 1985; the two cellular carriers are Cantel Mobile Communications and Mobility Canada. These carriers service more than two million Canadian subscribers and both companies estimate that business will grow at a rate of 20% to 25% annually [1]. Over ten thousand jobs have already been created in the Canadian cellular industry [2], but, as the demand for new and improved services continues, more engineering skills and research will be necessary for its successful growth.

A problem in cellular radio, which manifests itself by reducing the reliability of the received signal, is known as multipath fading. The objective of this thesis is to improve the quality of the received signal in a cellular multipath environment and thus acquire a more reliable information signal.

A solution to this objective is achieved by two separate projects in this thesis. Although both projects are applied in conjunction specifically at the cellular base station, due to a time restriction, the projects are presented independently.

The first project involves a new cellular base station antenna design, to be known in this thesis as the Cylindrical Slot Antenna. This antenna is

designed to achieve the typical base station antenna requirements but with an emphasis on overall size and cost. A prototype antenna has been developed in order to evaluate the antenna design. Further, an anechoic test set-up has been developed in order to evaluate the prototype antenna. The prototype is a physically scaled-down version of the design antenna and all measurements are frequency scaled to adjust to its physical size. The prototype is evaluated by the radiation pattern, input impedance, return loss and S21 measurements.

The second project involves a unique pattern diversity scheme which is based on the combination of a space diversity configuration and a passive combiner known as a Magic T. To evaluate the diversity scheme, a continuous wave uplink test system with mobile transmitter, operating in the ISM band, was developed. The received data from the test system was converted into probability and cumulative distribution curves. These curves are used to determine the relative diversity improvement of the diversity scheme.

2.0 Problem Statement

One of the most serious technical problems in cellular radio is caused by multiple versions of the desired information signal arriving at the receiving antenna. These multiple signals travel through the channel to the receiver via multiple paths which are created by surrounding objects either reflecting, scattering, or diffracting some portion of the transmitted signal [1]. This type of channel is known as a multipath channel and the signals travelling through the channel are subject to a degradation known as multipath fading.

A reflector, which is an object that is physically much larger than the wavelength of the transmitted signal, reradiates some portion of its incident signal. This can be a spectral or diffuse reflection depending on the relative smoothness of the object's surface. A spectral reflection occurs when the incident signal encounters a smooth interface and is reflected according to Snell's law. A diffuse reflection occurs when the incident signal encounters a rough interface and the signal is scattered. A scatterer, which is an object that is comparable in physical size to the wavelength of the transmitted signal, reradiates some portion of the signal in many directions. The radius, r , of the physical area in which the reflectors and scatterers significantly affect multipath fading, is often approximated by Equation 2.1 [2] centered at the location of the mobile station.

$$r = \frac{R \times BW}{2} \quad (2.1)$$

The third common phenomenon that affects the received signal is diffraction, which occurs when the line of sight signal (the direct path between

the transmitter and receiver) is impeded but, by seemingly bending around the impeding object, the signal arrives at the receiver. An example of reflection, scattering, and diffraction is presented in Figure 2.1.

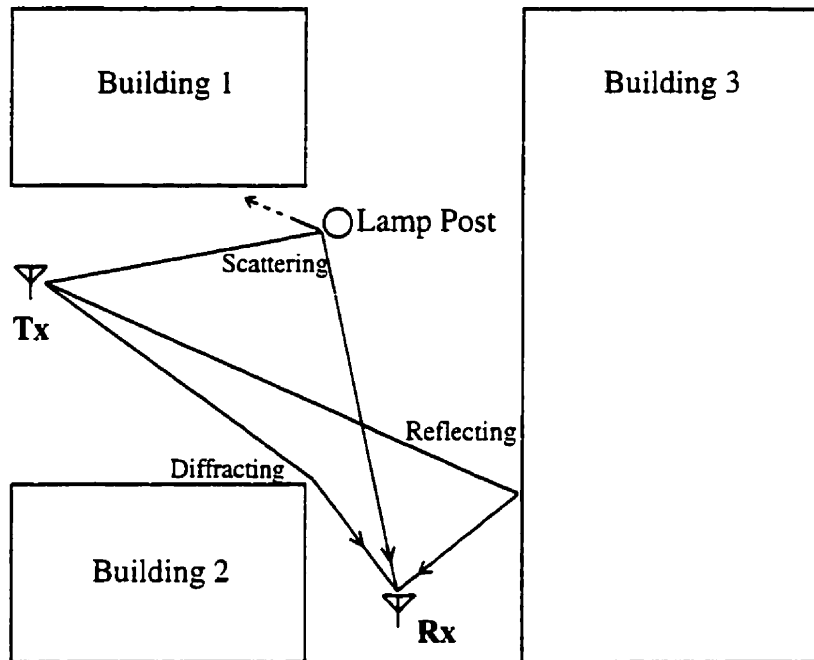


Figure 2.1 Reflectors, Scatterers and Diffractors

These multipath signals arrive at the receiver with different amplitudes, phases, and polarizations which either constructively or destructively combine to produce the multipath fading signal. The quality of the signal is generally improved by reducing the depth and duration of the fades within the multipath fading signal.

2.1 General Cell Systems

As in most mobile radio systems, the desired coverage area of the cellular telephony system consists of many smaller, individual, coverage areas-called cells. Each cell is supported predominately by one base station transceiver, operating within a specific range of frequencies.

A cell is defined by the contour of a given RF field strength value. This value is based on the RF power necessary for a good demodulated signal. The term "good" refers to a clearly understood received message. (See Section 2.1.1.) Sometimes, not all locations within the cell boundaries have an RF field strength value above the necessary minimum. These areas are called dead spots or holes [3] and may be caused by an occurrence known as shadowing. Shadowing occurs when an obstructing object absorbs or reflects away the available signal and therefore creates an area with a weak RF field strength. These areas can only be tolerated in very low traffic locations thereby minimizing their effect on the cell system and maintaining the overall "good" standard.

Cells have irregular shapes and sizes; cell sizes can be categorized into three general groups: the macrocell, the microcell, and the picocell.

Macrocells, the largest cells, have a coverage radius of up to 50 km. The base station antenna is elevated well above all surrounding objects; and, the base station transmitter operates at large transmit powers ($\cong 1000\text{W}$ EIRP). This type of cell is very similar to that of AM or FM radio broadcasting systems and is predominantly used in this stage of cellular telephony.

With the larger cell size, fewer base stations are required to service the desired geographical area. But, as the number of users and frequency of user

calls increase - capacity demands on the existing systems grow, some cells and/or clusters (see Figure 2.2) may not be able to support all the traffic within their service area. A solution for increasing capacity, within a macrocell with a restricted frequency spectrum, is to reduce the cell size. Reducing the size of a macrocell is referred to as cell splitting. Cell splitting can be a permanent or dynamic procedure depending on the capacity and frequency of the traffic in the cell. Cell splitting involves reducing the area of the old cell size into a number of smaller cells, while each new cell services approximately the same traffic load as the old cell [4]. Another solution for increasing capacity within the frequency restricted macrocell involves sectorization of the cells. By using base station antennas with the appropriate radiation patterns, a cell can be split into a number of different sectors - usually at 120° or 60° intervals. A distortion, known as co-channel interference, is reduced due to increased directivity of the radiation patterns of the sectorized cells. Co-channel interference is caused by interference from other users in the vicinity, operating at or near the same frequency as the designated user. The required distance between cells supporting the same frequencies, for acceptable co-channel interference, is directly dependent on cell size and transmitter powers. With reduced co-channel interference, the signal to interference ratio (S/I) is improved. When the number of cells within a cluster consisting of sectorized cells is reduced, the increased S/I develops into an increased spectrum efficiency and therefore an increased capacity [5].

Microcells are smaller than macrocells and have a coverage radius of up to 1 km. The base station antennas supporting the microcells are generally lower in elevation than the base station antennas supporting macrocells due to the reduced required coverage areas. With a smaller cell size, the necessary

transmitter power from the base and mobile stations is reduced. The decreased power requirements reduce the complexity of the mobile transceiver. The decreased base station transmitter power requirements increase the number of cells needed to service the entire geographical area. The larger number of required cells directly increases the complexity of the base stations. The asymmetry of complexity of the base and mobile stations has economical and perhaps even medical advantages. The increased complexity at the base station can often be more easily accommodated technically and, therefore, more economically than at the mobile station. Also, the decreased signal power transmitted from the mobile station, as permitted by using smaller cells, addresses some concerns with respect to the UHF power that is radiated into the head of the mobile user. Many studies [6] have been done on this subject but clear conclusions cannot or have not as yet been determined. Many researchers are studying the effects of radiation on the human head and are working to develop antennas that reduce this possibly harmful radiation [7].

Picocells, the smallest cells, have a coverage radius of up to 100 meters. Picocells are used to service very small areas such as individual floors within a building or even the individual rooms within the floor of a building. The elevation of the base station antenna supporting the picocell is only higher than the very immediate surrounding objects, i.e. the highest point in a room. This cell size has an important role in wireless local area networks - an area with great potential for both telecommunication suppliers and users. Macrocells and microcells are most commonly employed in outdoor propagation environments while picocells are typically employed in the smaller indoor propagation environments.

The arrival of multiple distorted copies of the desired information signal (multipath signals) at the receiving antenna, lengthens or spreads out the required time necessary to capture the relevant signals. A common measure for this lengthening in time, known as delay spread, involves transmitting an impulse signal through the channel and measuring the time it takes for the majority of the relevant multipath signals to arrive at the receiving antenna. The delay spread is used to determine the coherence bandwidth. Two received signals with a frequency separation less than the coherence bandwidth will demonstrate statistically similar fading characteristics. A frequency separation greater than the coherence bandwidth results in statistically dissimilar fading characteristics. In typical outdoor environments, as the cell size decreases, the delay spread and the propagation characteristics, such as the dynamic range of the signal fades, also decrease thus reducing the effects of multipath fading on the received signal. Therefore in smaller cells, the degree of the measures required to counter multipath fading is reduced [8].

Cells [9] are arranged in clusters; each cluster uses the entire allotted cellular frequency spectrum. The cells within a cluster partially overlap and the coverage area of the clusters may also partially overlap in order to ensure continuous coverage from one cell area to another. (See Figure 2.2.) Each cell is assigned specific frequencies from the cellular frequency spectrum; cells from neighboring clusters, which support the same frequencies, must be well separated in order to minimize distortion. As a mobile user, with an active call, travels from one cell to another and through one cluster to another, the operating frequency and the supporting base station for the call must change so a continuous service can be achieved. This is a complex procedure and is known as hand-off.

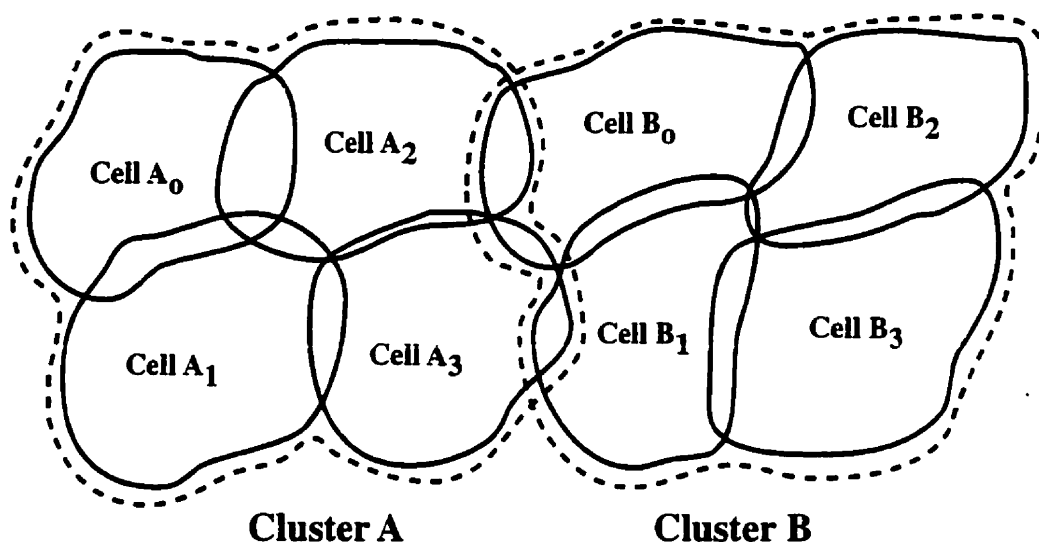


Figure 2.2 Cluster

The principle attenuation of the RF signal from the transmitting antenna to the receiving antenna, excluding the losses due to multipath fading, shadowing, and co-channel interference, is known as propagation loss. In a simple propagation environment, such as propagation over a flat earth, the power at the receiving antenna is equal to the transmitted power reduced by the propagation loss.

Significant factors in determining the propagation loss of a system are the height of the antennas, location of the antennas, and the gain of the antennas. A formula for determining the propagation loss in a flat earth situation, Equation 2.2 [10], takes these significant factors into account but only considers the direct wave and one spectrally reflected wave and does not take into account environmental or terrain factors. This type of path loss is known as plane earth attenuation (A_{pe}).

$$A_{pe} = -120 + 20 \log\left(\frac{h_t h_r}{d_{km}^2}\right) + G_t + G_r \quad (\text{dB}) \quad (2.2)$$

Where h_t and G_t refer to the transmitting antennas's absolute height and gain respectively. The variables h_r and G_r represent the receiving antenna's absolute height and gain respectively. The variable d_{km} represents the separation distance between the transmitting and receiving antenna measured in kilometres.

The transmitter power can be increased to effectively overcome the propagation loss and, therefore, potentially increase the cell size but there are limits to the maximum transmitter power. These limits have been established by economics and industry/government standards. Although an increase in transmitter power may potentially increase cell size, the restrictions on the RF transmitter power provide an upper bound to this increase.

Referring to Equation 2.2, the propagation loss at a constant distance from the transmitting antenna can be decreased by either increasing the gain of the antennas or increasing the absolute height of the antennas.

The absolute height of the antennas affects the propagation loss. As the antennas' height increases, the propagation loss decreases. There are limits to the maximum height of an antenna which consequentially provide an upper bound to the reduction in propagation loss and, therefore, to the potential increase in cell size. In a more typical propagation environment, such as an urban environment, the relative elevation of the antennas compared to surrounding objects, the effective height, affects the cells size. Generally, as the effective height of the antennas increases above the surrounding objects, the coverage area of the cell tends to be larger. As the antenna elevation decreases below the elevation of the surrounding objects, the signal may be

contained by these reflectors and scatters. Consequentially the coverage area may remain essentially unchanged due to the effective antenna height even with an increase in transmitter power. An illustration of the effect of the elevation of the antenna relative to surrounding objects, is presented in Figure 2.3.

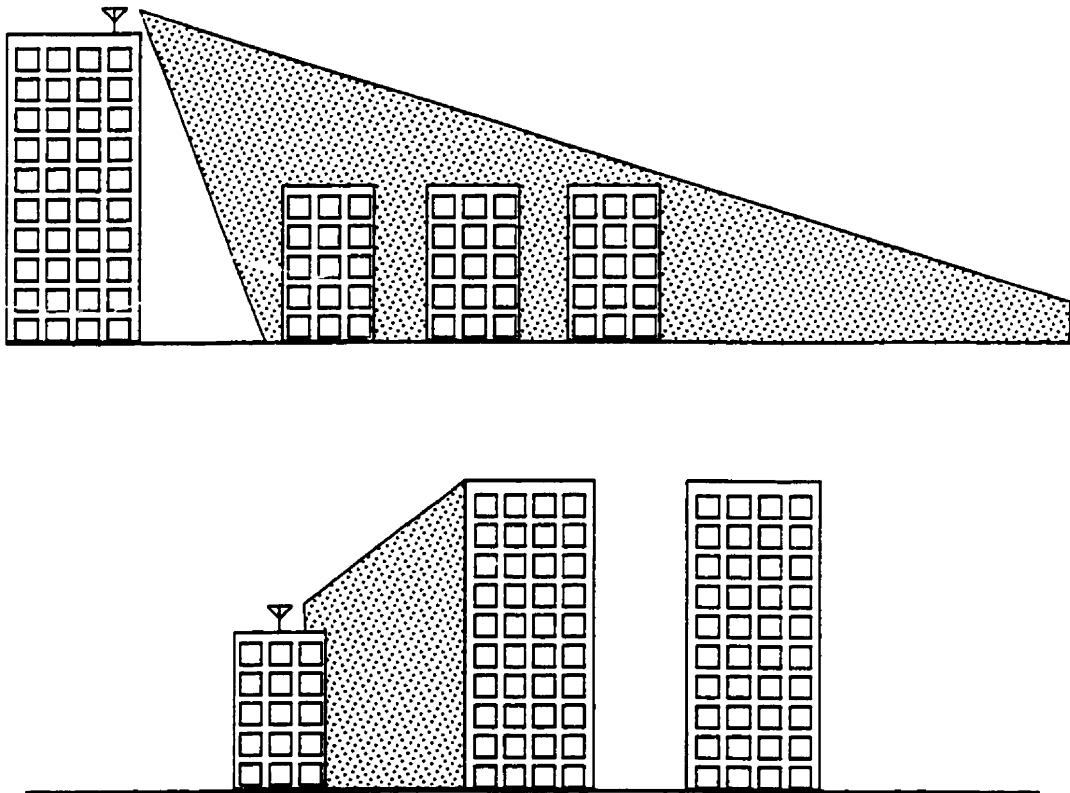


Figure 2.3 Antenna Positioning

Many models have been developed which attempt to more accurately predict propagation loss by taking into account different environmental and path parameters. One of the more recognized prediction formulas was developed by M. Hata [11] whereby equations have been fit to the experimental data acquired by Y. Okumura et al. The data for the model was acquired in Tokyo, Japan,

between the frequencies of 200 MHz and 1920 MHz with separation distances of 1 to 100 km from the base station. The model can be adjusted to account for suburban, open, isolated mountain areas, rolling hills, sloping terrain, and mixed land-sea paths.

This model can be used as the design foundation for the requirements of the RF section of a cellular system. Experimental results can be used to provide the necessary fine-tuning to the cellular system design.

2.1.1 Current Cellular Systems

The first generation of cellular telephony utilizes analog RF modulation techniques in a frequency division multiple access (FDMA) scheme; the second generation of cellular telephony utilizes full digital techniques incorporating new access techniques such as time division multiple access (TDMA) and/or code division multiple access (CDMA) [12]. Digital systems can support more users per base station per MHz than the analog counterpart. While user capacity demands increase and digital coding and VLSI technologies improve, the fully digital cellular technology will become more economically viable to the cellular suppliers and subscribers. In Canada, the analog standards are governed by the Advanced Mobile Phone Standard (AMPS) and the digital standards are governed by the Interim Standards, IS-54 and IS-95. The digital standards work within the framework of the analog standard in order to allow a smooth industry transition from analog to digital. In the analog standard, the mobile station transmit frequency allocation is within the band 824 MHz to 849 MHz, and the base station transmit frequency allocation is within the band 869 MHz to 894 MHz. There are 832 duplex channels each with a 30 kHz bandwidth of

which 21 are used for set up and initialization. The far field (see Equation 3.2) transmitted signal is an electromagnetic wave operating in the transverse electric and magnetic (TEM) mode. (See Figure 2.4.) The electric and magnetic fields, while perpendicular to the direction of wave travel, are also perpendicular to each other. As the electric field travels in the z direction it varies sinusoidally in the x direction. The magnetic field, which is perpendicular to the electric field, travels also in the z direction but varies sinusoidally in the y direction.

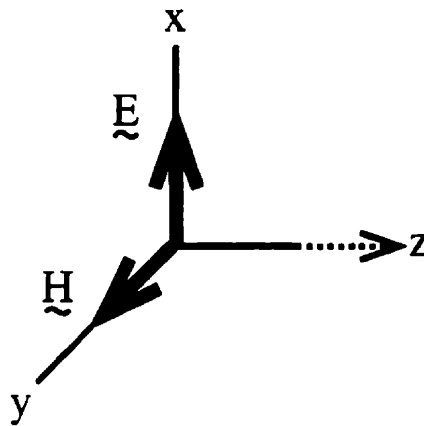


Figure 2.4 TEM Wave

The quality of the received signal is determined by the perceived quality determined by the listener. In flat terrain, the perceived quality of the received signal must be between good and excellent judged by 75% of the users in 90% of the cell coverage area [13]. In a hilly terrain, 90% of the users must rate the quality of the received signal to be between good and excellent in 75% of the cell coverage area [13].

2.2 Multipath

The total multipath signal, as presented in Figure 2.5, can be separated into two categories, long term fading and short term fading. Long term fading is a relatively slow fading signal onto which the short term fading signal is superimposed. The propagation loss of the RF signal is the main component in long term fading. This fading indicates the time varying mean of the received signal and generally has a log normal probability distribution. In this thesis, solutions to the detrimental effects of long term fading on the reliability of the received signal are not addressed. Other more effective solutions for long term fading must be used, i.e. automatic gain control systems. Short term fading is a fast fading phenomenon caused by the multipath signals arriving at the receive antenna. The movement of the environment surrounding the transmitter and receiver and the movement of the transmitter and/or the receiver cause a rapidly time-varying multipath signal. This type of fading can often be characterized by a Rayleigh or Rician probability density function depending on the relative power in the line of sight signal path. A common technique used to minimize the effect of short term fading is antenna diversity.

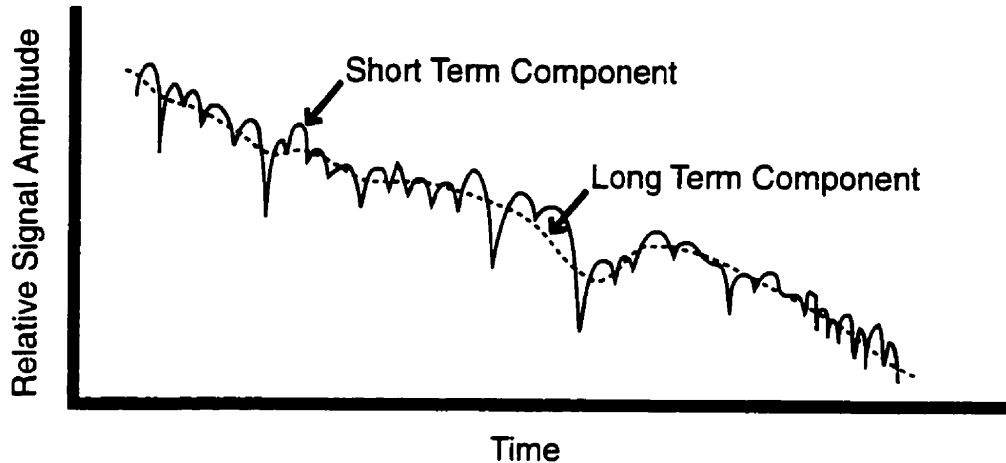


Figure 2.5 Sample of Multipath Fading Signal

2.3 Diversity Techniques

Diversity schemes can improve the reliability in the quality of the signal in the multipath environment by providing a number of independent, or almost independent, fading channels. Diversity techniques can be implemented at the base station and/or the receive station to obtain system improvement. The correlation coefficient, which is a relative measure of dependence, between the diversity channels can be relatively high and still obtain significant diversity improvement [14]. If the antenna scheme is the major component to the diversity technique then it is known as antenna diversity. Some of the common antenna diversity schemes are space, polarization, field, and pattern.

Space diversity is a common and simple scheme requiring two or more antennas at the receiving site. These antennas must be separated by a specific distance to ensure that the signals received are optimally uncorrelated. The distance between antennas is dependent on the size of the angular sector of the majority of the incoming signals to the site. The incoming signals and,

consequently, the incoming angular sector are affected by the receive antennas' physical location relative to surrounding scatterers and reflectors. Therefore, the incoming angular sectors of the mobile station and the base station are dramatically different. (See Figure 2.6.)

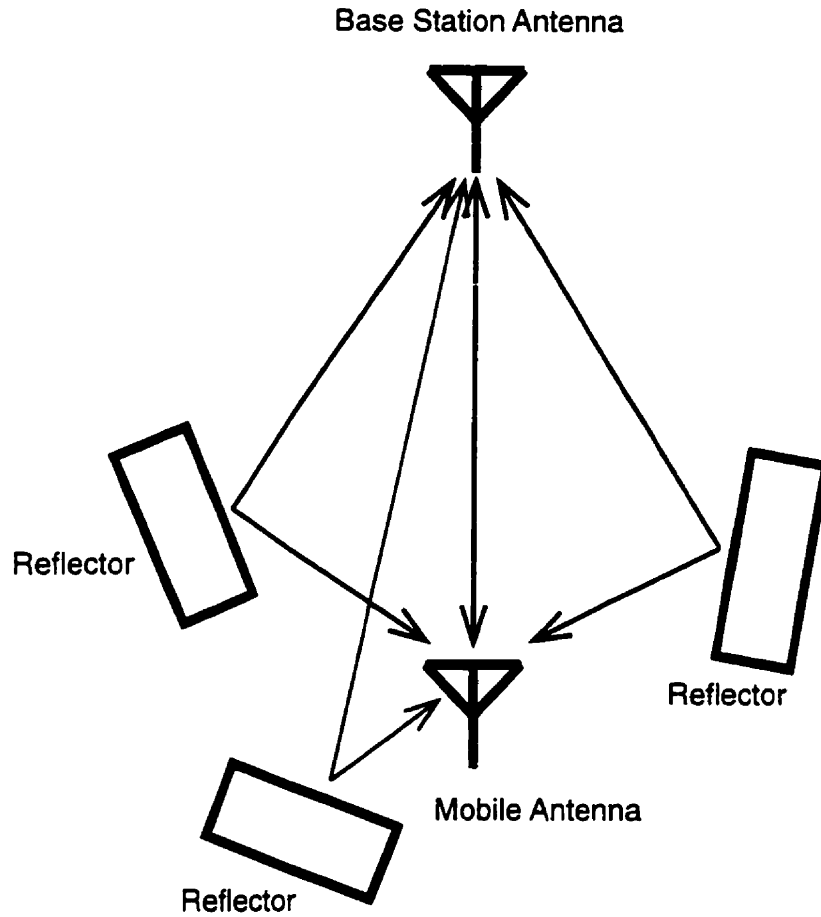


Figure 2.6 Example of Angular Sectors at the Base and Mobile Sites

Normally, the mobile receiver is located at or near street level amongst the majority of all scatters and reflectors. Therefore, multipath signals arrive from all angles to the mobile, resulting in an extremely wide angular sector. The appropriate separation distance is determined by Equation. 2.3 [15].

$$\rho_r(d) = Jo^2(\beta d)$$

Where ρ_r is the received correlation coefficient and β is the propagation constant and d is the separation distance of the receiving antennas.

Normally, the base station is well elevated above the majority of all surrounding reflectors and scatterers causing the multipath signals to arrive within a small angular sector. The appropriate separation is then determined using the graphs in Reference 16. These graphs have been numerically calculated and depend on the bandwidth of the angular sector, on the relative angle of the angular sector, and on the velocity of the mobile unit.

Since the physical area required for the antenna separation may often be more practically obtained at the base station than at the mobile station, space diversity is more commonly incorporated at the base station.

Polarization diversity relies on unlike reflecting coefficients and unlike scattering coefficients for the differently polarized signals. While the multiple polarization orientations of the same information signal will be correlated at the transmitter, the different reflecting and scattering coefficients may create statistically uncorrelated signals at the receiver. The different polarizations, generally vertical and horizontal, can be used at the receiver to obtain diversity improvement. Neglecting cross-polarization as an effective polarization scheme, changes to the transmitting configuration and receiving configuration are required to implement this type of diversity. Appropriately designed polarization antennas may be co-located and, therefore, minimize the physical area required at the base station and mobile station.

Field diversity is very similar to polarization diversity, but, instead of focusing on multiple polarizations, the electric and magnetic fields are used to

create the diversity signals. The TEM fields at the transmitting antenna are indeed interdependent but, as the wave travels through the channel, the fields are affected by different reflecting and scattering coefficients which may result in highly uncorrelated fields at the receiving antennas. As in polarization diversity, properly designed field diversity antennas may be co-located.

Pattern diversity relies on multiple radiation patterns to individually receive different multipath signals. The overall desired coverage area is subdivided into a number of narrow angular sections by independent radiation patterns; the signals received within these sectors may be highly uncorrelated. Different radiation pattern configurations are required depending on the specific environment surrounding the receive antenna. As in space diversity, only changes to the receiving configuration are required to implement this diversity scheme. Appropriately designed antennas may often be co-located and, therefore, minimize the physical area required at the receiving site.

While all of these schemes can be applied to either the base station or the mobile station, the gains from the individual diversity schemes cannot be generically compared. The specific environment in which the diversity scheme will be applied is a presiding influence in the ranking of the schemes as the pros and cons of each scheme are varied in different environments.

In all the antenna diversity schemes presented, multiple antennas are required as the major component in each configuration. Thus, a persistent design concern is the mutual coupling of radiated fields from the individual antennas within the array. Mutual coupling occurs when objects in close proximity interact with the antenna and affect the free space current distribution along the antenna. In a first order approximation, the degree of coupling decreases as the distance between the coupling objects increases. The free

space characteristics of the individual antennas must be adjusted in the system design to account for the specific operating environments.

When the signals to be used for diversity improvement are received, the signals must be evaluated and correctly manipulated to provide the best overall signal. Common techniques [14] to accomplish this are switched selection combining, equal gain combining, and maximal ratio combining. Switched selection combining selects one signal branch with the largest relative amplitude from all diversity input signals. Equal gain combining, equally combines all the phase adjusted diversity signals. Maximal ratio combining, combines the weighted phase adjusted signal branches by increasing the gain of the phase adjusted signal with the largest carrier to noise ratio and selectively attenuating the other phase adjusted signals. Although maximal ratio combining produces the best actual performance in analog combining, it is also the most complex of all the analog combining techniques. In analog systems, switch selective combining achieves less diversity improvement but is a much simpler technique than maximal ratio combining and, therefore, is often considered the best of the three techniques, particularly in these early development and application stages of diversity techniques.

3.0 Measurement Methods

A measurement system for each project has been developed to respectively evaluate the solutions presented in Chapters Four and Five.

For the first project, a mini-anechoic chamber test set-up has been developed in order to evaluate the new base station antenna design. This mini-anechoic chamber test set-up is used to measure the radiation pattern, input impedance, polarization and power gain of small to medium size antennas operating in and above the UHF bandwidth.

For the second project, a narrowband uplink system with a mobile transmitter has been developed to evaluate the unique base station pattern diversity scheme. The uplink system is used to sample and measure the power in the envelope of received diversity signals in order to determine the effectiveness of the pattern diversity scheme.

Since both projects of this thesis are hardware oriented, the instrumentation and measurement methods developed and applied are strongly emphasized.

3.1 Cellular Base Station Antenna

There are numerous performance parameters which can be used as evaluators for antenna systems. A select combination of these evaluators is required to provide sufficient information and therefore determine the suitability of a particular antenna system in a specific environment.

The more commonly required antenna parameters are efficiency, radiation pattern, input impedance, polarization and gain. In general, all these

parameters are frequency dependent and must be determined throughout the entire frequency bandwidth of interest.

3.1.1 Efficiency

Antenna efficiency is the measure of the radiated power compared with the total input power to the antenna system. "The time average power radiated in free space is the same power that would be dissipated in a resistance in the absence of any radiation" [1]. This resistance is known as radiation resistance. The input power, which is not radiated, is dissipated in one of four general loss categories [2]: conduction losses, dielectric losses, coupling losses, and mismatch losses.

The efficiency of an antenna system can be measured or analytically calculated. The efficiency of small antennas can be measured using a Wheeler cap method [3], while the efficiency of medium to large antennas is commonly measured using gain and directivity measurements determined in a highly accurate anechoic chamber. The efficiency of antennas of all sizes can be analytically calculated, but this analysis is computationally very intensive. Due to the complexity of determining the antenna efficiency by either measurement or analysis methods, the efficiency parameter is not evaluated for the antenna in this thesis. The efficiency of the presented antenna design is assumed to be high, due to low loss materials used in the design and an overall good input match.

3.1.1.1 Losses

In a metallic conductor, a very small amount of energy is required to move electrons in the lower filled states into unoccupied higher energy states, thus, creating an electron flow [4]. The mobility and charge density of electrons in the conduction band determine its conductivity. This conductivity, together with length and diameter of the metallic conductor, play a role in determining the resistance of the metal. The power absorbed by the conductor resistance, known as conductor loss, is converted into heat and is not retrievable to the antenna. The conductor loss in an antenna may be higher than expected due to a phenomenon known as skin effect which occurs in conductors at radiation frequencies. This effect forces the current flow to the surface of the conductor and substantially reduces its effective cross-sectional area, therefore raising the effective conductor resistance and consequently the conductor loss. For example the depth of penetration a transmitted signal along a copper wire at 1 GHz is approximately 2 μm .

The predominate type of charge in dielectric materials is bound charge. Bound charges are electric dipoles composed of positive and negative charges [5]. These dipoles have the ability to store energy by shifting the relative positions of the charge elements from their normal positions. These polarizations account for the predominant type of current in low loss dielectrics, known as displacement current. Displacement current is described as the time-varying current in a non-conducting medium in which net volume charge density is not present. From the ratio of conduction current to displacement current, known as tangent loss, the intrinsic impedance can be determined and

accordingly used in the time-averaged power equations to determine the effective dielectric loss. (See Reference 5.)

Coupling losses are due to the presence of objects surrounding the antenna. These objects alter the antenna's free space characteristics and result in a mutual impedance which is dependent on the geometry and the electrical character of the surrounding objects. (See Section 3.1.3.)

Mismatch losses result from the power reflected back to the source, at the input to the antenna system, due to its mismatched input impedance. The TEM wave travels along the transmission line with a specific characteristic impedance until encountering the load. Assuming that the source impedance and the transmission line characteristic impedance are properly matched, the load must be the conjugate match of the source impedance. Otherwise, some portion of the incident TEM wave is reflected back to the source, thus taking power out of the system that is potentially deliverable to the load.

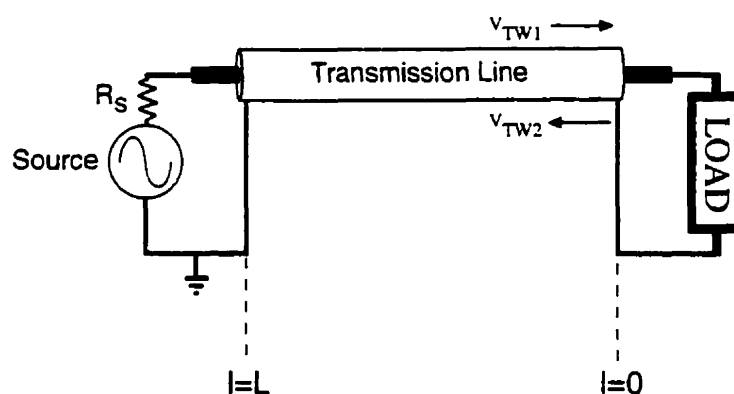


Figure 3.1 Transmission Line

The reflected power at $l=0$, is dependent on the load impedance and characteristic impedance of the transmission line. (See Figure 3.1 and Equation 3.1 [6].)

$$\Gamma_{\rho}(l=0) = \left(\frac{Z_L - Z_0}{Z_L + Z_0} \right)^2 \Bigg|_{Z_0 \text{ is real}} \quad (3.1)$$

Where Γ_{ρ} is the reflected power coefficient, Z_L is the load impedance, and Z_0 is the characteristic line impedance.

3.1.2 Radiation Pattern

The radiation pattern is a graphical representation of the normalized coverage area of the TEM wave from an antenna system. The radiation pattern of the far field waves is usually presented in either 2D or 3D graphs. “The far field zone is defined as the region of the antenna field where the angular field distribution is essentially independent of the distance from the antenna” [7]. Antennas are generally used to communicate information over relatively large distances (many wavelengths), therefore, the far field is ultimately the zone of interest. Radiation pattern graphs may be the representation of the magnitude of either the electric or the magnetic field, although the magnitude of the electric field is most routinely employed.

The general methods of determining the radiation patterns were established before World War II. In the subsequent years, many improvements have been developed to increase overall measurement accuracy [8]. The most common type of indoor facility for measuring the radiation pattern of an antenna, in the UHF region and higher, is the anechoic chamber. This type of test facility or test range has a specific shape and size depending on the frequencies of interest. Generally, the inner side walls and ceiling of the test range are covered with a highly absorptive and non-reflective RF material to reduce reflections and, therefore, approximate a free space environment. The basic

concept of the anechoic chamber is to transmit a signal from a source antenna, with a known radiation pattern, then measure the direct wave signal strength radiating from the antenna under test (AUT). The field strength, as measured by the S21 parameter (see Section 3.1.2.1), is recorded and usually normalized for each particular orientation at a specific frequency. Normalization of the radiation pattern involves determining the maximum received signal power and reducing all measurements by this maximum value. There are eight main components of an anechoic chamber measurement system: chamber, signal source, source antenna, receiving antenna, positioning system, calibrated receiver, recording system and data processor. (See Figure 3.2 [9].)

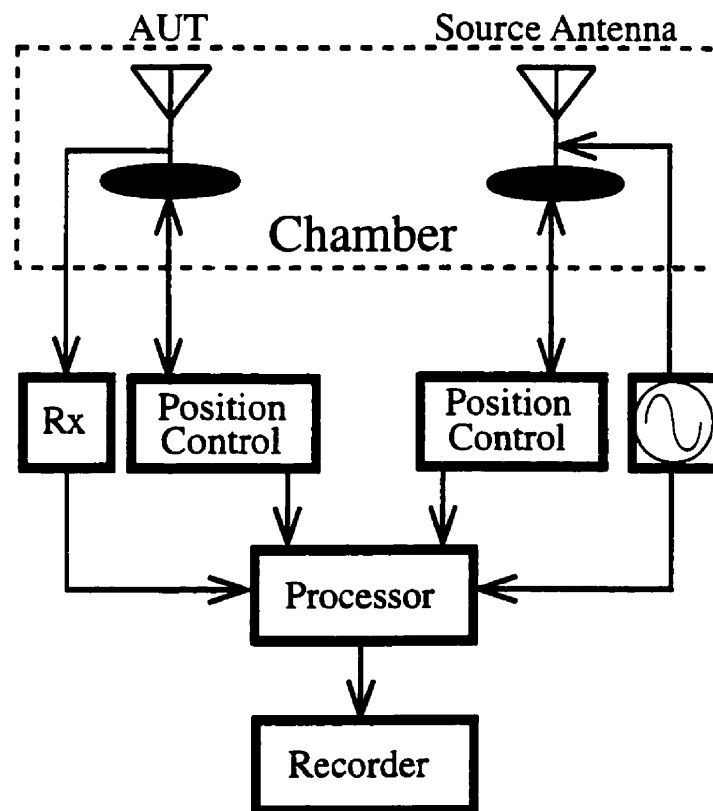


Figure 3.2 Anechoic System Block Diagram

To measure the far field radiation pattern, the source antenna and the AUT must be separated by the minimum distance determined by the Fraunhofer equation. (See Equation 3.2 [7] and Figure 3.3.)

$$r \geq \frac{2D^2}{\lambda} \quad (3.2)$$

Where D is the maximum antenna dimension, λ is the wavelength of the transmitted field, and r is the necessary antenna separation distance.

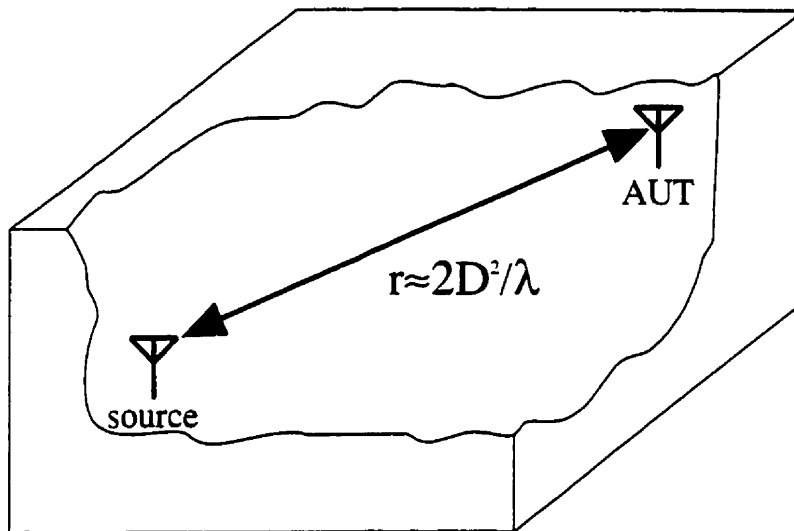


Figure 3.3 Separation Distance of Antennas in Far Field

In order to obtain preliminary radiation pattern measurements and facilitate the antenna design process, a mini-anechoic chamber was designed and built at the University of Calgary. When the final antenna design to developed, the antenna should be evaluated in a precisely tuned industrial anechoic chamber to obtain accurate results. The complete measurement system consists of a chamber, network analyzer, motor and microprocessor.

The outer dimensions of the wooden chamber are 2.44 m x 2.44 m x 1.22 m. The inner chamber walls and ceiling are covered with an RF absorptive material which consequently reduces the inner dimensions to 1.5 m x 1.5 m x 0.75 m. The RF absorptive material, rantec EHP-18 CL Foam Absorber, has a return loss specification of approximately -30 dB at 500 MHz, -40 dB at 1 GHz and -45 at 3 GHz. The inner chamber floor is covered by a large aluminum sheet with an approximate 2 mm thickness which reduces the overall cost of the chamber. The aluminum sheet provides a good ground plane for the test antennas but also creates at least one strong ground reflection. Through proper antenna placement and by normalizing all measurements, the effects of a strong ground reflection on the measured radiation pattern are effectively eliminated. (See Section 3.1.5.) Since the signal measurements are all taken at the same location within the anechoic chamber, the effect of the multipath is consistent throughout all results. Therefore, the normalizing procedure eliminates the effect of the multipath from the radiation pattern measurements.

The source antenna and AUT are located at opposite corners within the chamber, thus providing a maximum 1.85 m antenna separation. This distance is greater than the minimum required separation for far field operation when operating in the cellular radio frequency bandwidth. (See Equation 3.2.) The AUT is placed on a rotatable table which is rotated by a geared motor controlled by a computer interface. The computer interface program sets the rotation angle and step size, then initiates each incremental segment rotation and records the signal as measured by the calibrated network analyzer. The network analyzer incorporates the signal source and the calibrated receiving system in one instrument.

A verification test was performed on the anechoic chamber to ensure that the measurement system provides valid results with acceptable accuracy for its purpose. A loop antenna with a known radiation pattern was used as the AUT. The measured and theoretical results of the vertically polarized horizontal radiation pattern were very similar. (See Figure 3.4.). Thus the output from this measurement set-up is concluded to be a very good indicator of the actual free space radiation patterns of the AUT.

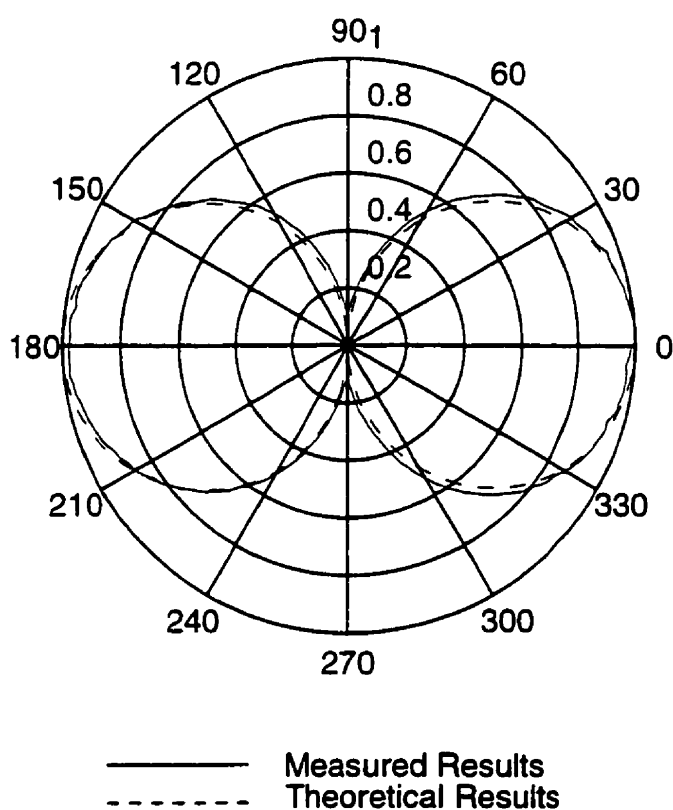


Figure 3.4 Verification Results for Anechoic Chamber

There are many sources of error in an anechoic chamber. The size and shape of the chamber and the RF absorbing material are all specifically chosen to obtain approximate free space measurements in the frequency bandwidth of interest. But not all the reflected signals or multipaths are completely eliminated

in the zone surrounding the AUT, therefore the reflected signals add to the direct wave and disrupt the free space condition.

The proximity of the inner chamber surfaces to the test antennas and the proximity of the source to the AUT create coupling losses in the system due to mutual coupling of these objects. There are also polarization and impedance mismatches between the AUT and the test equipment which cause accuracy errors. These errors can be minimized and the accuracy of the anechoic chamber can be improved by making complex reflection and polarization measurements to calibrate the test chamber.

3.1.2.1 S21 Measurements With Probe

The vertically polarized vertical radiation pattern cannot be measured using the anechoic chamber but an indirect measure of the radiation pattern can be obtained through the S21 measurements obtained with a simple dipole probe tool and network analyzer. Assuming a two-port device model with a properly terminated load, the S21 parameter is the measure of the output wave, b_2 , compared to the incident wave, a_1 . (See Equation 3.3 and Figure 3.5.)

$$S_{21} = \frac{b_2}{a_1} \Big|_{\text{port 2 properly terminated}} \quad (3.3)$$

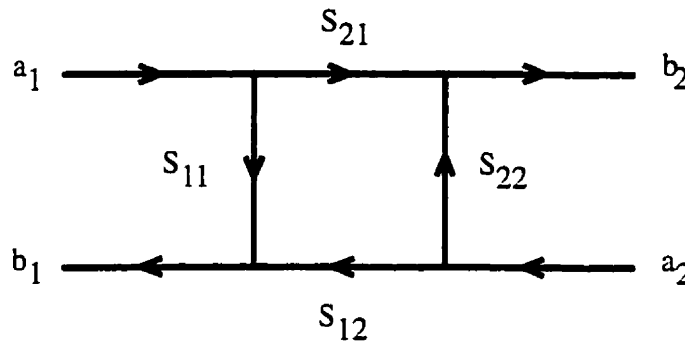


Figure 3.5 S parameters

The dipole probe tool is simply a short dipole antenna connected to the port #2 of the network analyzer through a split coaxial balun. A balun is used to suppress current flowing on the outer conductor of the unbalanced coaxial line and to maintain the balanced property of the dipole [10]. Using the network analyzer and the dipole probe tool, both the magnitude and the phase of the S_{21} measurements can be evaluated at each radiating element. The S_{21} measurements of slots two through four are normalized using the measurements of slot one. The normalized S_{21} measurements can be compared and the approximate vertical radiation pattern can be deduced.

3.1.3 Impedance

The measured input impedance of all antenna systems consists of self and mutual impedance components. The self impedance normally involves a resistance, which results in power being absorbed by the antenna due to radiation and loss resistance; and a reactance, which accounts for all energy stored in the near field antenna zone. Due to the dynamic nature of the environment surrounding antennas, changes in the mutual impedance components cause a time-varying overall input impedance.

The desired input impedance of most systems, while using appropriate transmission lines, is a conjugate match of the source impedance. This procedure provides optimum power transfer from source to load; in an RF system the standard impedance is 50Ω . To provide a good match over the desired bandwidth, both the self and mutual impedances must be relatively stable.

A strict free space environment eliminates the mutual impedance component and, hence, only the antenna's self impedance component remains. The approximate free space measurements can be acquired by measuring the impedance of an antenna in an anechoic chamber. The impedance measurements are easily measured by using a Hewlett Packard HP-8510C network analyzer. To accurately measure the input impedance, the network analyzer must be calibrated over the desired bandwidth, using standard test loads and the appropriate coaxial test cables. A one-port calibration technique is used for antenna measurements; antenna systems are normally considered two-port devices but the second port is already appropriately terminated by its radiation resistance. The impedance values are easily interpreted from a Smith chart. The Smith chart is composed of constant resistance, reactance, conductance and susceptance circles from which the impedance or admittance of a load is denoted.

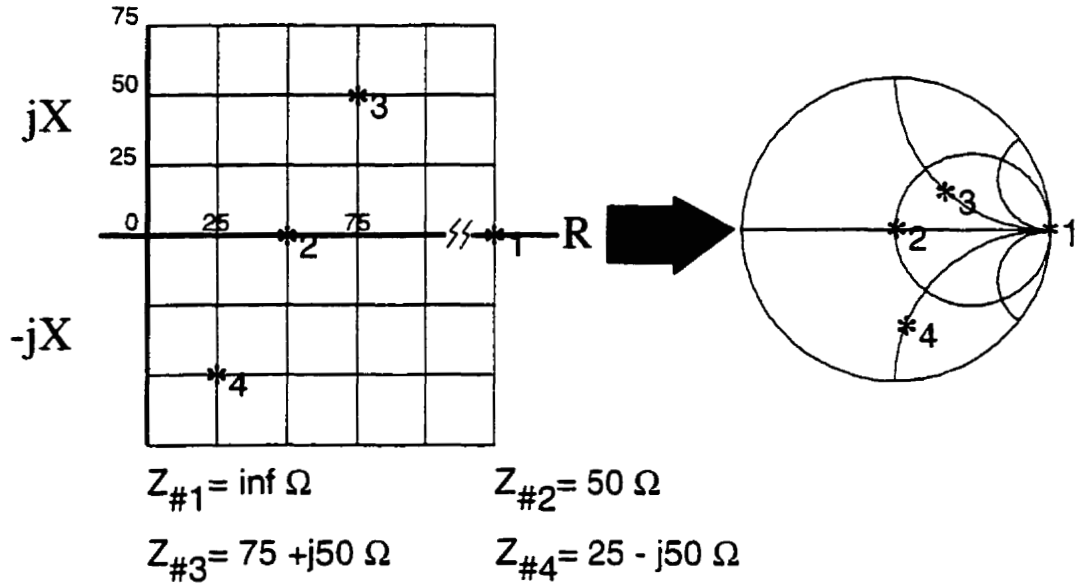


Figure 3.6 XY Graph to Smith Chart Translation [11]

As the environment surrounding the antenna changes, the input impedance must be relatively constant within the desired bandwidth, indicating a well isolated antenna. To demonstrate the antenna's sensitivity to the environmental changes, the impedance results can be noted while an object is moved about in close proximity to the AUT.

3.1.3.1 S11 Parameter

A parameter which is closely related to input impedance is the S11 parameter. The S11 parameter can be translated into an input impedance using Equation 3.4 [6].

$$Z_{in}(l) = Z_0 \left(\frac{1 + S_{11}(l)}{1 - S_{11}(l)} \right) \quad (3.4)$$

Where $Z_{in}(l)$ is the input impedance at distance l from the load. Assuming a two-port device model with a properly terminated load, the S11 parameter [6] is a measure of the reflected wave, V_{TW2} or b_1 , compared to the forward wave, V_{TW1} or a_1 . (See Equation 3.5 and Figure 3.4)

$$S_{11} = \left. \frac{b_1}{a_1} \right|_{\text{port 2 properly terminated}} \quad (3.5)$$

The S11 values are very easily measured using the same set up as required for the input impedance measurement. The complex S11 values are most easily interpreted from a Smith chart, although the return loss, which is the magnitude of the complex S11 values, may be effectively displayed on an XY graph. On the Smith chart, the Cartesian coordinates are the real and imaginary parts of the normalized impedance coefficients, while the polar coordinates are the magnitude and phase angle of the reflection coefficients [12]. Referring to reflection parameters, the point in the center of the Smith chart indicates that there is no reflection and all power is absorbed by the AUT; a point on the outer circle of the Smith chart indicates that all power is reflected back from the AUT and that power is not absorbed. All points within these two extreme coordinates indicate a combination of the power reflected and absorbed by the AUT.

3.1.4 Polarization

Polarization describes the direction of variation of a specific field in the TEM wave as it travels through space. Generally, the polarization of an antenna is categorized into one of three groups: linear, circular and elliptical. Although

linear and circular instances are actually only special cases of an elliptical state. The AMPS and Interim Standards dictate a linear, vertically polarized, electric field for all cellular transceivers, as presented in Figure 3.7 [13].

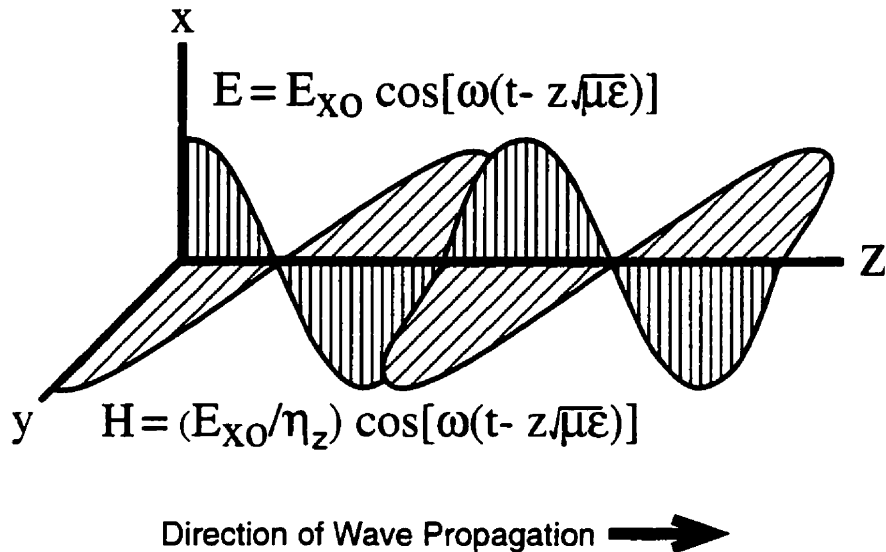


Figure 3.7 TEM Wave in Free Space

The ground plane flooring produces a strong reflected signal within the chamber; the ground plane reflects different polarizations with dissimilar outcomes [14]. While anticipating that, at least, one strong ground reflection will add to the desired direct wave, this reflected signal must be controlled so as not to cancel the direct signal by arriving out of phase with the direct signal at the location of the AUT. On an ideal ground plane, a vertically polarized reflected field is in-phase with its incident field, while a horizontally polarized reflected field is out of phase with its incident field. The path length of the reflected field must be accordingly adjusted to arrive approximately in-phase with the direct wave. Therefore, for a vertical polarization, the length of the path for the reflected field must not be an odd multiple of $\lambda/2$ longer than the direct path

length; for a horizontal polarization, the path for the reflected signal must be close to an odd multiple of $\lambda/2$ longer than the direct path length. The height of the test antennas with respect to the ground plane and their separation distance determine the effective path lengths.

The polarization of the AUT can be evaluated in the anechoic chamber measurement set-up, by acquiring and comparing a number of radiation pattern measurements using source antennas with different polarizations. In the anechoic measurement test system, both the vertical and horizontal polarizations of the horizontal radiation pattern can be measured, although only the vertically polarization horizontal radiation pattern is evaluated. A horizontally polarized source antenna could be used for measuring the horizontally polarized, horizontal radiation pattern; a vertically polarized source antenna is used to measure the vertically polarized, horizontal radiation pattern.

To adjust for the dissimilar reflections of the vertical and horizontal polarizations, the vertically polarized measurements are made with a vertically polarized source antenna, positioned very near the ground plane elevated to approximately 0.05 m. The horizontally polarized measurements are made with a horizontally polarized source antenna elevated 0.32 m from the ground plane. (See Figure 3.8.) Due to the physical space limitations of the anechoic chamber, the polarization measurements cannot be fully evaluated, but the prototype cylindrical slot antenna is assumed to be mostly vertically polarized because of the type of radiation elements used.

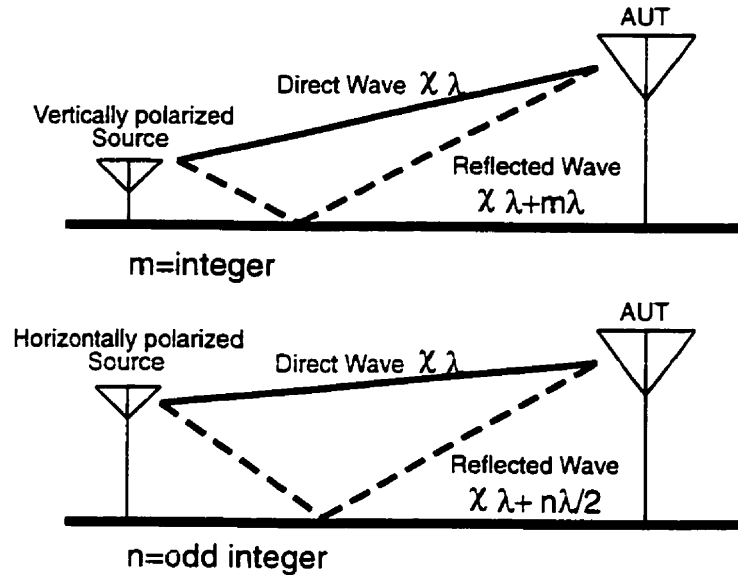


Figure 3.8 Required Path Lengths in Anechoic Chamber

3.1.5 Gain

Gain is a measure of an antenna's ability to radiate power compared to its source input power. Gain, $G(\theta, \phi)$ [15], is defined as 4π times the radiation intensity, $U(\theta, \phi)$, compared to the total input power, P_{in} .

$$G(\theta, \phi) = \frac{4\pi U(\theta, \phi)}{P_{in}} \quad (3.6)$$

Gain is closely related to the efficiency parameter, η , except gain takes into account the directivity, $D(\theta, \phi)$, of the antenna [15] [16]. Directivity is defined as the power intensity of the antenna compared to the power intensity of a specific reference antenna, i.e. a lossless isotropic radiator. An isotropic radiator is an ideal element which radiates power equally in all directions.

$$G(\theta, \phi) = \eta D(\theta, \phi)$$

Often a more significant parameter to RF engineers is maximum gain, G , which is simply the maximum value from the spatial gain results, $G(\theta, \phi)$.

To determine the gain of the AUT in an anechoic test set-up, the measured power results must be translated into gain measurements. The Friis Transmission equation is used for this translation. (See Equation. 3.8 [17].).

$$G = \left(\frac{4\pi R}{\lambda} \right)^2 \frac{P_r}{P_t} \quad (3.8)$$

There are two prevailing types of gain measurement methods, absolute gain and gain transfer. Absolute gain measurements require no prior knowledge of the antennas used in the test. In this method, there are two similar measurement schemes; one involves two like antennas while the other involves three unlike antennas. In both these schemes, the Friis formula is the basis to the evaluation of the gain results. Gain transfer measurements are made using a standard reference antenna. In order to determine the test antenna's overall gain, results of the power measurements for the reference antenna are compared to the results of the power measurements for the AUT. The gain parameter of the prototype cylindrical slot antenna has not been determined due to time restraints.

3.2 Diversity Scheme

To improve system performance in the multipath fading environment, a passive combining device is used in conjunction with two cellular base station antennas to achieve a diversity improvement through a unique pattern diversity scheme. (See section 4.2.1.) Although system performance is expected to improve, the diversity scheme and its system performance are not the only ambitions of this thesis. Another important thrust behind this project is the design and development of a test system to compare the relative diversity improvement of the pattern diversity scheme to a space diversity scheme.

The objective of the test system is to measure the power in the envelope of the received space and pattern diversity branch signals, in order to determine the cumulative distributions and compare the relative diversity improvements. The desired result from the test system is to demonstrate, by examining the cumulative distribution graphs, that the pattern and space diversity signals are less correlated overall than the two space diversity signals. The less correlated branch signals can be effectively combined to reduce fade depths and duration and, therefore, minimize the effect of a multipath environment.

The test system has been broken down into three sections: the transmitter, the receiver and the data retrieval section. In the transmitter section, an unmodulated tone is transmitted from a mobile platform. In the receiver section, four fading signals are received using diversity techniques. In the data retrieval section, the magnitude of each of the four received fading signals is sampled, measured and stored on a computer output file. After sufficient samples are obtained, the data is then converted into probability density graphs

and cumulative distribution graphs for final system analysis in the results section in Chapter Five.

3.2.1 Transmitter Section

The objective of the transmitter section is to transmit a 910 MHz unmodulated, one watt tone from a mobile platform. (See Figure 3.13.) Due to the reflectors and scatterers in the vicinity of the base and mobile stations, the transmitted signal arrives at the receiver by more than one path. The received signal components combine and produce a distorted version of the transmitted signal. Each path signal involves a time varying attenuation, $a_i(t)$, phase, $\Phi_i(t)$, and delay time, $\tau_i(t)$. The resultant channel characteristic is the vector sum of all these incoming time varying signals. The random and time-varying cellular channel can be modeled by a linear time-varying filter. The low pass impulse response of the channel is given in Equation. 3.9 [17].

$$h(t, \tau) = \sum_i a_i(t) e^{-j\phi_i(t)} \delta(t - \tau_i(t)) \quad (3.9)$$

While neglecting additive noise, the low pass received signal, $r(t)$, is the result of the convolution, with respect to τ , of the low pass input signal, $u(t)$, and the low pass channel characteristics, $h(t, \tau)$. (See Equation 3.10 and figure 3.9. [18])

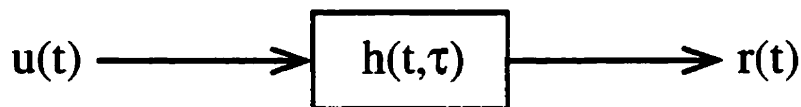


Figure 3.9 Channel

$$r(t) = \sum_i a_i(t) e^{-j\phi_i(t)} u(t - \tau_i(t)) \quad (3.10)$$

The AMPS cellular bandwidth is considered to be a narrowband signal because of the narrow channel bandwidth relative to the coherence bandwidth. Therefore, the channel characteristics are considered approximately constant over the entire bandwidth, but still time dependent. (See Equations 3.11 and 3.12 [18].)

$$r(t) = h(t, 0) u(t) \quad (3.11)$$

$$r(t) = u(t) \sum_i a_i(t) e^{-j\phi_i(t)} \quad (3.12)$$

The transmitted signal in this test is an unmodulated tone. Therefore, neglecting the Doppler effects, the received signal describes the channel characteristics. (See Equation 3.13 [18].)

$$r(t) = A \sum_i a_i(t) e^{-j\phi_i(t)} \quad (3.13)$$

The probability distribution of the random process, $r(t)$, may be described by different distribution functions depending on the environment. Due to specific parameters in this test, such as the antenna locations and the mobile transmitter path, the characteristics of the output signals compare closely to the Rayleigh probability distribution function. The Rayleigh assumption is then used in all calculations required to convert the output data from the data retrieval section to the necessary graphs in the final analysis.

The entire transmitter section is transported in a vehicle which travels around a fixed path about the University of Calgary campus. (See Figure 3.10.)



Figure 3.10 Map of Path Traveled

The vehicle travels around the fixed path at approximately 10 km/hr for approximately 20 minutes for each antenna separation. (See Section 3.2.2.) Due to the sampling rate, vehicular speed and test duration, approximately 20,000 samples are measured and recorded. According to Reference 18, a set of 20,000 samples provides a sufficient number of samples to accurately determine the statistical probability and cumulative distribution graphs from the four diversity signals.

The vehicle must travel at a reasonably constant speed to ensure the validity of the correlation results. If the vehicle travels faster than 10 km/hr, then the distance travelled between sequential switches (switching period, 0.5 ms) would increase and the correlation of the transmitted signal within each switching sequence (switch cycle, 2 ms) would be reduced. Consequently, the output of each switch during an active switch period could not be assumed to occur all at the same time with negligible error. (See Section 3.2.3.) If the vehicle travels slower than 10 km/hr, then the independence between the sequential sampling (sampling period, 60 ms) of the same switch feed would be

reduced. Consequently, adjacent samples would contain correlated information which would be measured and, thus, redundant information would be recorded and more samples would need to be obtained for statistically independent data.

The 910 MHz signal originates from a Marconi 2022 signal generator operating at -4 dBm. The output of the signal generator feeds the input port of a Minicircuits ZHL-42 high power amplifier through a short Belden RG-174U 50 Ω cable. The ZHL-42 is a broadband linear power amplifier with a 32 dB gain producing approximately 28 dBm of output signal. This value is limited by the 1 dB compression point of the ZHL-42 amplifier. The output of the ZHL-42 amplifier feeds the antenna through a short Belden RG 58A 50 Ω cable. The radiating element is a disccone antenna, it acts like a simple monopole antenna with similar radiation characteristics, but with an extended bandwidth because of its conical shape. The antenna is vertically polarized and has an approximate gain of 2.15 dB. The antenna is supported by a 1" plastic tubing which extends out of the vehicle window. (See Figures 3.11 and 3.12)

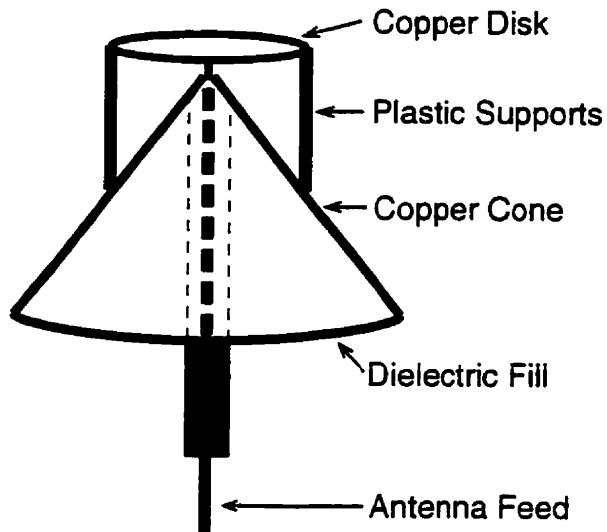


Figure 3.11 Discone Antenna

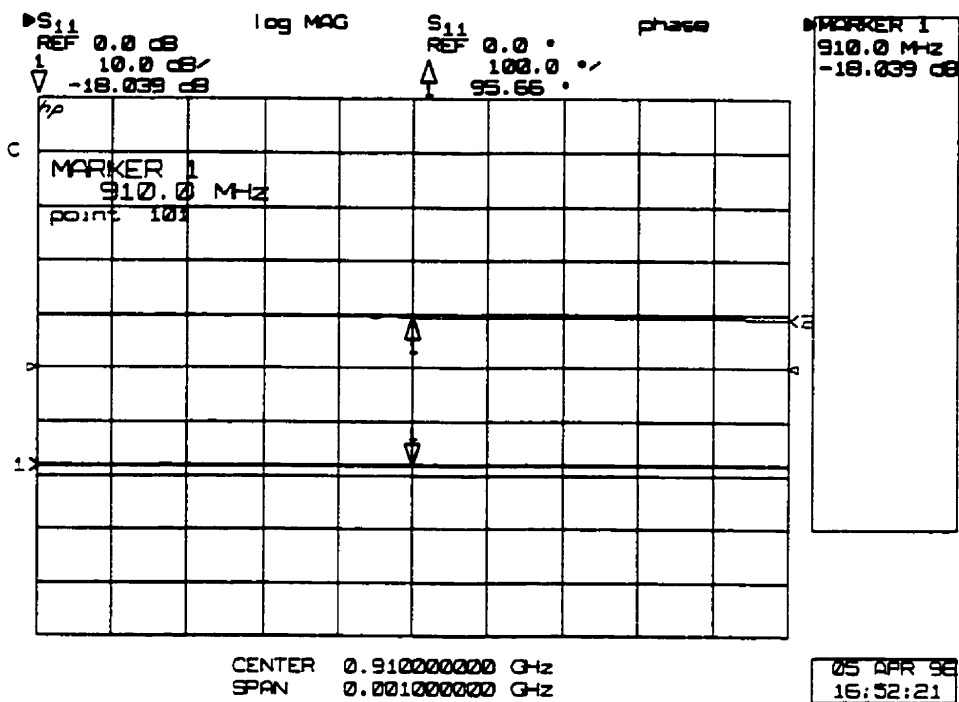


Figure 3.12 S11 of Discone Antenna

An XT 30-2 Xantrex DC power supply is required to provide the necessary +15 V DC bias voltage for the ZHL-42 amplifier. The power supply and the signal generator require a 110 V, 60 Hz supply voltage. These sources are supplied from a Tripp-Lite 200 power inverter connected to a 12 V heavy duty battery.

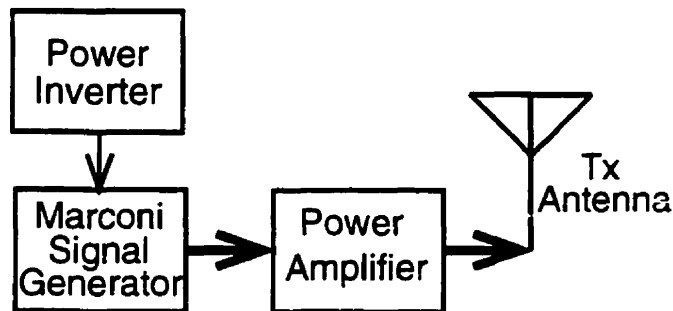


Figure 3.13 Transmitter Section Block Diagram

3.2.2 Receiver Section

The objective of this section is to receive two space diversity antenna signals from the transmitted 910 MHz tone and then create two pattern diversity signals. This section develops the four antenna diversity signals which are to be compared. (See Figure 3.17.)

Two cellular base station antennas, antenna model - Kathrein K73-30-6, are used in the space diversity scheme. These antennas are mounted on the south-side on the roof of Discovery Place, approximately 10 m from ground level. Discovery place is located at 3553-31 Street N.W. in Calgary, Alberta - approximately one block north of the Mechanical Engineering building on the University of Calgary campus. The base station antennas are directed southwards towards the northern section of the campus.

Diversity improvement from space diversity signals depends on the degree of correlation of the received signals. The degree of signal correlation depends on the antenna separation. Two different antenna separations, 5λ and 40λ (1.65 m and 13.19 m @ 910 MHz), are used to evaluate the proposed pattern diversity scheme. The different separation distances result in different correlations between the diversity channels. The theoretical correlation values for these separations and orientations can be interpolated from data given in Reference 16.

The RF signal output from each base station antenna is filtered by a cavity resonator filter [19]. These narrowband pass filters are required to reduce the extraneous signals within the band of operation and to protect against saturating the next stage of this section - the power amplifiers. The total input power to each power amplifier is determined by the summation of the power in each frequency component within the operational spectrum. This total input power must be limited to the maximum input power specifications in order to avoid destroying the amplifiers.

The power amplifier stage is composed of two RF amplifier components. The first component is a Minicircuits ZEL-0812 low noise amplifier and the second component is a Minicircuits ZHL-1000H broad band amplifier. These two RF amplifiers produce a combined gain of, approximately, 61 dB on each signal branch. To reduce the possibility of oscillations due to the cascading of the low noise and the broad band amplifiers, an isolator is inserted between the two components. This isolator reduces the reflections, due to the slight impedance mismatches, from the input of the second amplifier back to the output of the first amplifier. Without an isolator, the cascaded amplifiers can produce oscillations up to 1V p-p in the frequency band of interest [20]. The DC

supply for the RF amplifiers is provided by two 15 V battery packs consisting of ten D cell batteries each. This configuration is used instead of a variable power supply because of the instability of the outputs of the readily available power supplies and, also, to eliminate potential ground loop problems within the system. This amplification section is required to reduce the potentially high noise figure (see Section 3.2.4) of the system and counter the large attenuation of the next stage of this section - the coaxial cable.

The RF signals are routed from the output of the power amplifier section, on the roof, to the utility room, on the second floor of Discovery Place, through two 30.5 m RG400U Belden coaxial cables. The measured loss per branch of the 30.5 m coaxial cable at 910 MHz is 21 dB. The phase shift due to the cable and band pass filter in each leg are very similar; the phase difference is less than one degree. (See Figures 3.14, 3.15 and 3.16.)

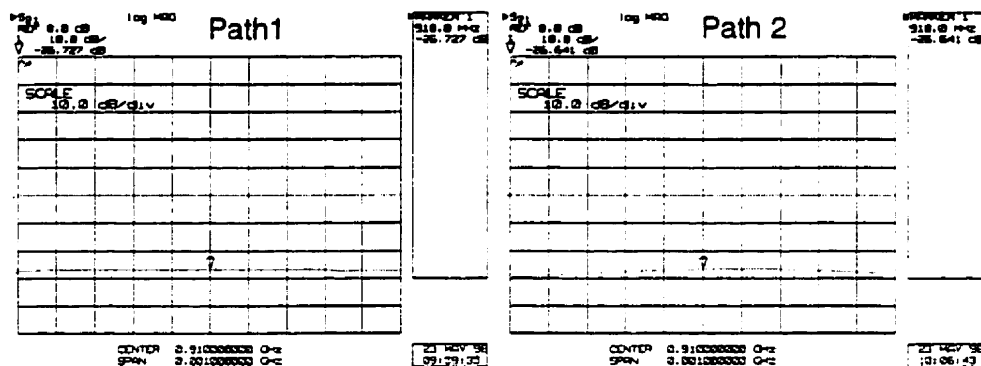


Figure 3.14 . Path Attenuation Profiles

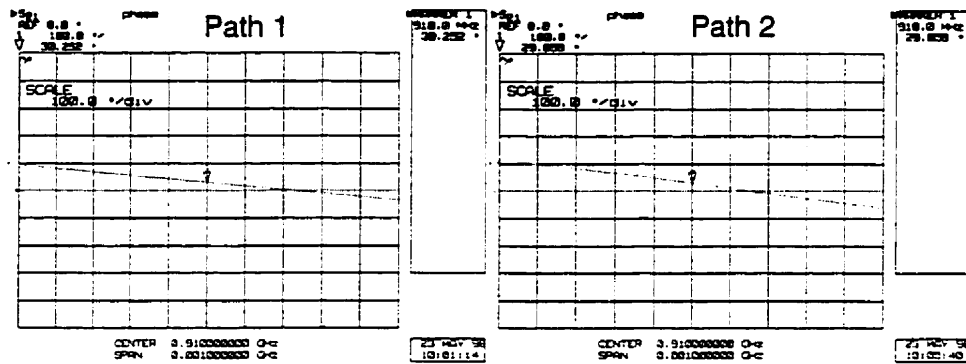


Figure 3.14 Path Phase Profiles

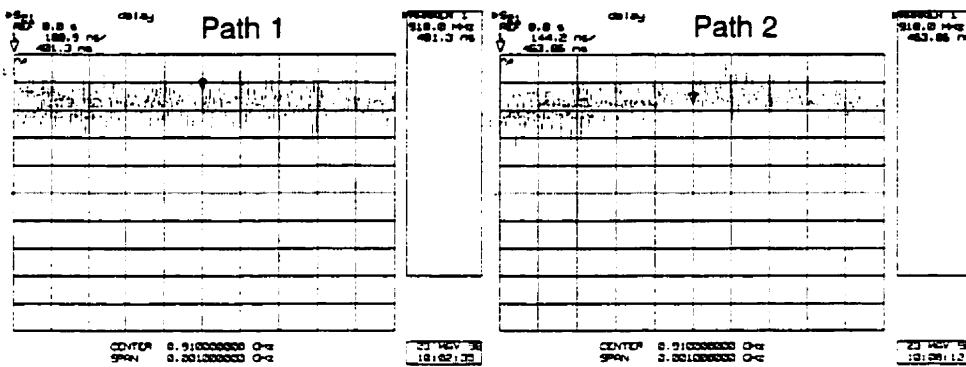


Figure 3.15 Path Delay Profiles

Within the utility room, the respective path signals are split into two more paths using two Minicircuits ZFSC-2-2500 power splitters. One output from each splitter is fed into one of two inputs of the combining device, through 0.085 semi-rigid cable. The length of the cables from the splitter to output of the receive section and the length of the cables from the splitter to the combining device have been tuned to provide precise timing and attenuation through all paths.

At this stage, there are four diversity signals, consisting of two pattern diversity signals and two space diversity signals. The pattern diversity signals

are available from the two output ports of the combining device, while the space diversity signals are available from the other ports of the power splitters.

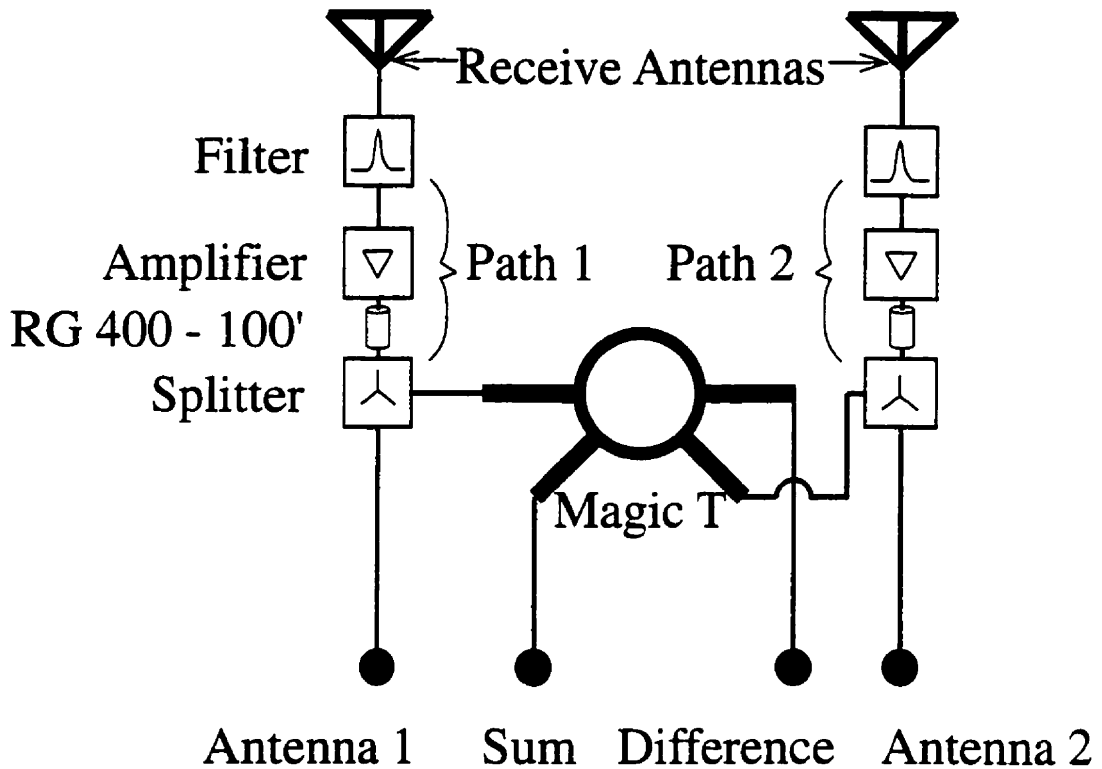


Figure 3.17 Receiver Section Block Diagram

3.2.3 Data Retrieval

The objective of this data retrieval section is to sample and measure the four test signals from the receiver section and to store the resultant values in an output file [20][21]. The ideal situation would be to sample each of the test signals at exactly the same time and continue sampling periodically. Unfortunately, due to equipment restraints, the multipath signals cannot be sampled at exactly the same time but are instead sampled sequentially. The first signal is sampled then the second, third, and fourth signals are respectively

sampled after which there is a delay period before the entire cycle is repeated. This method is not quite ideal but provides reasonable results due to the high correlation of each individual signal over the sampling interval, see Reference 15.

A 4-to-1 switch is used to sequentially route the four output signals from the receiver section into the one branch output signal for the data retrieval section. Each input signal is routed to the output branch for a switching period of 0.5 ms (switching period) during each switching interval of 2 ms (switch interval). The switch cycle is repeated every 60 ms (sampling period or switch cycle).

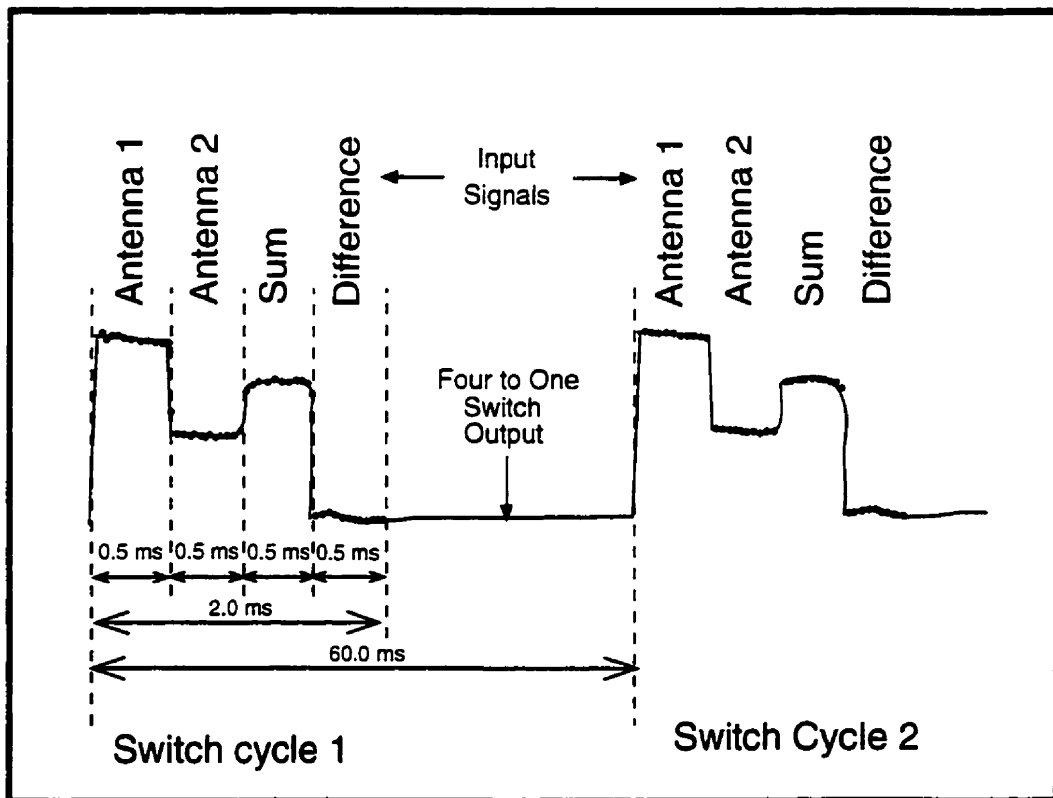


Figure 3.18 Measurement Times

Between the sequential switching of 0.5 ms, the vehicle travels a maximum distance of 1.39 mm from the receiving antennas. In one complete sample cycle, 2 ms, the vehicle travels a maximum of 5.54 mm. The 0.5 ms timing (switching period) between the sequential samples was limited by the settling time of the A/D component of the data retrieval section. The suitable time was experimentally determined by increasing the time block until precise and stable results were obtained from the A/D using known inputs. The period between switching cycles (sample period, 60 ms) is determined by the necessary time required in order to transmit an independent signal through the cellular channel compared to a previous point in time. The formula used, Equation 3.14 [22], is based on a time diversity scheme and applies, accordingly, to this experiment.

$$\tau_s \geq \frac{1}{2 \left(\frac{v}{\lambda} \right)} \quad (3.14)$$

Where τ_s is the time period and v is the velocity of the mobile.

The 4-to-1 switch consists of three 2-to-1 Minicircuits ZFSWA-2-46 switches. Two front end 2-to-1 switches (four inputs) feed one back end 2-to-1 switch (one output) in the 4-to-1 switch configuration. (See Appendix A.) The measured isolation between the input branches of the 4-to-1 switch is approximately 40 dB. The isolation is determined in the overall dynamic range of the system in Figure 3.19. A signal source is applied to one receiver power amplifier while the other branch power amplifier input is loaded with a 50 Ω impedance; the isolation is the difference in the relative output power from the A/D. This isolation was performed on both branches with similar average results.

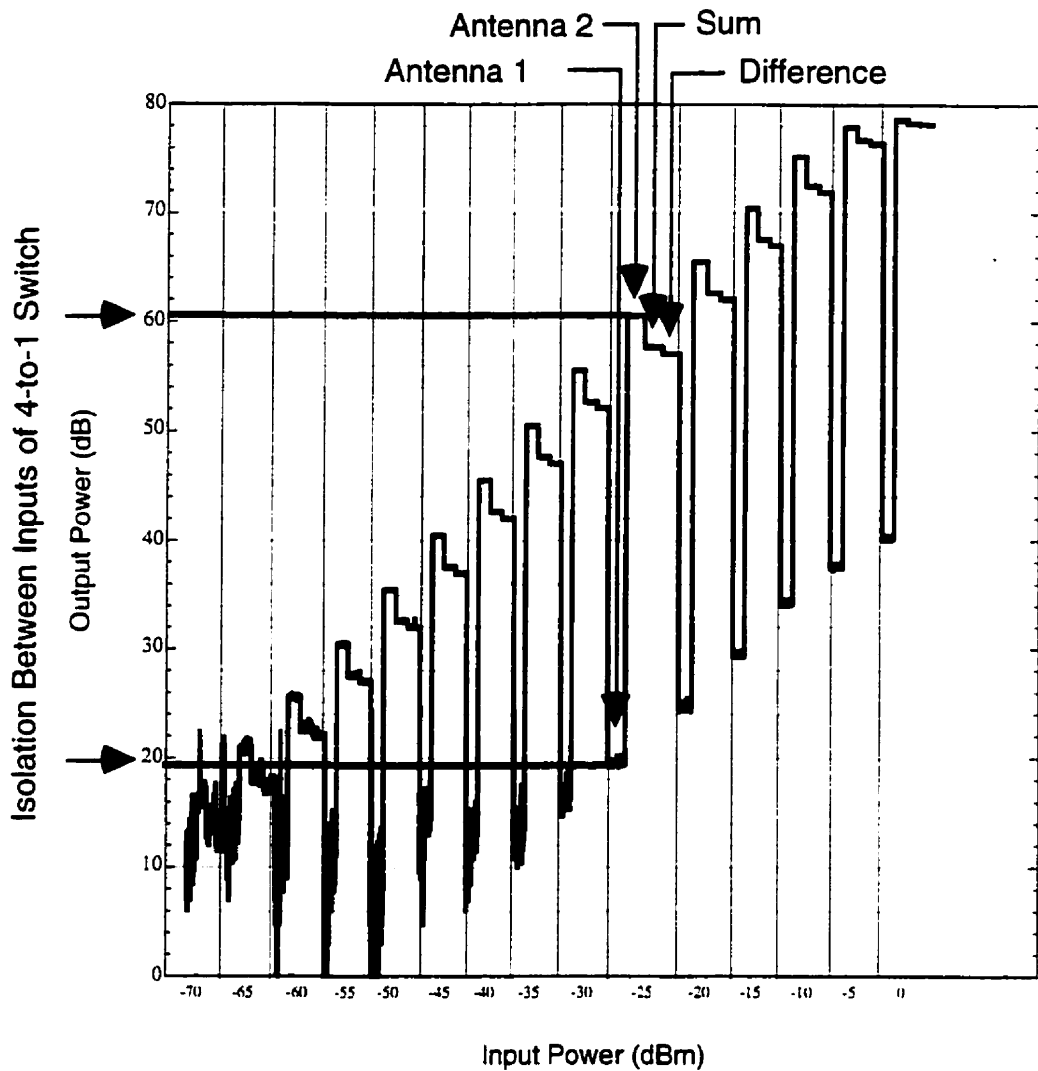


Figure 3.19 Dynamic Range of Receiver and Data Retrieval Sections

In order to provide accurate control timing for the 4-to-1 switch, the TTL voltages from the NB-DIO 32F National Instruments I/O plug in board, in the Macintosh Quadra 900 computer, are used as trigger signals. The NB-DIO 32F is a "high speed, 32 bit parallel digital input output interface for Macintosh

computers" [23]. Unfortunately, the three ZFSWA-2-46 switches require 0V and -8V control voltages and not the 0V and 5V TTL voltages of the I/O board. The TTL control voltages must be converted to the appropriate values necessary for the switches. This conversion is done using two operational amplifiers in a non-inverting configuration while using the supply voltage as the output limit for a -8V to 8V voltage swing. The output signals from the non-inverting configuration are rectified by a diode to produce the necessary 0V and -8V signals. (See Figure 3.20.) The operational amplifiers used have high slew rates in order to maintain the system timing.

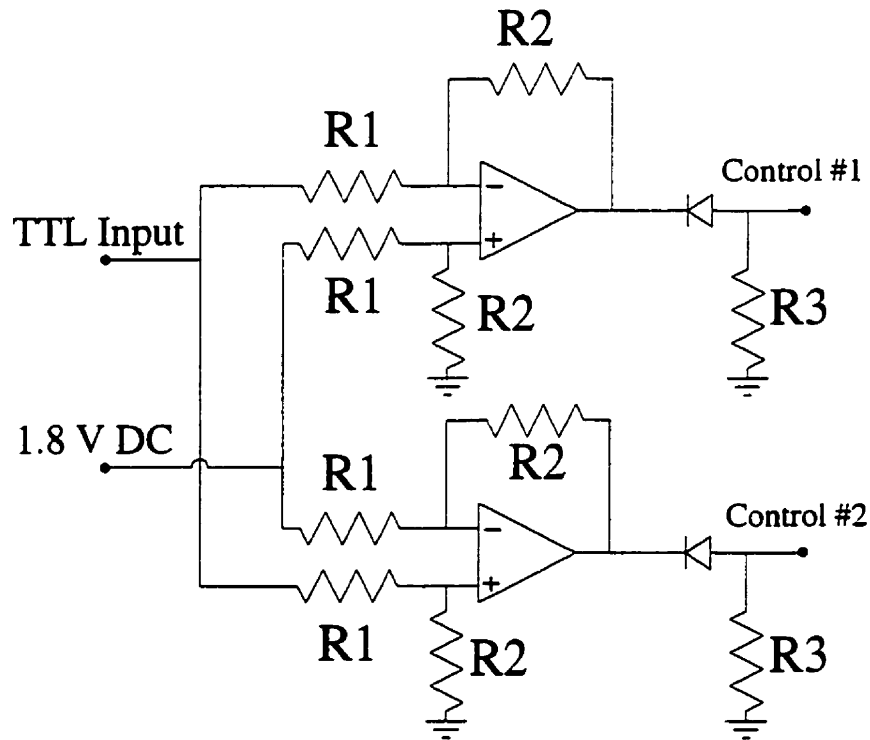


Figure 3.20 Switch Control for 4-to-1 Switch

Using a Minicircuits ZFL-2000B medium power broadband linear amplifier, the output from the 4-to-1 switch block is amplified by, approximately,

20 dB. The output signal from the medium power amplifier is down-converted to a 10 kHz in-phase signal, I, and quadrature signal, Q, using a unique system known as the Impulse Response Identification System (IRIS) [20][24]. The IRIS system is a very powerful transceiver which can be used in many propagation and system evaluations, although in this test the IRIS is simply used as a down-converter. The 910 MHz signal is mixed, in a HP-8981A K-10 Microwave down converter, with a 1110.01 MHz signal from a HP 83650A Synthesized Sweeper. The resultant, 200.01 MHz, signal is amplified by another ZFL 2000B to reduce the effects of conversion loss and is then mixed down further, in a HP 8981A Vector Modulation Analyzer, with a 200 MHz signal from a HP 8656B signal generator. The overall output, originating from the 910 MHz tone, is a 10 kHz I signal and a 10 kHz Q signal.

The output signals are fed to the National Instruments NB-A2100 A/D board within the Quadra 900 Macintosh computer. The NB-A2100 A/D board is "a high accuracy audio frequency A/D and plug in board. Having two 16 bit channels simultaneously sampled analog inputs with 4 times over sampling delta modulation" [25]. The A/D board is AC coupled to the inputs and operates at 48 kHz. Therefore, the sampling rate is well above the two times over sampling Nyquist requirement of the input signal frequency. Both input channels to the A/D are sampled 12 times during each 0.5 ms period. Each sample of channel A, the in-phase signal, is squared and individually added to the squared sample of channel B, the quadrature signal. At the end of 12 samples, 0.5 ms, the sample sums are added and averaged. This average number is then stored in a output file on the Macintosh's hard drive while another sampling cycle continues.

Both the NB-DIO-32F and NB-A2100 plug in boards are programmed in the TMS320C30 assembly language. The overall data retrieval section is controlled by the Labview program developed by National Instruments. The Labview program initializes the appropriate memory locations and initiates the NB-DSP230X Series Interface. The NB-DSP230X Series Interface [26] is a digital signal processing plug-in module which manages the memory, loads executable codes, controls execution and communication between the boards and the Macintosh computer. The Labview [21] and TMS320C30 [21] programs are located in the Appendix B.

All equipment in the data retrieval and receive sections are grounded at the same grounding point, in order to reduce the noise associated with ground loop problems. Ground loop problems occur when grounds throughout a system have different potentials and these potentials feed back into the measurement system which increases the noise floor. A technique called "lifting the grounds" is used to ensure that only one central grounding point exists and, therefore, eliminates ground loops. The signal grounds of all but one instrument are removed or lifted to eliminate the different ground potentials.

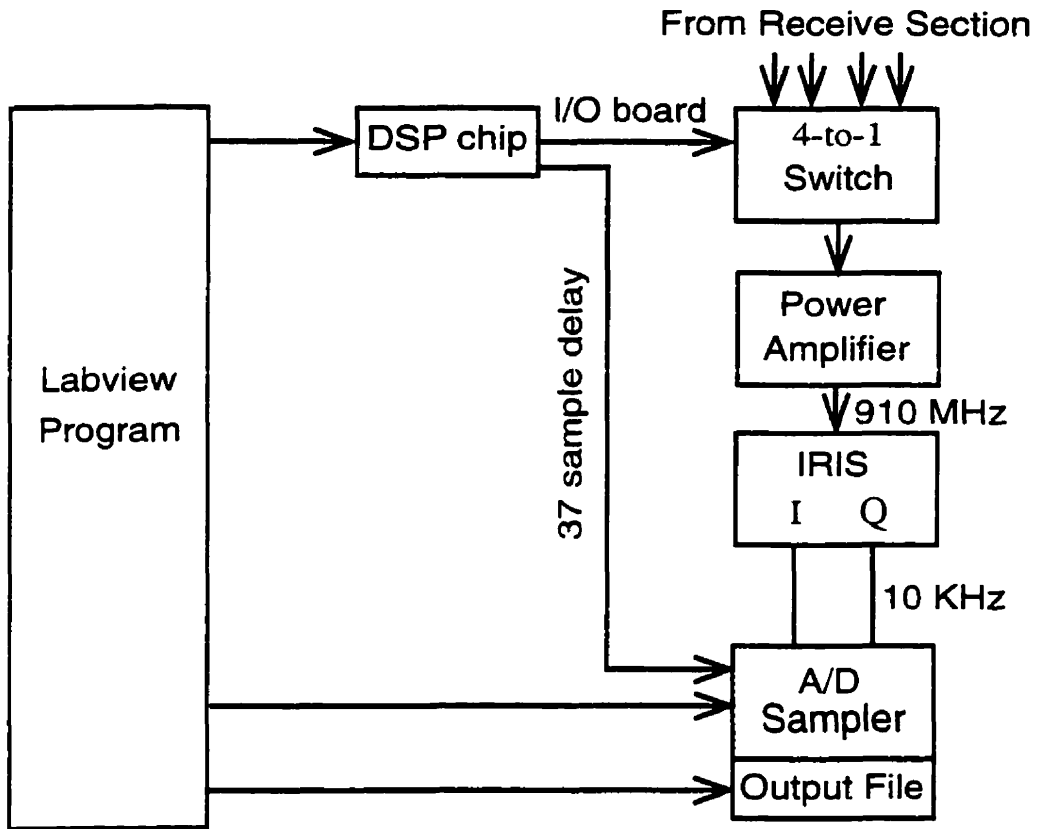


Figure 3.21 Data Retrieval Section Block Diagram

3.2.4 Noise Figure

To reliably detect an RF signal, the minimum received signal power must exceed the maximum noise power of the system by a specific value - the minimum SNR. The available signal power at the antennas of the receive section is determined by the transmit power less the appropriate propagation attenuation, in this case, the attenuation due to plane earth propagation, shadowing and multipath loss.

The dominant source of noise power is caused by thermal noise which occurs in conducting media due to the random motion of charge carriers. The

noise power present at the input to the antennas of the receiver section is determined by Equation. 3.15 [27].

$$NF = K \times T \times BW \quad (3.15)$$

The input SNR is calculated from the available power (dBm) less the noise power (dB). As the input signal travels through the test system, the input SNR is reduced due to the noise factors of each individual piece of equipment. The reduction of the output signal to noise ratio, (S/N), compared to the input signal to noise ratio, (S/N)_{i-1}, is known as the noise figure, F_i. (See Equation 3.16 [28].)

$$\left(\frac{S}{N}\right) = \frac{1}{F_i} \left(\frac{S}{N}\right)_{i-1} \quad (3.16)$$

Using the Friis formula [29], the noise factor of the system can be approximated. (See Equation 3.17 [29].)

$$F_i = F_1 + \frac{F_2 - 1}{G_{a1}} + \dots + \frac{F_{i-1} - 1}{G_{a1}G_{a2} \dots G_{a(i-2)}} \quad (3.17)$$

The individual noise figures, F_i, and gains or losses, G_{ai}, of each block within the system can be determined from the appropriate manufacturer information specifications. The approximate noise figure of the system from filter to IRIS is 4.68 dB. For calculations of the system noise figure, see Appendix C.

All equipment within the system have finite dynamic ranges. The minimum anticipated received power compared to the maximum received power must not exceed the dynamic range of the individual blocks within the

system. The minimum input power to the system is limited at, approximately, -100 dBm, while the maximum input power is limited at, approximately, -40 dBm. The dynamic range of the system is 60 dB. The surrounding environment to the receive antennas and the path through which the mobile platform travels, directly determines the received power. The path selected results in a Rayleigh short term fading signal with signal powers within the limits of the measurement system. The limits of the receive system were determined experimentally using signal generators.

The minimum measured signal levels are indicated in Table 3.1.

Instrument Output	Gain (dB)	Signal Output (dBm)
Tx power amp	+30	+28
Tx antenna	+2	+30
Propagation	-145	-115
Rx antennas	+14	-101
Amplifier	+61	-40
Cable	-21	-61
Splitter + Switch	-11	-72
Amplifier	+20	-52

Table 3.1 Minimum Input Signal to Receiver Antennas

The receive section within this test configuration limits the dynamic range of the input signals. The noise floor at the receiver, including the effects of the system noise figure, is -145 dBm. The noise floor was calculated, using a bandwidth of 10 kHz, in Equation. 3.14. The minimum bandwidth would seem

to be determined by the narrow band pass filters, 40 kHz, but the oversampling and averaging of the A/D sampler reduces the overall bandwidth of the system to approximately 10 kHz.

The maximum measured signal levels are indicated in Table 3.2.

Instrument Output	Gain (dB)	Signal Output dBm)
Tx power	+30	+28
Tx antenna	+2	+30
Propagation	-84	-54
Rx antennas	-14	-40
Amplifiers	+61	+21
Cable	-21	0
Splitter + Switch	-11	-11
Amplifier	+20	+9

Table 3.2 Maximum Input Signal to Receive Antennas

As protection against saturating any instrument in the IRIS system, the input signal at the front end is compressed at, approximately, +10 dBm, hence limiting the maximum input signal.

4.0 Cylindrical Slot Antenna

The objective of this antenna design is to create an antenna with characteristics similar to existing cellular antennas, i.e. radiation pattern and input impedance, but with an emphasis placed on its overall size and cost. The Cylindrical Slot Antenna, has 3 basic components: the supporting structure, the radiating element, and the feeding network.

The supporting structure for this design is a vertical copper cylinder into which horizontal slots are cut. These slots act as the radiating elements of the antenna. The source signal is fed to the slots through a feed network consisting of copper strips mounted on a plexiglass sheet and secured within the copper cylinder. This final antenna design (see Figure 4.1) has been achieved through numerous and different design stages. Through overcoming the problems of the early stages the cylindrical slot antenna was developed.

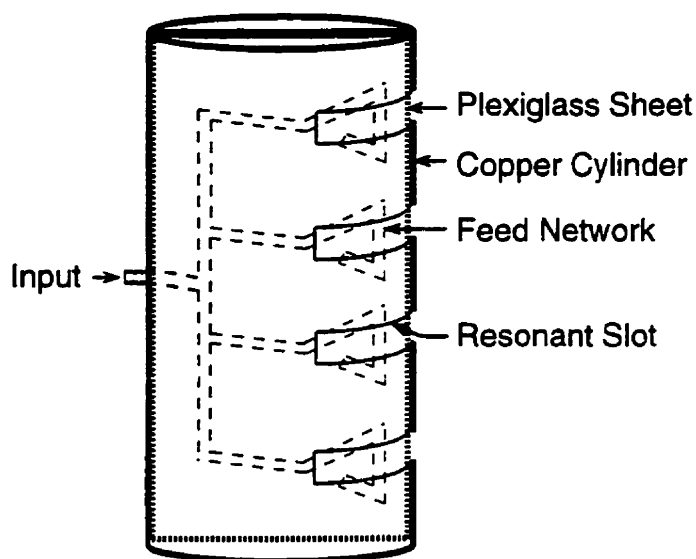


Figure 4.1 Cylindrical Slot Antenna

4.1 Copper Cylinder - Support Structure

A copper cylinder is used as the supporting structure for the antenna. In the prototype antenna, a copper pipe, commonly used in plumbing applications serves as the supporting structure. In a larger scale production of the antenna, a flat copper sheet rolled into a cylinder may be a more appropriate support structure when considering manufacturing costs.

The proposed cylinder is 0.9 m in length, 0.15 m in diameter and has a 0.0016 m wall thickness. A copper cylinder with these dimensions is very sturdy and rigid. A strong structure is necessary for the antenna to bear up against a hostile environment typical for many base station antennas. Cellular base station antennas are commonly the highest elevated structure within the cell (see Section 2.1) and, therefore, the antennas are without shelter from the environment, especially strong winds and storms.

For the radiating elements to operate properly, the supporting structure must also provide a good ground plane. The high conductivity and low resistivity of the copper cylinder provides a common ground potential for all the radiating elements.

A supply of copper pipe having a 0.1 m diameter was available at the University of Calgary. This copper pipe was used in the prototype design despite the reduced diameter. To account for the diameter discrepancy, the operational centre frequency was scaled to 1.275 GHz from 850 MHz. All measurements on the prototype antenna are scaled from the 850 MHz centre frequency to accurately predict the operation of the actual proposed antenna. The other parameters of the prototype supporting structure are consistent with the proposed design.

4.2 Slots - Radiating Element

Horizontal slots are cut into the copper cylinder and act as the radiating elements for the antenna. The overall size, length and width of the slot, determines the radiating element impedance; the slots have been designed to be resonant at the scaled centre frequency. The complete antenna design incorporates four resonant slots in a broadside array.

4.2.1 Individual Slot

The theoretical radiation pattern from a slot cut into an infinitely large ground plane is the dual of the most basic radiating element - the dipole antenna. The term dual refers to the interchange of the electric and magnetic

field equations of the dipole to describe the fields radiating from the slot antenna.

The far field closed form solution is given in Equations 4.1 through 4.8 [1] for a slot of length of 'a' and width of 'b', shown in Figure 4.2.

$$E_{\theta} = C \sin \phi \frac{\sin X}{X} \frac{\sin Y}{Y} \quad (4.1)$$

$$E_{\phi} = C \cos \theta \cos \phi \frac{\sin X}{X} \frac{\sin Y}{Y} \quad (4.2)$$

$$H_{\theta} = \frac{-E_{\phi}}{\eta_z} \quad (4.3)$$

$$H_{\phi} = \frac{E_{\theta}}{\eta_z} \quad (4.4)$$

$$H_r = E_r = 0 \quad (4.5)$$

$$C = \frac{j a b \beta E_0 e^{-j k_1 r}}{2 \pi r} \quad (4.6)$$

$$X = \frac{\beta a}{2} \sin \theta \cos \phi \quad (4.7)$$

$$Y = \frac{\beta b}{2} \sin \theta \sin \phi \quad (4.8)$$

Where θ is the angle created by the z axis to the point of interest about the slot while ϕ is the angle created by the x axis to the point of interest about the slot.

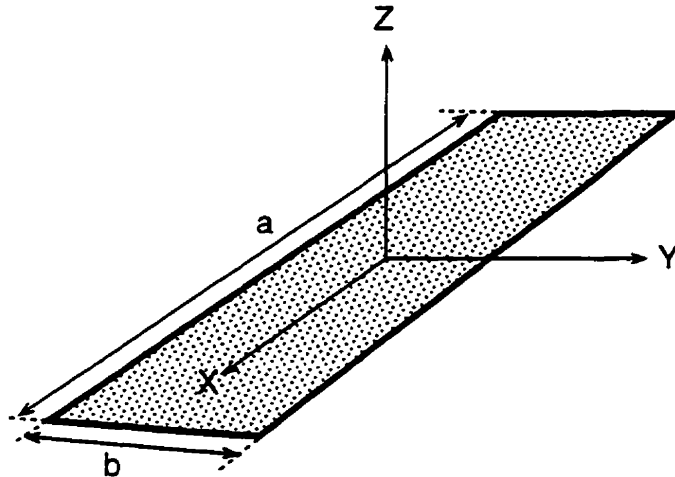


Figure 4.2 Slot Orientation for Equations. 4.1 through 4.8

The radiation pattern and directivity of a thin slot with an $a = \lambda/2$ length, oriented as in Figure 4.2, is the same as the $\lambda/2$ dipole oriented along the y axis except that the polarization is rotated by 90° .

The impedance of a thin dipole can be determined from the graphs in Reference 4.2. The impedance of a $\lambda/2$ dipole can be modelled as a combination of a series inductor, a capacitor and a resistor. The impedance of the slot is also the dual of the impedance of a dipole and can be modelled as a combination of a parallel inductor, a capacitor and a resistor. The impedance of both the dipole and slot is dependent on the element length and width compared to wavelength. The impedance of an approximate thin $\lambda/2$ resonant slot in a large ground plane is given in Equation. 4.9 [3].

$$R_{slot} = \frac{Z_0^2}{4R_d} = 487 \Omega \quad (4.9)$$

Where R_s is the slot resistance and R_d is the dipole resistance.

The input impedance and radiation pattern of a slot cut into a rounded cylinder is not equal to that of a slot cut into a large flat ground plane. As is the case of most radiating structures, a closed form solution for a radiating slot cut into a cylinder is probably not attainable. Therefore, the slot characteristics must be determined through simulation programs and/or lab experiments. An array of slots cut into a flat ground plane (slot planar array) was used in the early antenna design stages to give direction to this project. Due to the limitations of the readily available electromagnetic simulation programs, the antenna design was generally developed through trial and error using basic electromagnetic principles as a guide.

4.2.2 Resonant Slot

The term resonant refers to the impedance of the radiating element. Ideally, the impedance of a resonant element is realized by the resistive component and lacks the reactive component.

The width and length of the slot compared to the operating wavelength determines the slot impedance. It is desirable for the slot to be predominately resistive in order for the source signal to be absorbed by the radiation resistance and not be stored in the near field zone. The first step in designing the prototype antenna was to develop an effective model for the slot in order to determine the required length, with a set width, for resonant operation. The slot is tuned using the Hewlett Packard Microwave and RF Design System (MDS), the network analyzer, the copper pipe, and a special feed network. A small slot with a 1 cm width is cut into the copper pipe and is connected to the special feed network shown in Figure 4.3.

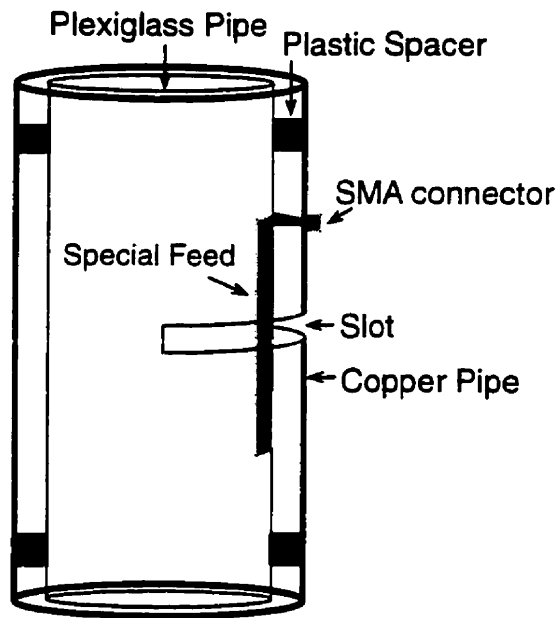


Figure 4.3 Set-up to Measure Resonant Slot (Not to Scale)

The copper strip of the special feed network extends down the inner plexiglass cylinder, approximately 1 cm from the outer copper cylinder, effectively cutting perpendicularly through the centre of the horizontal slot. Using the network analyzer, the one slot antenna is measured and the data is stored. The data is transferred to the MDS program and a model of the slot and the feed network is developed [4]. (See figure 4.4.) The slot length is increased and the procedure is repeated until the MDS model indicates a resonant impedance at the scaled centre frequency. The MDS test program is presented in Appendix F.

The experimentally determined slot length, of a 1 cm wide resonant slot operating at 1.275 GHz, is 12.1 cm.

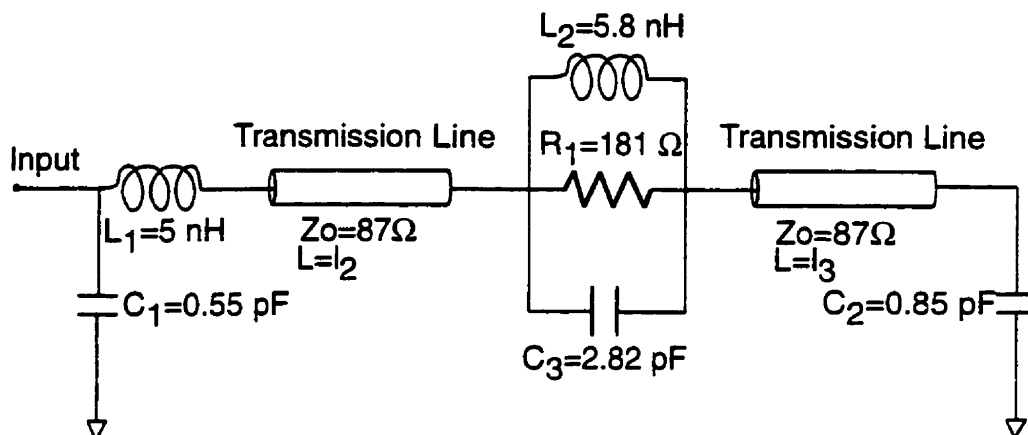


Figure 4.4 Special Feed network and Slot Model

4.2.3 Slot Array

Four resonant slots will be used in an array to obtain the appropriate overall radiation pattern. The four slots are spaced at $\lambda/2$ intervals along the axial component of the cylinder. These slots are all fed in-phase with equal power to produce a broadside array pattern. To give direction to the design procedure, the approximate radiation patterns for the antenna are found using Equations 5.2 through 5.4 [5] which are the basic array equations. In the array equations, horizontal slots were used as the radiating elements thus creating the slot planar array.

The radiation pattern in Figures. 4.5 and 4.6, except for the large back lobes, provide adequate coverage patterns to suit base station requirements. The large back lobes will be reduced in the actual base station antenna design due to the grounded support structure.

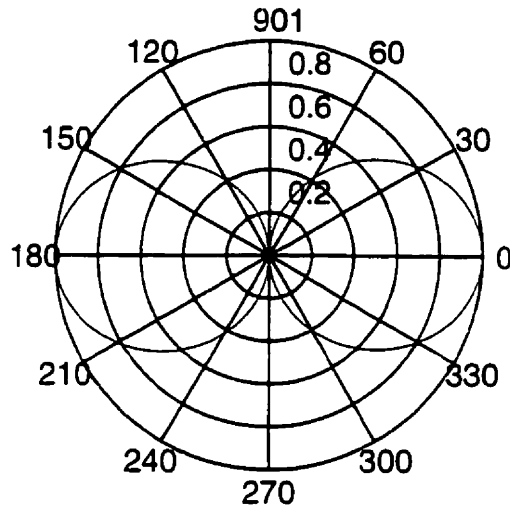


Figure 4.5 Horizontal Radiation Pattern of Planar Array

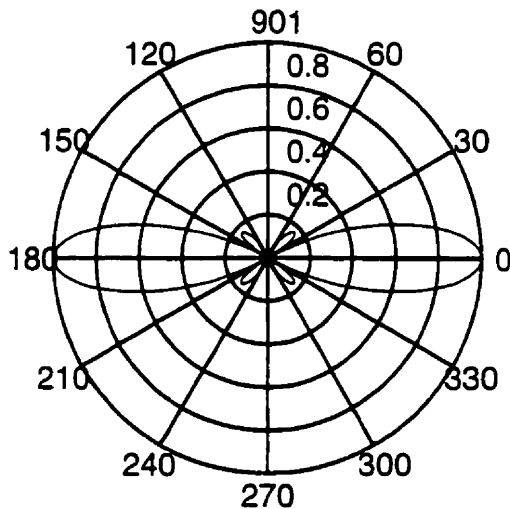


Figure 4.6 Vertical Radiation Pattern of Planar Array

4.3 Feed Network

The feed network is designed to deliver equal, in-phase signal power to each slot and present an overall 50Ω input impedance to the signal source. The final feed network design consists of sections of copper strips secured to a plexiglass sheet and mounted into the copper cylinder. The characteristic

impedance of the copper sections are directly determined by section width and orientation within the cylinder. The length of the copper strips determine the degree of rotation or translation of the load impedance around the Smith chart.

The feed network is not directly attached to the slot in the copper cylinder. The feed network operation is based on the current being diverted around the slot. As the signal travels down the copper feed strip and encounters the open ended load at the end of the strip, an equal and opposite current travels along the copper pipe and is eventually diverted about the slot. This diversion of current develops the appropriate fields and consequentially develops the radiating TEM wave. (See Figure 4.7.)

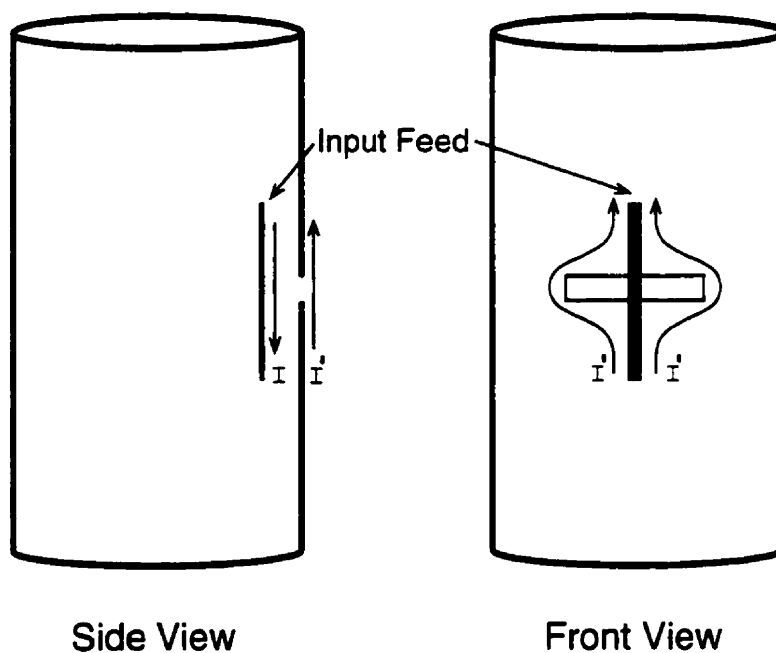


Figure 4.7 Current in Feed and about Slot

The impedance of each slot must be the same and must be equally translated to a common feed point, resulting in an overall 50Ω input impedance. The feed network design was stepped through many different

stages until the final feed network design was produced. Extensive work was applied to a feed network secured on a plexiglass cylinder instead of that on a flat sheet. (See Figure 4.8.) This design operated on the same principles as the final design, indicated in Figure 4.7, but the design theory was simplified due to the constant line separation of the copper cylinder and feed line. This feed network secured in the copper cylinder acted as a simple coaxial transmission line with offset centre conductor.

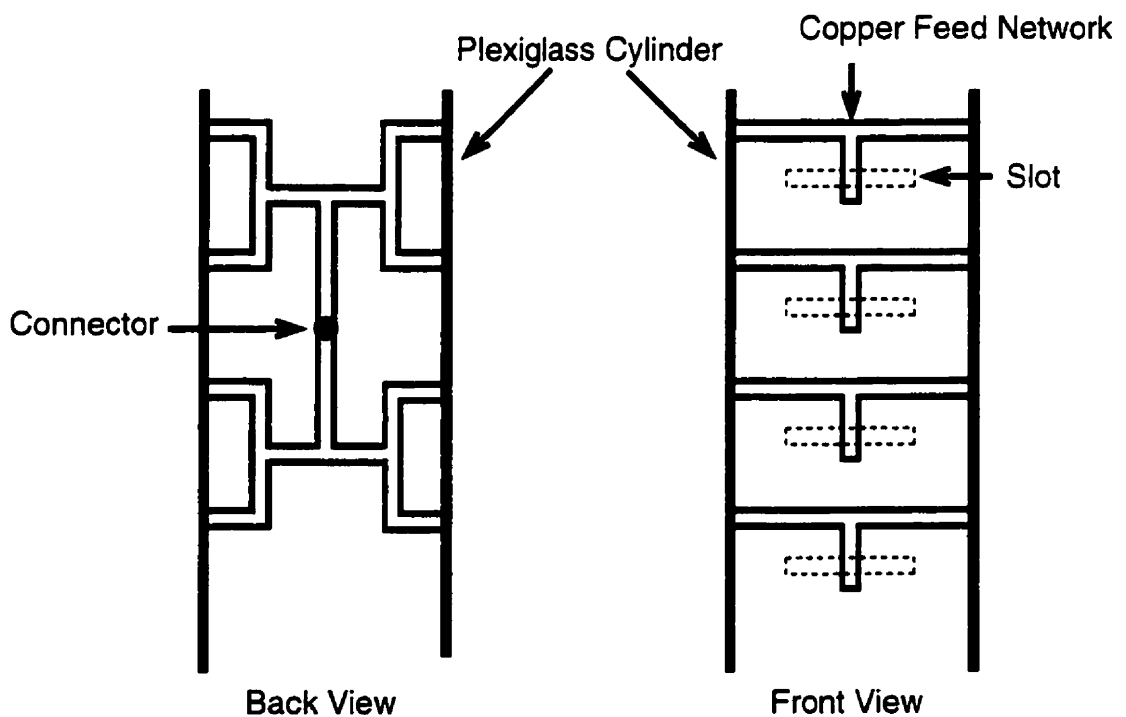


Figure 4.8 Feed network Mounted on Cylinder

Unfortunately, due to the physical feed line layout, the individual components were asymmetrically coupled and thus degraded the performance. The final feed network is a more complex design due to the many orientations of the copper strips within the cylinder.

The impedance of the slot is translated to a main feed line through the basic feed, presented in Figure 4.9. The basic feed component consists of an open ended copper strip with a 0.8 cm width. Each basic feed is individually tuned to obtain optimum performance.

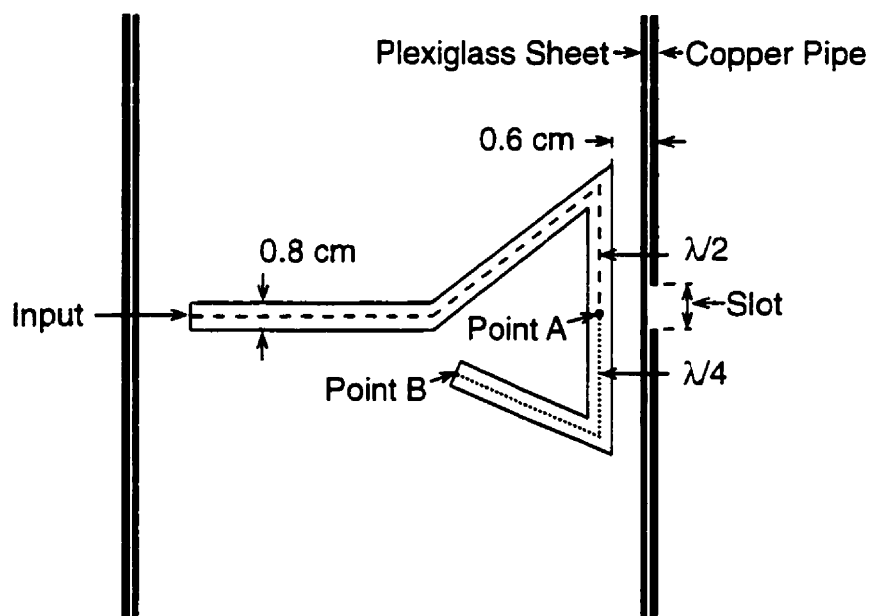


Figure 4.9 Basic Feed Component (Not to Scale)

The vertical section of the feed perpendicularly crosses the center of the slot. For best coupling between feed and slot, the open end of the feed is to be translated to a short located at point A on Figure 4.9. This translation is due to the line length from point A to B. The basic feed line model is presented in Figure 4.10. The two parallel tank circuits provide an opportunity for increased bandwidth, which can be created by a controlled coupling of each individual tank circuit.

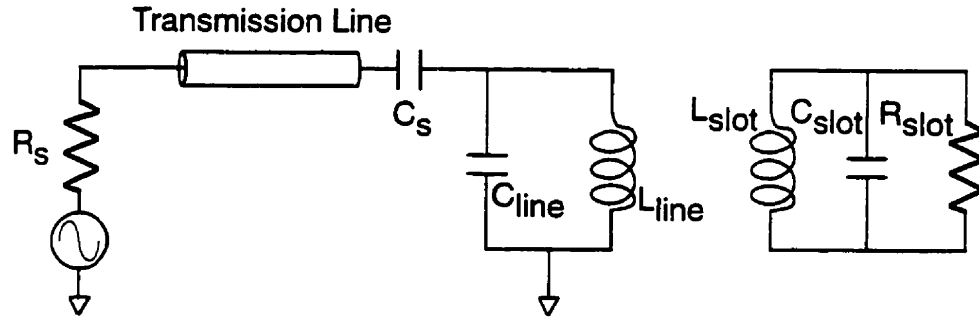


Figure 4.10 Basic Feed Network Model

The overall feed network is presented in Figure 4.11. Using the network analyzer, each slot was tuned for optimum performance. The top two basic feed components, slots three and four, are tuned for similar responses at point A on Figure 4.11 on the Smith chart (Figures 4.12 and 4.13). Similarly, the bottom two feed components, slots one and two, are tuned for similar responses at point B on Figure 4.11 on the Smith chart (Figures 4.14 and 4.15). Similar input impedances, i.e. similar in general shape of response and in general location of centre frequency, at these points are required to ensure that the source signal is divided, equally, between both paths at the point intersection and that correct phases occur at the individual slots.

The combination of slots one and two at point A on Figure 4.11 (Figure 4.16) and the combination of slots three and four at point B on Figure 4.11 (Figure 4.17) is then tuned for similar responses at point C on Figure 4.11 on the Smith chart (Figures 4.18 and 4.19). Similar input impedances at these points are, also, required to ensure that the source signal is divided, equally, between both paths at the point intersection and that correct phases occur at the individual slots.

Each individual basic feed component is tuned by increasing or decreasing the line length and/or the addition of a series capacitance. A series

capacitance is created by simply removing a small section out of the line. The individual, basic feed components are joined and tuned using an increased line width.

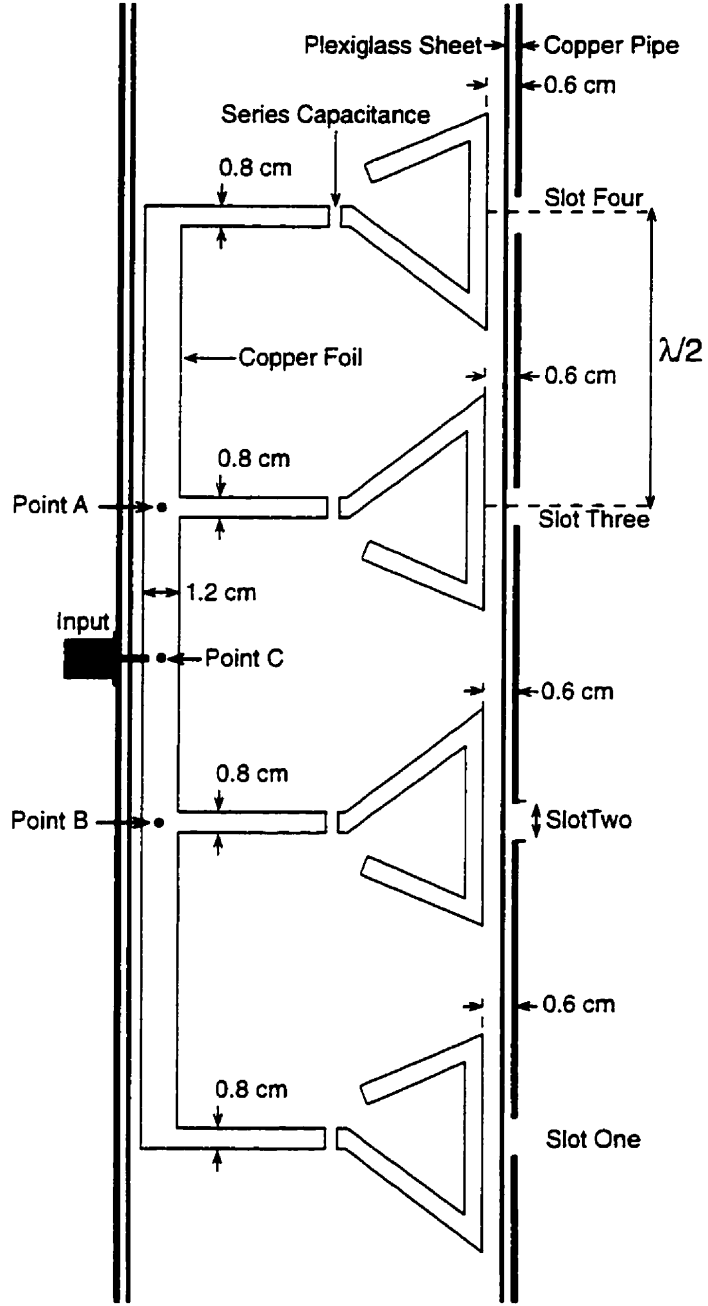
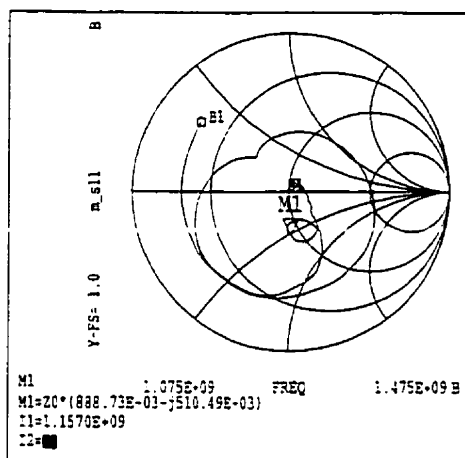
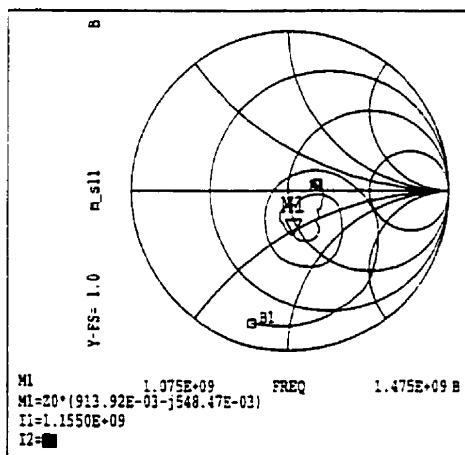


Figure 4.11 Overall Feed Network (Not to Scale)



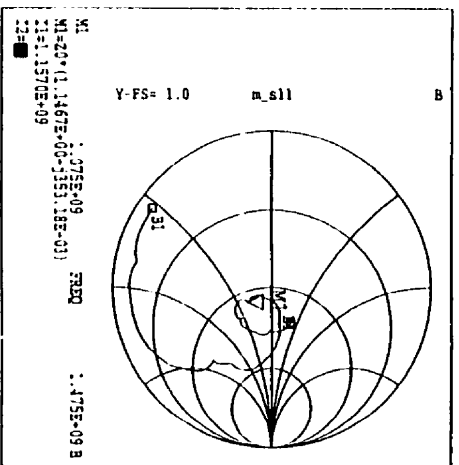
m_s11=slot1a2.DATA.S[1,1]

Figure 4.12 Response at Point A for Slot One



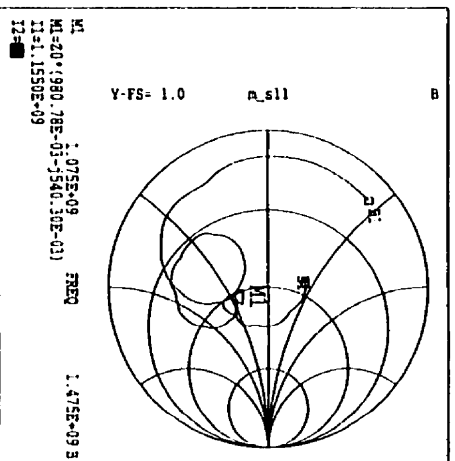
m_s11=slot2.DATA.S[1,1]

Figure 4.13 Response at Point A for Slot Two



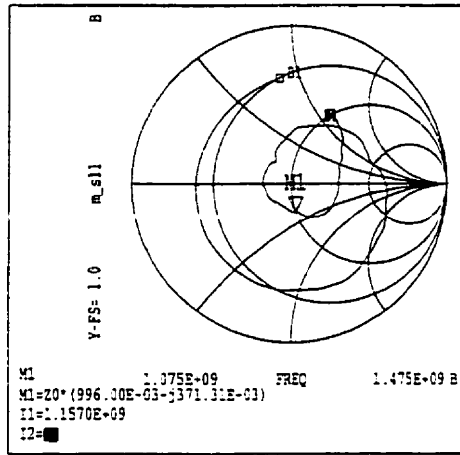
m_s11=slot3.DATA.S[1,1]

Figure 4.14 Response at Point B for Slot Three



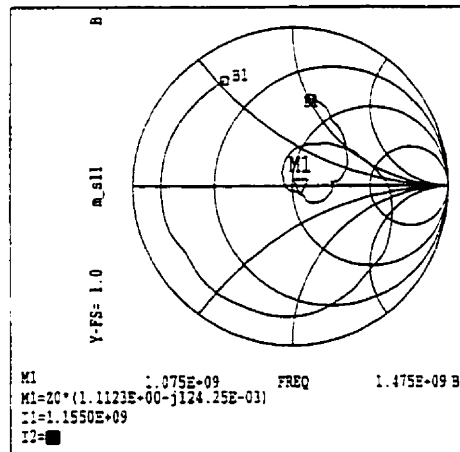
m_s11=slot43.DATA.S[1,1]

Figure 4.15 Response at Point B for Slot Four



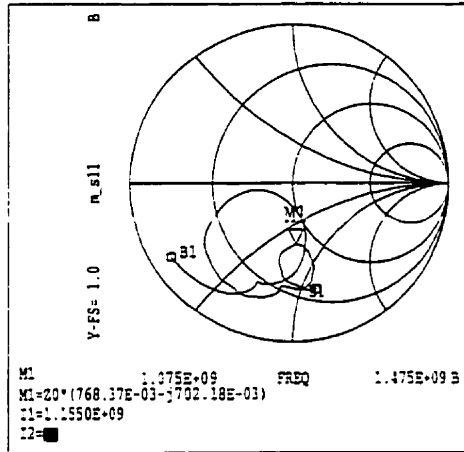
m_s11=slot12.DATA.S[1,1]

Figure 4.16 Response at Point A for Slots One and Two



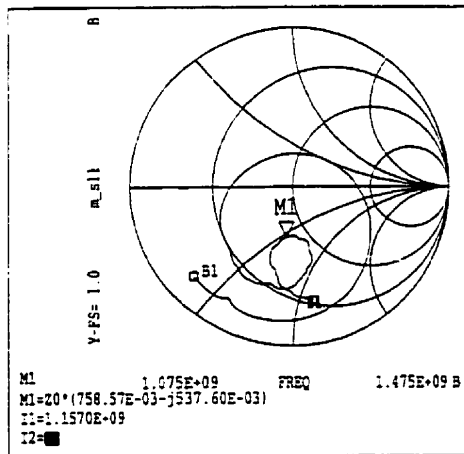
m_s11=slot43.DATA.S[1,1]

Figure 4.17 Response at Point B for Slots Three and Four



m_s11=slot12acen.DATA.S[1,1]

Figure 4.18 Response at Point C due to Point A



m_s11=slot43acen.DATA.S[1,1]

Figure 4.19 Response at Point C due to Point B

4.4 Cylindrical Slot Antenna Measurement Results

Using the prototype antenna and the network analyzer, the individual feed components were tuned to create the overall feed network. (See Figures 4.12 through 4.19.) Using a trial and error process, the feed network was tuned.

There are many degrees of freedom in the design of the feed network, such as the line width, the line length, the position of the series capacitance, the amount of the capacitance, the coupling distance of the line to the outer copper cylinder, and the overall shape of the basic feed component.

Due to the dimensions of the feed network parameters used in the prototype antenna, the resulting operational center frequency is slightly lower than the desired centre frequency of 1.275 GHz. The operational centre frequency of the prototype antenna is 1.15 GHz. The change in centre frequency has now slightly mistuned each slot, the slot length was designed to create a resonant slot at 1.275 GHz not at 1.15 GHz. Therefore the reactive component of the slot input impedance is slightly larger. Also, the vertical distance separating the slots is not effectively equal to $\lambda/2$ at the new centre frequency and thus the phase of the signal at the slots is not equal.

The required cellular bandwidth translated to the 1.156 GHz center frequency results in a 0.136 GHz bandwidth - extending from 1.088 GHz to 1.224 GHz.

4.4.1 Radiation Measurement

The horizontal, vertically polarized radiation pattern measurement of the four slot antenna is presented in Figure 4.20. The radiation pattern

measurements are produced by the mini-anechoic test set-up. The Matlab program that was used to acquire the radiation plots, `rad_plots.m`, is presented in Appendix D.

The measured front lobe is very similar to the original design requirements of a planar slot array. (See Figure 4.20.) The Cylindrical Slot Antenna has a 100° horizontal beam width measured at the standard 3 dB level which is slightly larger than the 80° beam width of the slot array. As desired, the measured back lobe has been greatly reduced when compared with that of the planar slot array. The vertically polarized horizontal radiation pattern of the prototype antenna varies very little throughout the entire measured bandwidth of 1.075 GHz to 1.475 GHz.

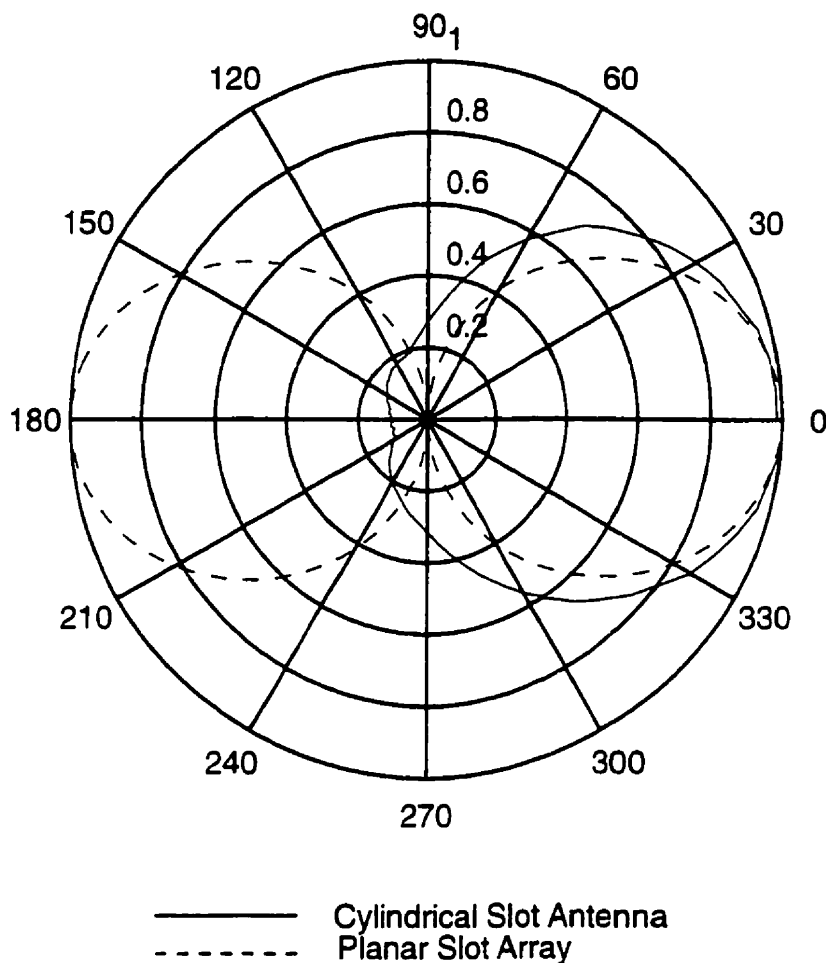
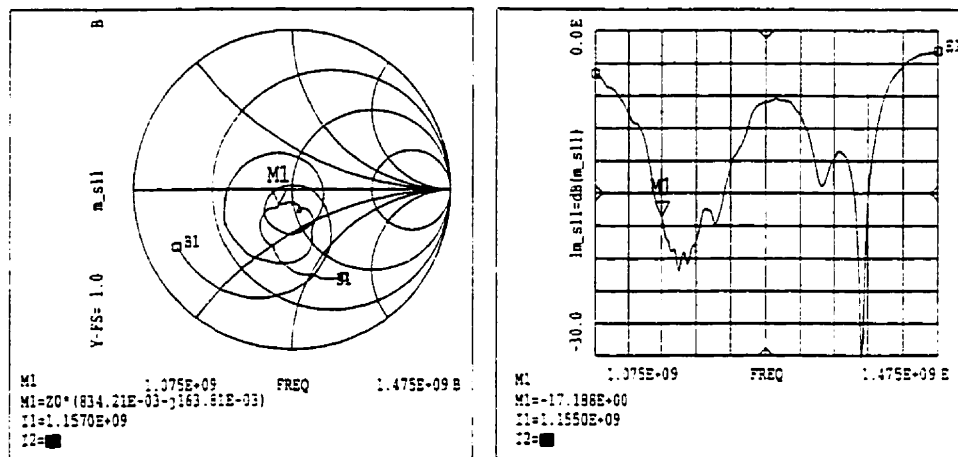


Figure 4.20 Horizontal, Vertical Polarization Radiation Pattern of Prototype and Planar Array @ 1.275 GHz

4.4.2 Input Impedance and S11 Parameter

The input impedance and return loss of the prototype antenna are presented in Figure 4.21. Due to the tuning parameters used, the feed network was tuned to a lower operational centre frequency of 1.156 GHz. The Smith chart denotes the input impedance of the prototype antenna over a large bandwidth - 1.075 GHz to 1.475 GHz. The extended bandwidth helps to understand the operation of the prototype antenna.

The input impedance presented in Figure 4.22 is centred about the middle of the Smith chart - the normalized $50\ \Omega$ input impedance point. The circling of the input impedance about the center point indicates a wide operational bandwidth. Another good indication, used to detail the overall bandwidth of the prototype antenna, is the return loss. A 0.340 GHz bandwidth is available using a -5 dB return loss reference.



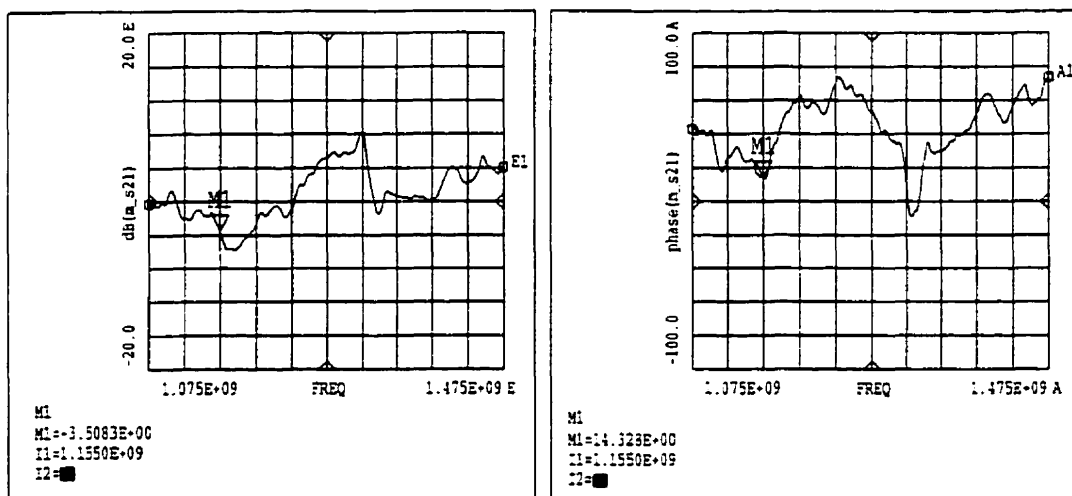
m_s11=final.DATA.S[1,1]

Point M1 indicates result at centre frequency of 1.15 GHz

Figure 4.21 Prototype Antenna Input Impedance and Return Loss

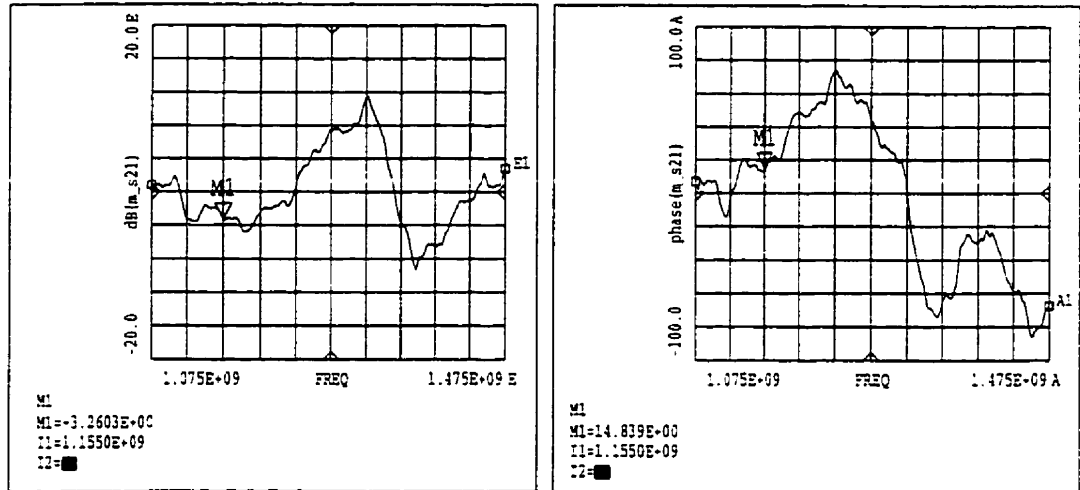
4.4.3 Electric Field Measurements

The feed network must provide equal, in-phase power to each slot in order for the slots to operate as a broadside array. The vertical electric field radiating from each slot is measured, near the slot, to determine the uniformity of the feed to each slot. The measurements from the dipole probe tool are normalized and the relative electric field from the individual slots can be compared. Slots two through four are normalized using the measured field from slot one. These normalized S21 plots are presented in Figures 4.22 through 4.24.



$$m_s21 = \text{probe2.DATA.S}[2,1] / \text{probe1.DATA.S}[2,1]$$

Figure 4.22 Normalized S21 Parameter of Slot Two



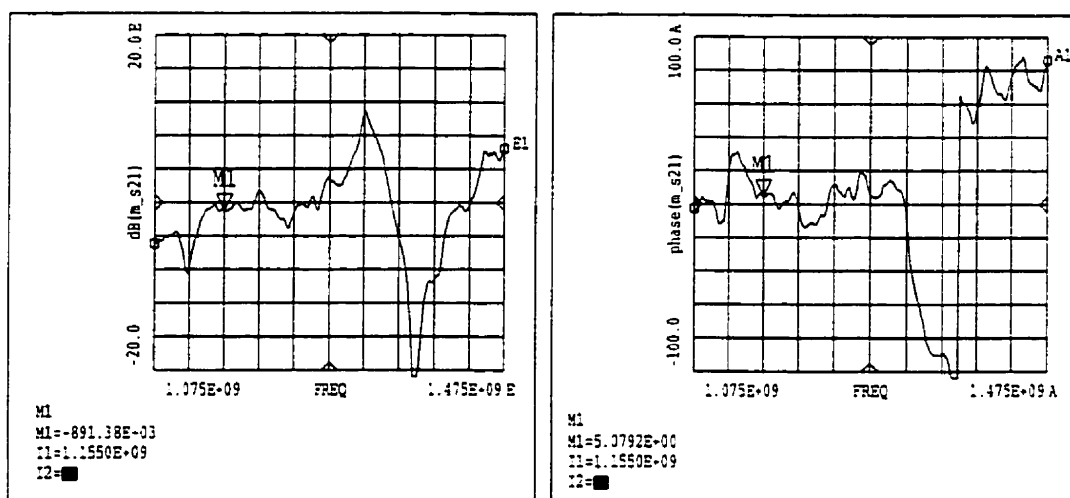
$$m_s21=probe3.DAT.S[2,1]/probe1.DAT.S[2,1]$$

Figure 4.23 Normalized S21 Parameter of Slot Three

The S21 magnitude values, at the operational centre frequency, for slots one and four are relatively the same. The S21 phase measurements of these slots are also very similar. The S21 measurements indicate that these slots are radiating very close to equal, in-phase power.

The S21 magnitude measurements for slots two and three are very similar but are approximately 3 dB different from slots one and four. The S21 phase measurements of slots two and three are, also, very similar but are offset from slots one and four. The key problem accounting for the dissimilarities of the inner and outer slots is due to the mistuning of the feed network. Another problem, is due to the change of centre frequency to 1.156 GHz from the

designed centre frequency of 1.275 GHz. The slot separation and, consequently, the vertical line lengths of the feed network must be changed, in subsequent fine tuning cycles, to account for the change in operating wavelength. The frequency discrepancy can account for, approximately, 16° in phase offset between the inner and outer slots.



```
m_s21=probe4.DATA.S{2,1}/probe1.DATA.S{2,1}
```

Figure 4.24 Normalized S21 Parameter of Slot Four

The normalized S21 measurements are used in a simple array Matlab program, `var_array_vert.m`, to indicate the vertically polarized vertical radiation pattern. (See Figure 4.25.) The simulated vertical radiation pattern is very similar to the theoretical four slot planar array except for a slight increase in sidelobe power.

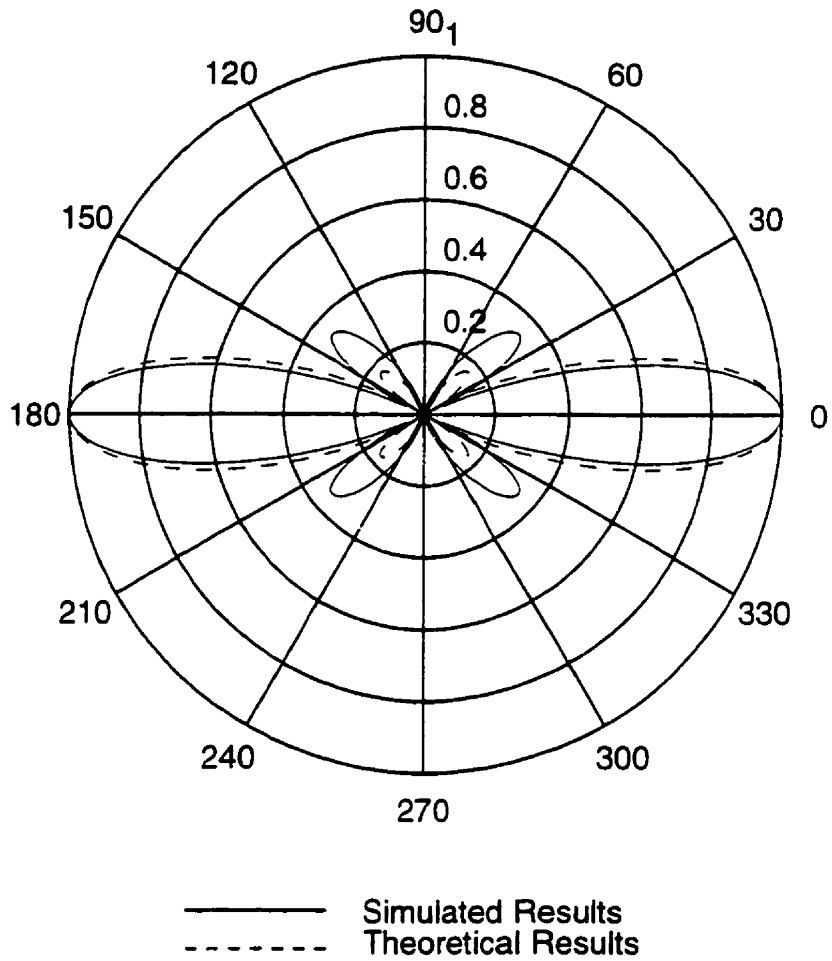


Figure 4.25 Simulated and Theoretical Vertically Polarized, Vertical Radiation Pattern @ 1.275 GHz.

5.0 Diversity Scheme

The pattern diversity scheme tested in this study is based on the interleaving of the minima and maxima of two independent radiation patterns. The basic premise of this diversity scheme is that from these two radiation patterns, due to uncorrelated multipaths, two highly uncorrelated signals can be received and effectively combined for an overall diversity improvement. An important component in this diversity scheme is a passive combiner, known as the Magic T. Although, the Magic T performs the interleaving of the radiation patterns, the shape of the radiation pattern is ultimately created by a space diversity scheme incorporated into the proposed diversity configuration. A continuous wave uplink system has been developed in order to test the proposed diversity system. (See Section 3.2.)

5.1 Magic T

The Magic T is known by many names such as a hybrid ring or rat race. This device has four ports; two are input ports and two are output ports. A general diagram of a microstrip Magic T is presented in Figure 5.1.

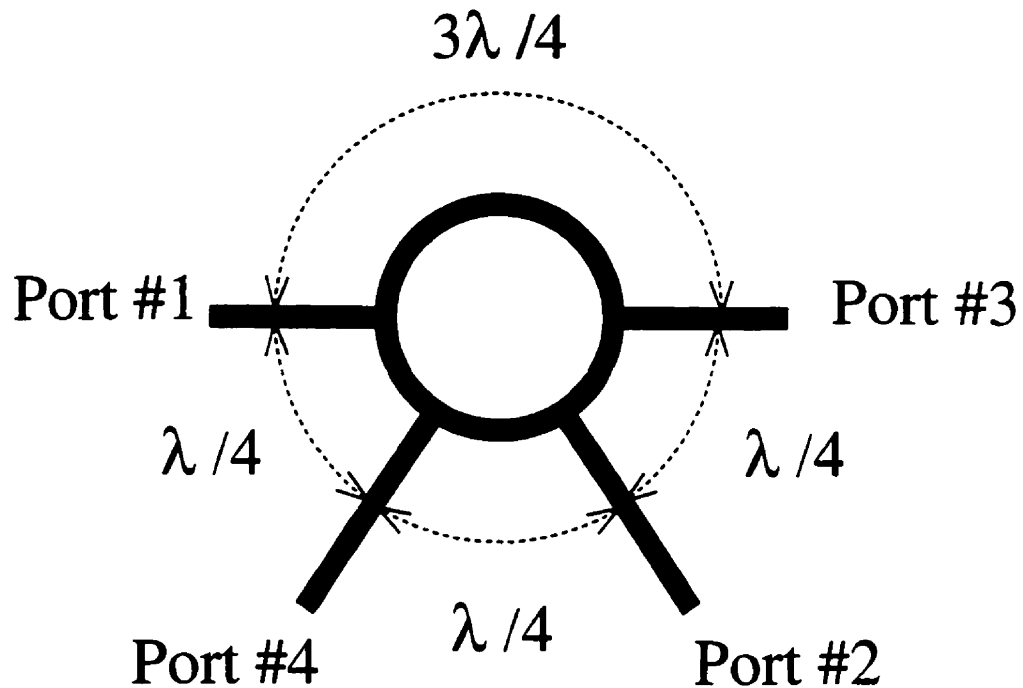


Figure 5.1 Magic T

The functionality of the Magic T depends on the phase shift imposed upon the travelling wave due to the transmission line. This phase shift depends on the length and characteristic impedance of the transmission line and the effective load impedance. (See Equation 5.1 [1].)

$$V = V_{TW1} e^{\alpha l} e^{j\beta l} \Big|_{Z_L=Z_0} \quad (5.1)$$

Referring to Figure 5.1, the following paragraph describes the general process of operation of the Magic T combining device. Signal A is fed into port #1, the signal is then equally divided between both directions or paths of the ring due to proper impedance loading. Assuming, for simplicity, that the velocity

factor of the transmission medium is one, then the normalized length is directly translated into a phase. As the signal propagates from port #1 to port #3, the $3\lambda/4$ path results in a phase shift of 270° of signal A. As the signal propagates from port #3 to port #2, there is another 90° phase shift resulting in a 360° or 0° phase shift of signal A. As the signal A travels the other path from port #1 towards port #4, the $\lambda/4$ path results in a 90° phase shift of signal A. The signal continuing, again, to port #2 has another 90° phase shift resulting in a 180° overall phase shift. Signal A is cancelled out at port #2 due to the signal paths resulting in a 180° phase difference. Following the same mechanism, the signal B is fed into port #2 which results in a phase shift of 90° of the signal at port #3 and port #4 and a cancellation of the signal at port #1.

At port #4, signal A has been phase shifted by 90° as is signal B. The signals are vectorially added and, since the signals are in-phase, the port has been named the 'sum output'. At port #3, signal A has been phase shifted by 270° and signal B has been phase shifted by only 90° . These signals are vectorially added and, since the signals are out of phase, the port has been named the 'difference output'. The attenuation of the signals fed into port #1 or port #2 is, approximately, 3 dB when they emerge at matched output ports. The phase characteristics of the Magic T are presented in Figure 5.2.

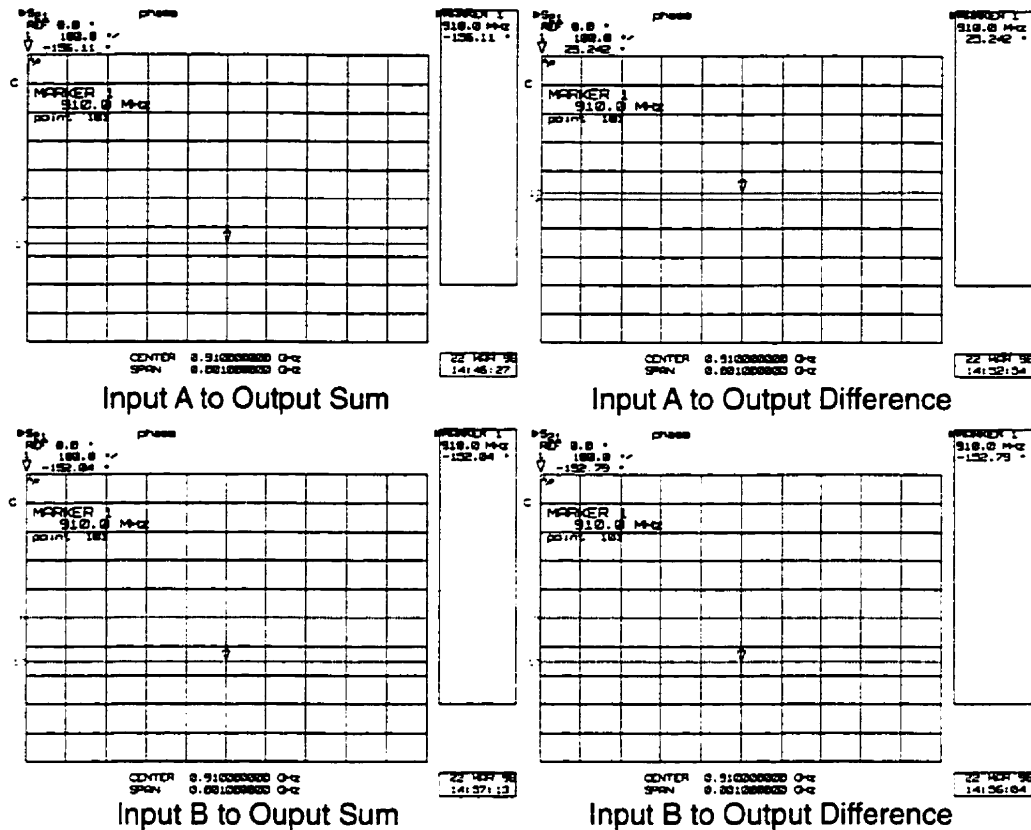


Figure 5.2 Magic T Phase Characteristics

5.2 Radiation Pattern

The desired overall radiation pattern consists of two independent radiation patterns, each of which consist of many slender lobes. The two independent radiation patterns are offset so the lobe maxima interleave. The two radiation patterns are used to independently detect different incoming multipath signals.

The creation of this special overall radiation pattern is a two-step process. (See Figure 5.4.) In the first step, two antennas with appropriate radiation patterns are sufficiently separated in order to create the desired array

pattern. The directive antennas must be sufficiently separated to create an array pattern consisting of slender lobes. This array pattern, $F(\theta, \phi)$, is calculated by a two-part procedure. In part A, the actual radiating elements are replaced by isotropic sources. The radiation pattern, $f(\theta, \phi)$, is calculated by vectorially adding the fields emanating from the individual sources. (See Equation 5.2 [2].) In part B, the isotropic radiation pattern is adjusted by the actual antenna radiation pattern, $g(\theta, \phi)$, resulting in the desired array pattern. (See Equations 5.3 and 5.4 [2].)

$$f(\theta, \phi) = \frac{1}{N} \frac{\sin(\frac{N\psi}{2})}{\sin(\frac{\psi}{2})} \quad (5.2)$$

$$F(\theta, \phi) = g(\theta, \phi)f(\theta, \phi) \quad (5.3)$$

$$\psi = kd \cos(\theta) + \beta \quad (5.4)$$

If the separation distance between the two antennas is greater than 1λ , the array pattern will consist of slender lobes. As the separation distance is increased, the number of lobes in the radiation pattern is increased and these lobes become increasingly slender. (See Figure 5.3.)

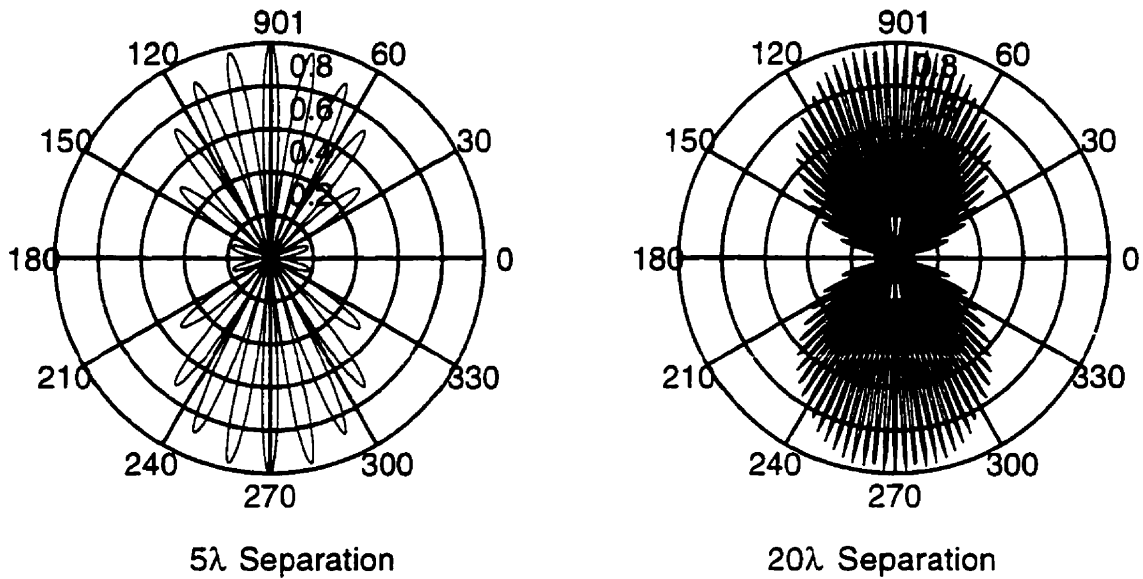


Figure 5.3 Radiation Patterns of Different Separations

In the second step of the creation of the pattern diversity radiation pattern, the combining device is used to create a radiation pattern similar to the one in step one, but with a phase offset. The output of each antenna is fed into the Magic T combining device. The radiation pattern from the sum output produces the desired array pattern determined in the first step, while the difference output results in a very similar radiation pattern, except it has been phase shifted by 180° . The maxima of the lobes from the difference output radiation pattern interleave with the maxima of the lobes from the sum output radiation pattern. The combining device is used in conjunction with the space diversity scheme to create the desired pattern diversity radiation pattern.

A general overview of the pattern diversity configuration is presented in Figure 5.4. The radiation pattern obtained from the sum and difference output ports of the Magic T result in the interleaving slender lobes of two independent radiation patterns.

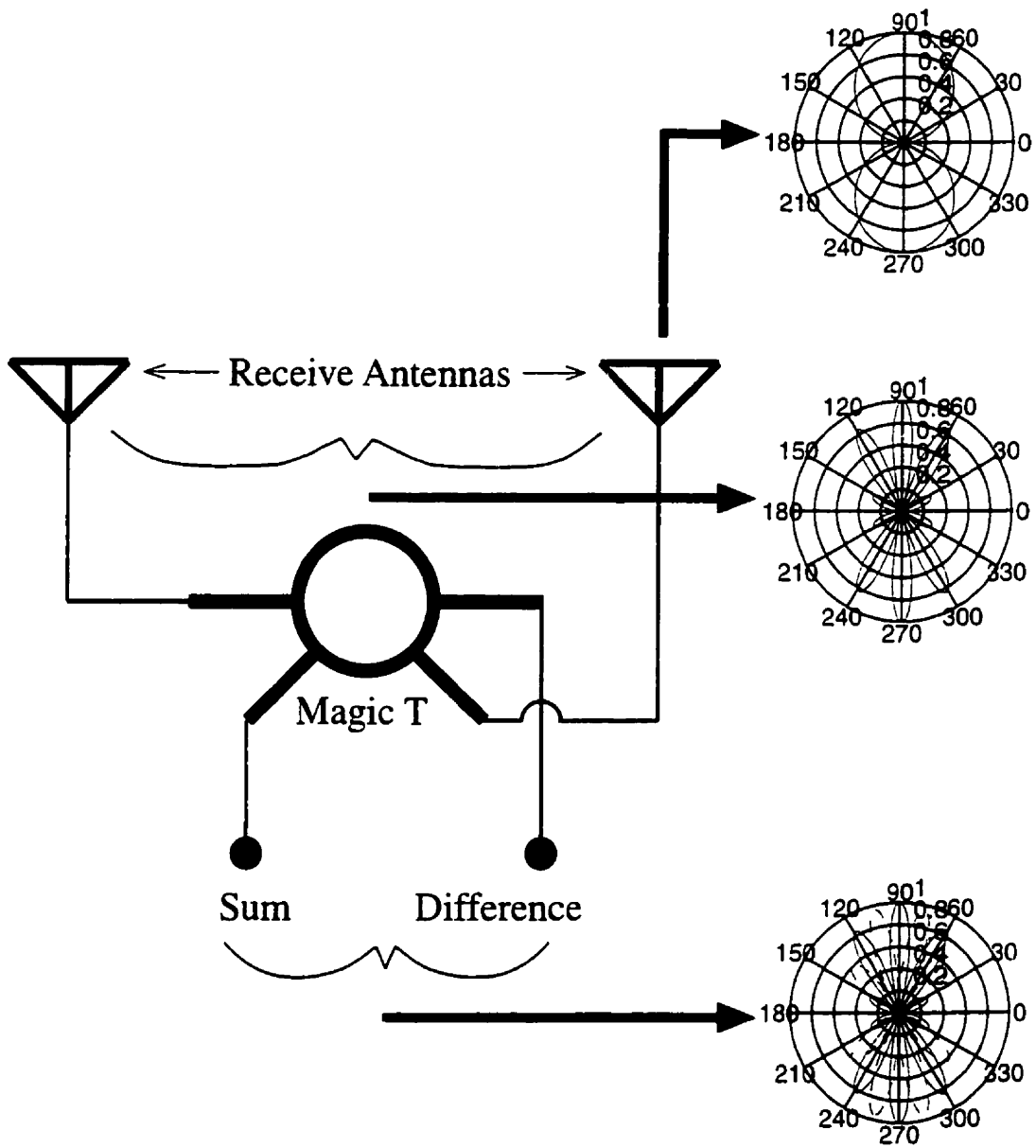


Figure 5.4 Radiation Pattern Development

5.3 Diversity at the Base Station

This specific form of pattern diversity can only be effectively applied to the base station and not the mobile station of a cellular network due to the need of a narrow angle of the incoming multipath signals. Multipath signals caused by reflectors and scatters are indeed reciprocal, but the angular sector of these incoming signals at the base and mobile stations are quite different. This difference is caused by the location of the stations relative to the reflectors and scatters. (See section 2.3.)

The slender interleaving lobes are the key elements in the proposed pattern diversity scheme. These slender lobes would not be advantageous in a situation with multipath signals incoming at all angles to the receive site, as is the general case of the mobile station. A pattern diversity technique with fewer and larger lobes would more effectively suit the mobile station [3]. Also the space required for effective antenna separation is not available on the cellular handset.

The narrow angular sector of incoming signals at the base station is better suited to the proposed pattern diversity scheme. The slender lobes are used to receive uncorrelated multipath signals from the narrow angular sector and translate the information into a diversity improvement.

5.4 Diversity Scheme Measurement Results

In order to determine the effectiveness of this diversity scheme, cumulative distribution curves, acquired from test data, are compared. The test data is acquired through a continuous wave, uplink test set-up using space and

pattern diversity configurations. These distribution curves are used to indicate the relative diversity improvement due to the selective combining of the different test data. From the relative diversity improvement, the effectiveness of the pattern diversity scheme can be established.

The received test signals are composed of both short term and long term fading components. The short term fading component is the direct result of multipath fading and must be isolated from the long term component. To obtain the desired short term fading signal with time invariant statistics, the local mean of each data file is calculated and then removed from the original signal.

After the long term component has been removed, probability distribution graphs of the short term signal are calculated. The probability distribution of the received data must compare to a Rayleigh distribution in order to validate the accuracy of the procedure used to separate the long and short term components.

In the final analysis of the data, cumulative distribution graphs are calculated from the short term fading component of individual signals and from the selection combining of these short term components.

5.4.1 Mean Value

The sampled data from each switch input (see section 3.2.3) is stored in an individual output file. The information recorded in the four files consists of the time of each sample and the sampled averaged envelope power.

The four switch inputs are not sampled at the exact same time but instead sampled sequentially due to the 4-to-1 switch in the receive section of the uplink system. The envelope data samples are time aligned to occur seemingly at the

same time. The error due to this procedure is assumed to be negligible because of the small distance travelled by the mobile transmitter during the respective sampling. (See Section 3.2.3.)

Since the transmitter is moving, the received signal has a time variant mean which indicates non-stationary random process. The objective is to find the cumulative distribution curves, related to first order statistics, and, ultimately, the diversity improvement of the system, related to second order statistics. To achieve the objective, a wide sense stationary random process is required which has time invariant first and second order statistics. If the envelope of the received signals has a Rayleigh distribution, a process with one degree of freedom, then a time invariant first order statistic ensures a time invariant second order statistic. The wide sense stationary signal is achieved by normalizing the random process with a local mean estimator [4][5][6]. Using a sliding window, the local mean can be removed from the data samples and the first and second order statistics of the Rayleigh signal will be time invariant. The length of the window is an important parameter, for if the window is too short or too long then the local mean will not be stationary. The best estimator of local mean has two characteristics: the average of the estimated value, $\hat{u}_m(y)$, tends towards the real mean, $u_m(y)$, and the variance of estimation which should be as small as possible. A window length of 40λ [4] provides a 1 dB standard deviation of the estimated mean of a Rayleigh fading signal. For simplicity a $40\lambda + 1$ sample window is used. Each switch input is sampled every 60 ms, which results in one sample of each switch input every $\lambda/2$. Therefore, $40\lambda + 1$ sample results in a 81 sample window length. The sliding window has 40 pre samples and 40 post samples centred around the sample time of interest. The 81 samples within the window are averaged to determine the mean value of the

centre sample. The received data files are presented in Figures 5.5 and 5.6.

The ordinate axis units used in these figures is determined by the A/D in the test system and is only considered when comparing results.

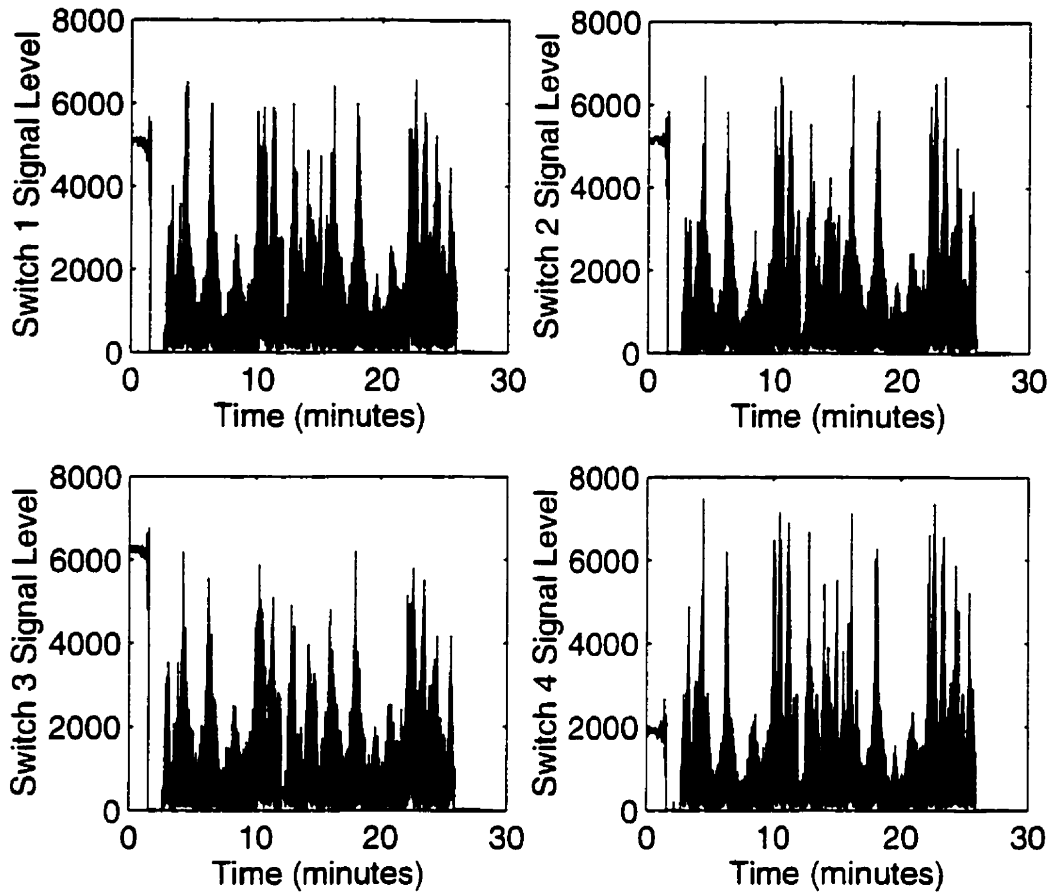


Figure 5.5 Received Signals with 5λ Separation between Antennas

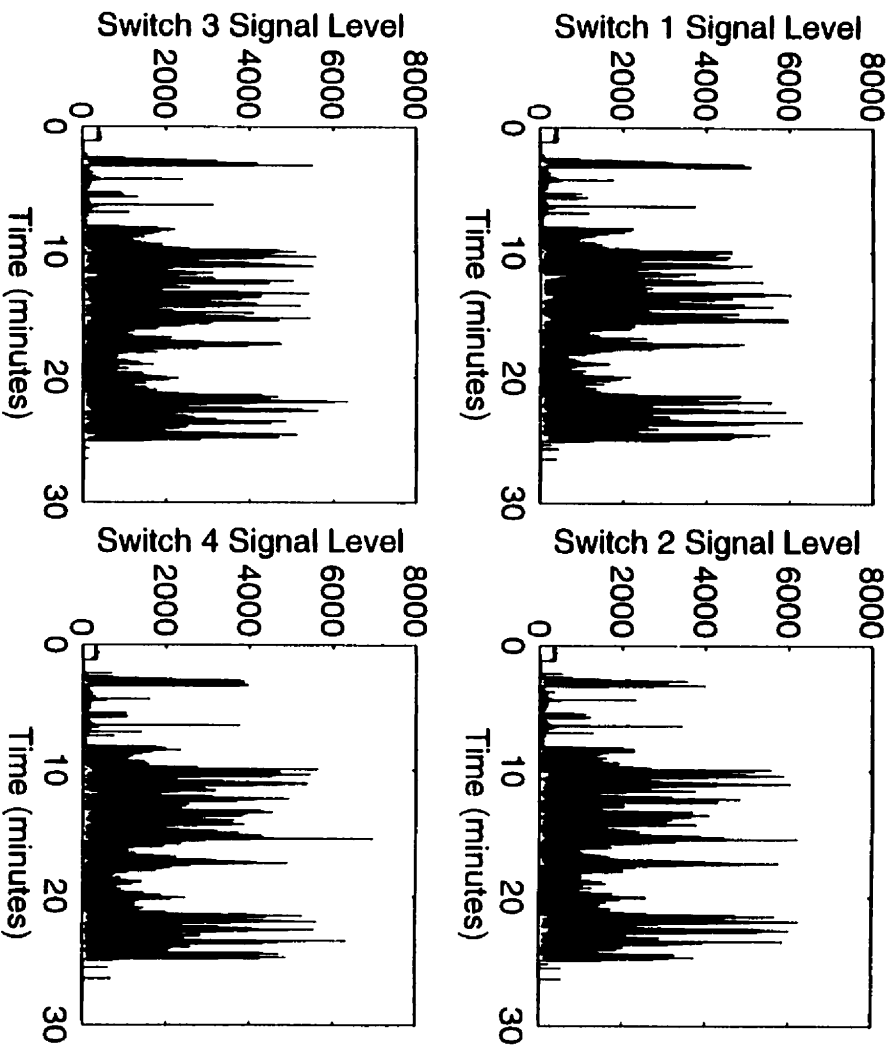


Figure 5.6 Received Signals with 40λ . Separation between Antennas

The original output sample value, $r(y)$, is normalized by the appropriate estimated mean value, $\hat{u}_m(y)$, at each sample point. (See Equation 5.6 [4].)

$$r(y) = u_m(y)r_o(y) \quad (5.5)$$

$$\hat{r}_o(y) = \frac{r(y)}{\hat{u}_m(y)} \quad (5.6)$$

The resultant output, \hat{r}_o , is a stationary variable and represents the short term fading signal. From the stationary short term fading signal, the probability

and cumulative distributions can be ascertained and then compared to evaluate the diversity improvement.

The first and last 40 samples of the short term fading signals are set to a normalized value of one, the overall mean of the short term signal, because of the pre and post samples required in the window estimator. The Matlab program, `mean_value.m`, which calculates then removes the estimated local mean from the signal, is found in Appendix E. The short term fading signals are presented in Figures 5.7 and 5.8.

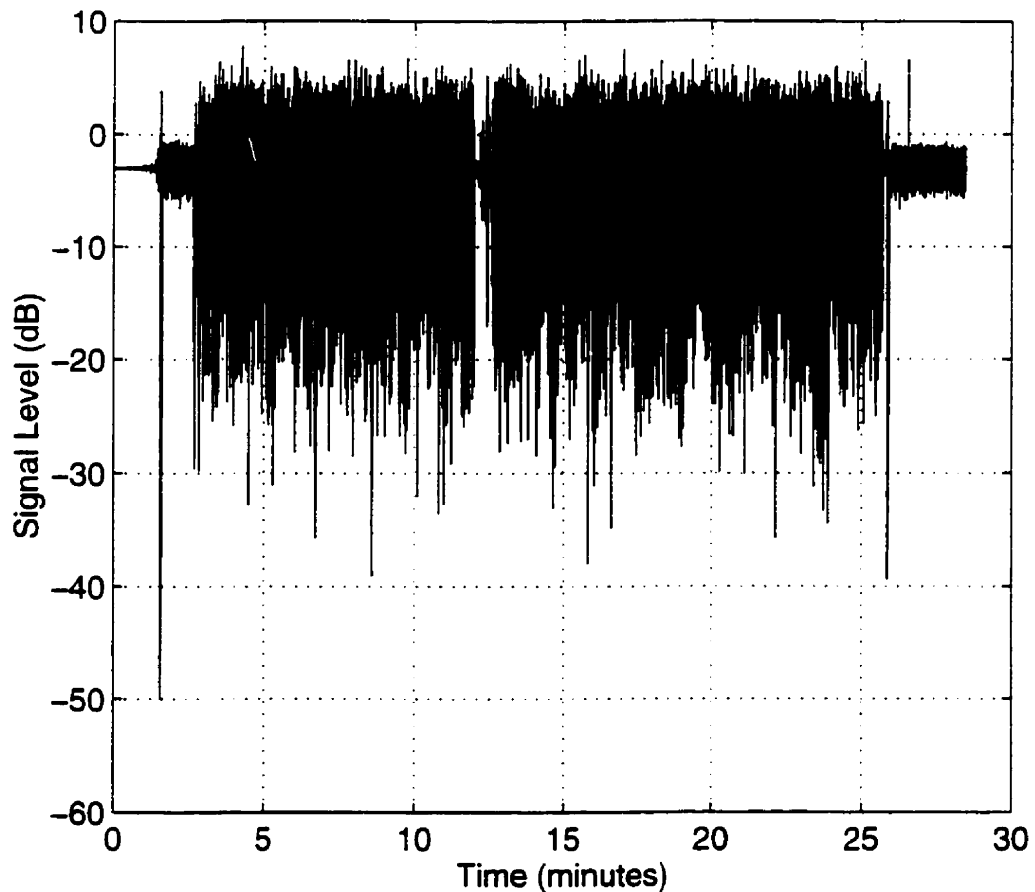


Figure 5.7 Switch 1 with Mean Removed at a 5λ Separation

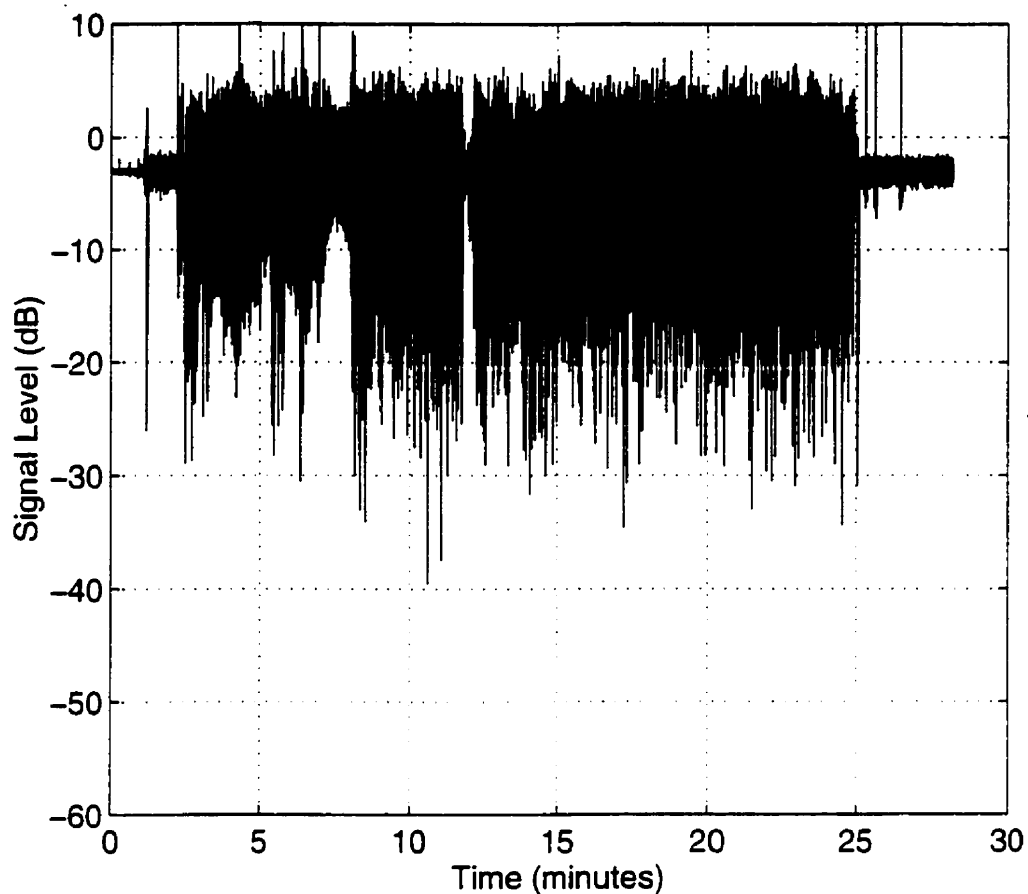


Figure 5.8 Switch 1 with Mean Removed at a 40λ Separation

5.4.2 Probability Distribution

Each short term fading signal is tested to determine its probability distribution. A Rayleigh probability distribution function is required to ensure the reliability of the results from the sliding window technique.

The measured data contains signal plus noise but since the signal and noise are independent, the probability distribution function of the data is simply the multiplication of the two distributions. However, due to high SNR, the

probability distribution function of the signal prevails in the overall probability distribution function of the data.

To determine the estimated probability distribution function, a histogram of each fading signal is determined using 15 evenly spaced bins. The number of bins used in the estimated probability distribution function is determined by trial and error until a fairly smooth curve is obtained. The number of samples, n_i , within each bin, b_i , is used in Equation 5.7 [5][6] to determine the estimated probability distribution, p_i .

$$p_i = \frac{n_i}{N\Delta a} \quad (5.7)$$

The theoretical Rayleigh and Gaussian probability distribution functions are also plotted using a mean value of one, the mean of the short term fading signal, in the Equations. 5.8 through 5.10 [7].

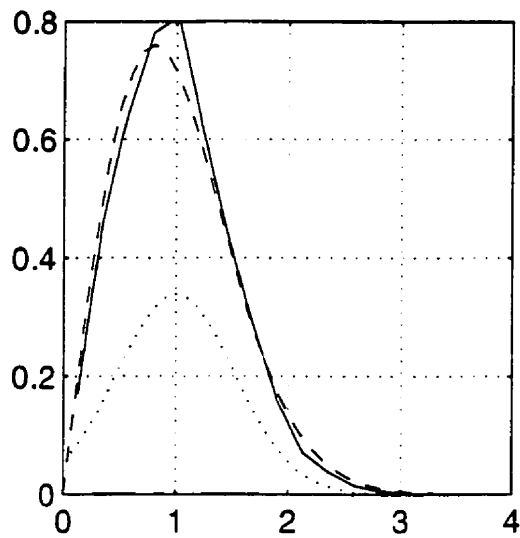
$$\hat{\mu}_m = \sqrt{\frac{\pi}{2}}\sigma \quad (5.8)$$

$$p_r(r) = \frac{r}{\sigma^2} \exp\left(-\frac{r^2}{2\sigma^2}\right) \quad (5.9)$$

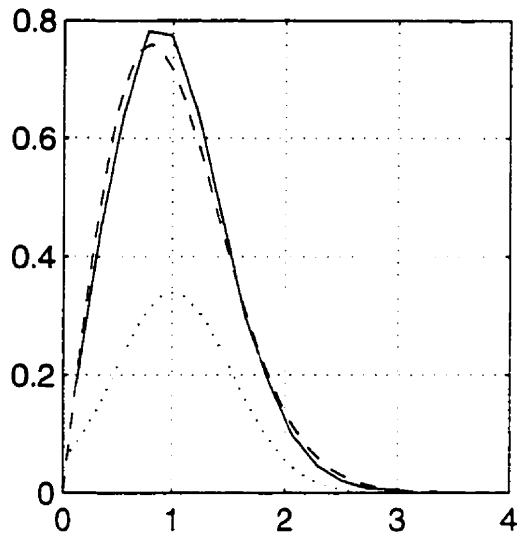
$$p_x(x) = \frac{1}{\sqrt{2\pi}\sigma} \exp\left[-\frac{(x - \hat{\mu}_x)^2}{2\sigma^2}\right] \quad (5.10)$$

The theoretical Rayleigh probability distribution functions and the estimated probability distribution functions, by visual comparison, match very closely, therefore, it is concluded that the fading signals have Rayleigh distributions and, thus, validate the procedures used in the sliding window technique. (See Figures 5.9 and 5.10.) The Matlab program, pdf.m, which

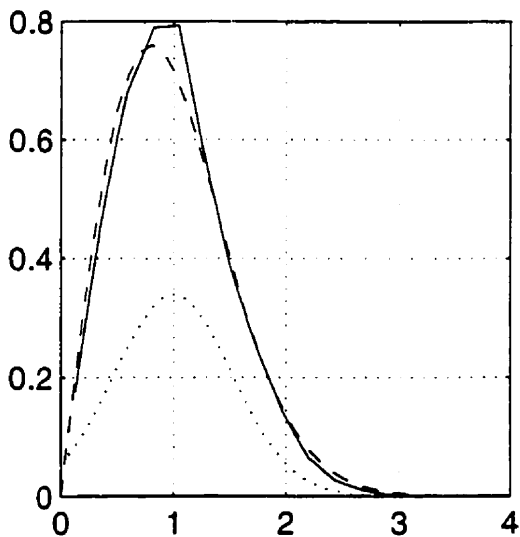
calculates then compares the short term probability distributions and the appropriate Rayleigh distribution is presented in Appendix E.



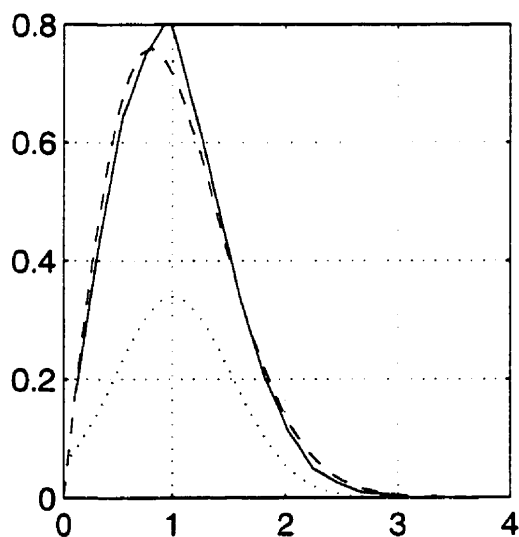
Input 1 - Antenna 1



Input 2 - Antenna 2



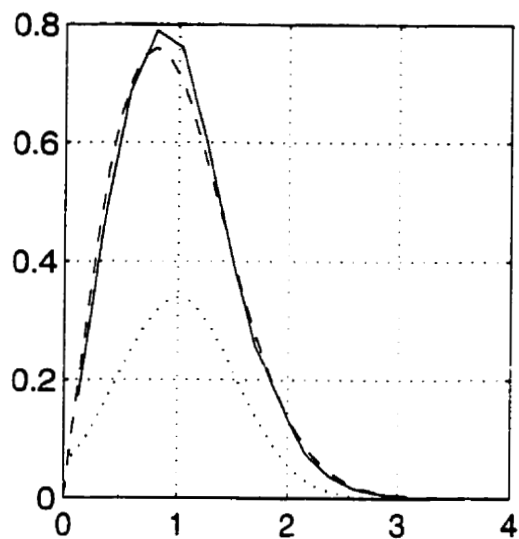
Input 3 - Sum



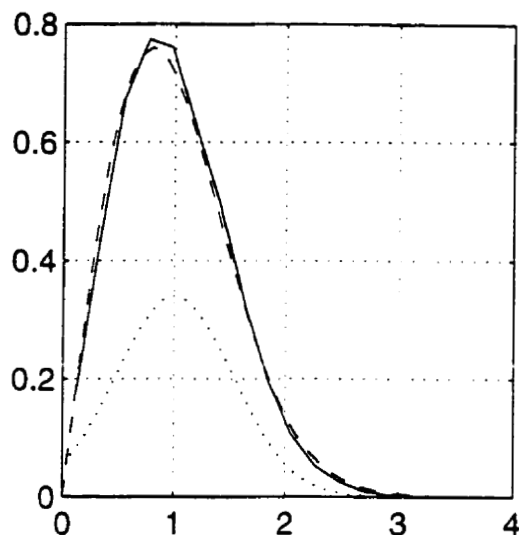
Input 4 - Difference

————— Measured pdf
 - - - - - Rayleigh pdf
 Normal pdf

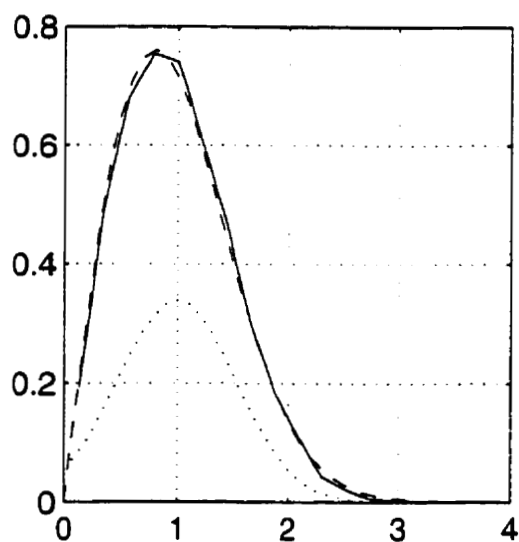
Figure 5.9 PDF of the 5λ Separation Inputs



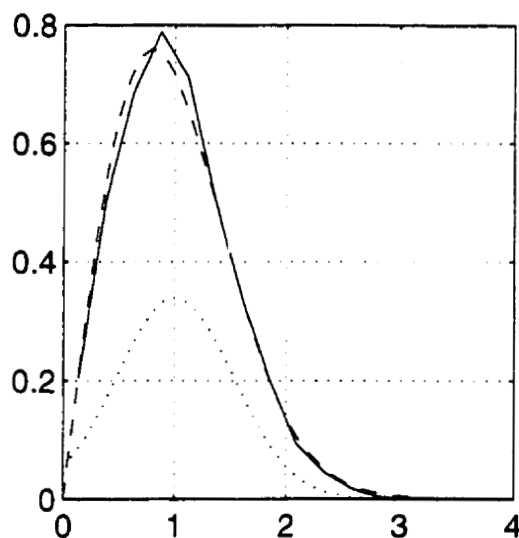
Input 1 - Antenna 1



Switch 2 - Antenna 2



Input 3 - Sum



Switch 4 - Difference

— Measured pdf
 - - - Rayleigh pdf
 . . . Normal pdf

Figure 5.10 PDF of the 40λ Separation Inputs

5.4.3 Cumulative Probability Distribution

The cumulative distribution graph denotes the probability that the received signal strength is above a specific threshold value determined by the abscissa. In comparing two cumulative distributions, the distribution with the least percent probability of the signal being below the abscissa reveals the short term fading signal with a statistically shorter fade duration and statistically milder fade depths. When using a combining technique to create the overall short term signal, the shorter fade duration and milder fade depths indicate that the combining short term fading signals are also statistically more uncorrelated than the other combining signals. The difference in signal level along the abscissa, between two cumulative distributions at the same probability, indicates the relative diversity improvement between diversity schemes.

The bins and number of samples within the bins determined in section 5.4.2 are used to calculate the cumulative distribution curves [8]. The abscissa is the same as that used in the probability distribution function plots, but the ordinate value, P_i , is determined by summing the number of samples in and below the specific threshold, $\sum n_i$, and normalizing this number by the total number of samples, N . (See Equation 5.11.)

$$P_i = \frac{\sum n_i}{N} * 100 \quad (5.11)$$

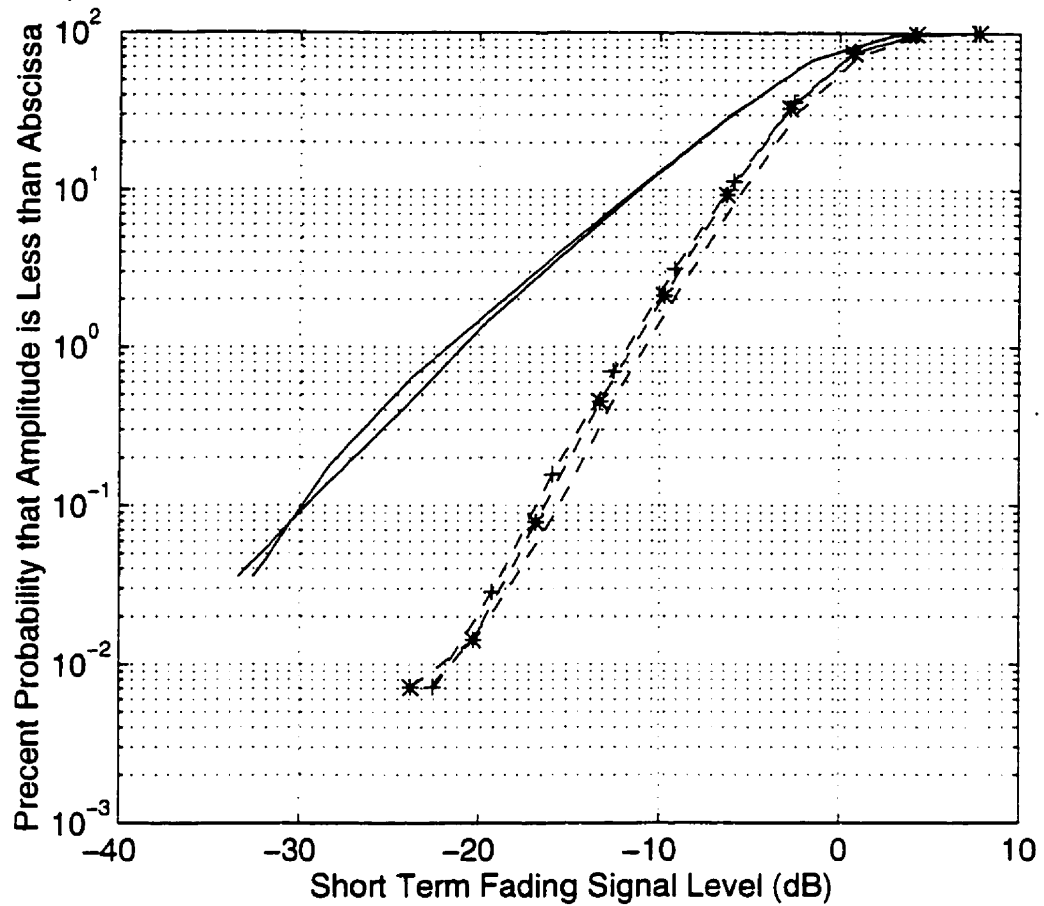
The combined fading signal is created using a technique known as selection combining. The four individual switch output files are combined in different configurations to attempt to produce a resultant fading signal with fades of less duration and depth than the original received fading signals. The signal

with the strongest amplitude is selected from the possible signals at each specific sample time to create a new combined signal. This type of combining does not produce the best overall combined signal compared to other combining techniques (see Section 2.3), but is easy to compute and, also, appropriate in this experiment because the phase of the received signals is not known.

The cumulative distribution of the received antenna 1 and 2 signals, the combination of the space diversity signals, the combination of the pattern diversity signals, and the combination of all signals are plotted for each antenna separation. (See Figures 5.11 and 5.12.) The diversity improvement, at the 1% probability, between the individual antenna signals 1 and 2 and the selective combining of these signals (space diversity) is 9.06 dB for a 5λ separation and 9.8 dB for a 40λ separation. The diversity improvement, at the 1% probability, due to the selective combining of all received short term fading signals over the space diversity results is 0.86 dB for both the 5λ and the 40λ separations.

The results of the cumulative distribution graphs in the regions of high or low probability are not necessarily reliable. From the approximate 20,000 samples in each test run, very few samples fall with the respective bins at such probabilities and, therefore, are not as statistically reliable.

The Matlab programs, `cdf.m` and `select_combining.m`, are found in Appendix E.



- Received Short Term Fading Signal from Antenna 1 and 2
- + - - - + - - - + Selective Combining of the Space Diversity Signals
- * - - * - - * Selective Combining of the Pattern Diversity Signals
- Selective Combining of all Short Term Fading Signals

Figure 5.11 CDF Graph for 5λ Separation

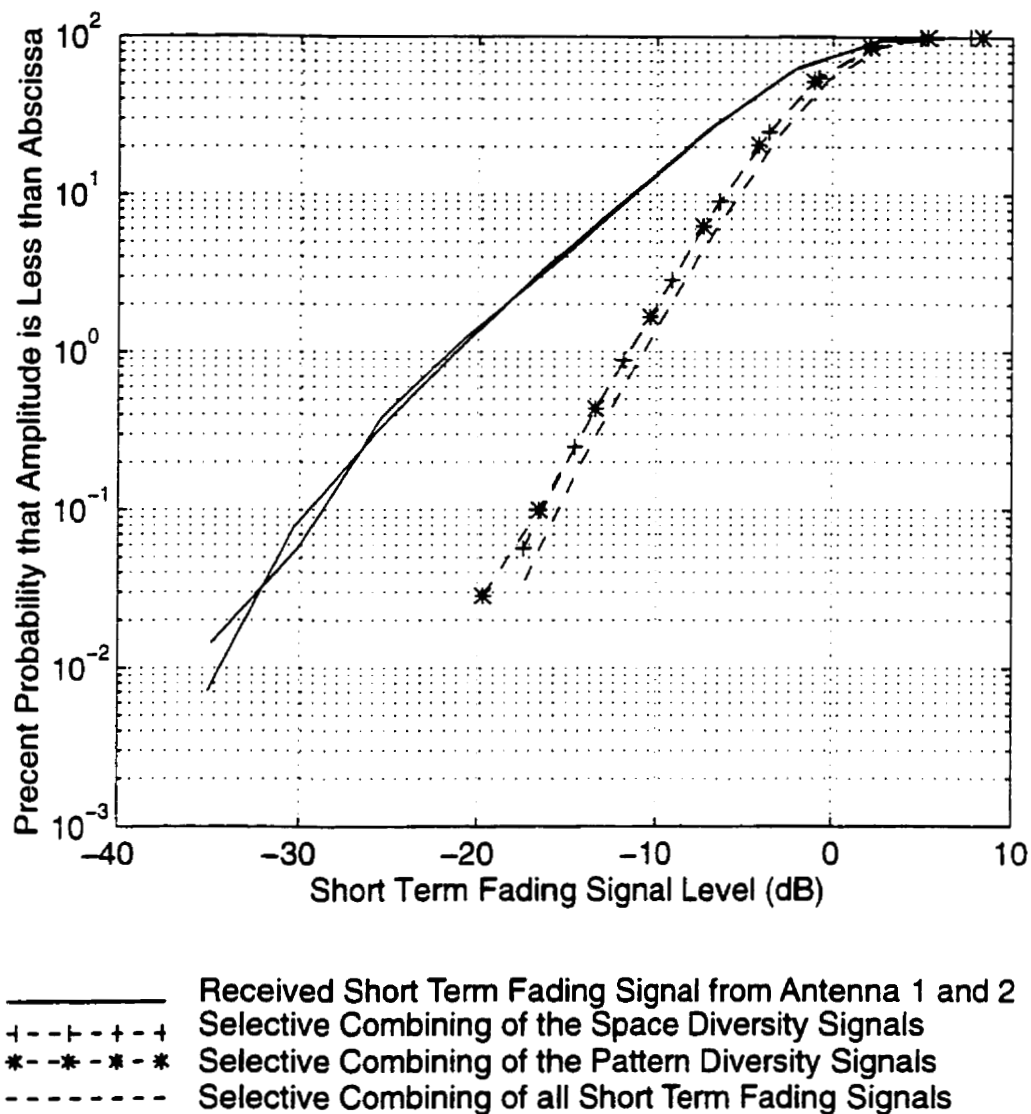


Figure 5.12 CDF Graph for 40λ Separation

5.4.4 Test Accuracy

To understand the limits of the continuous wave uplink measurement system, the accuracy of the system is required. The noise floor of the system and the noise riding on the signal are the limiting factors in the system. The quantization noise of the A/D is dominated by the system noise floor. The effect

on the accuracy of the system due to the noise floor and the noise riding on the signal is calculated, then presented in Figure 5.15. (See Appendix G [9][10].)

As presented in Figure 5.13, the resulting effect of noise on the system is reduced as the received signal power is increased. Recalling that the received signal power is limited by the saturation specifications of the equipment in the system.

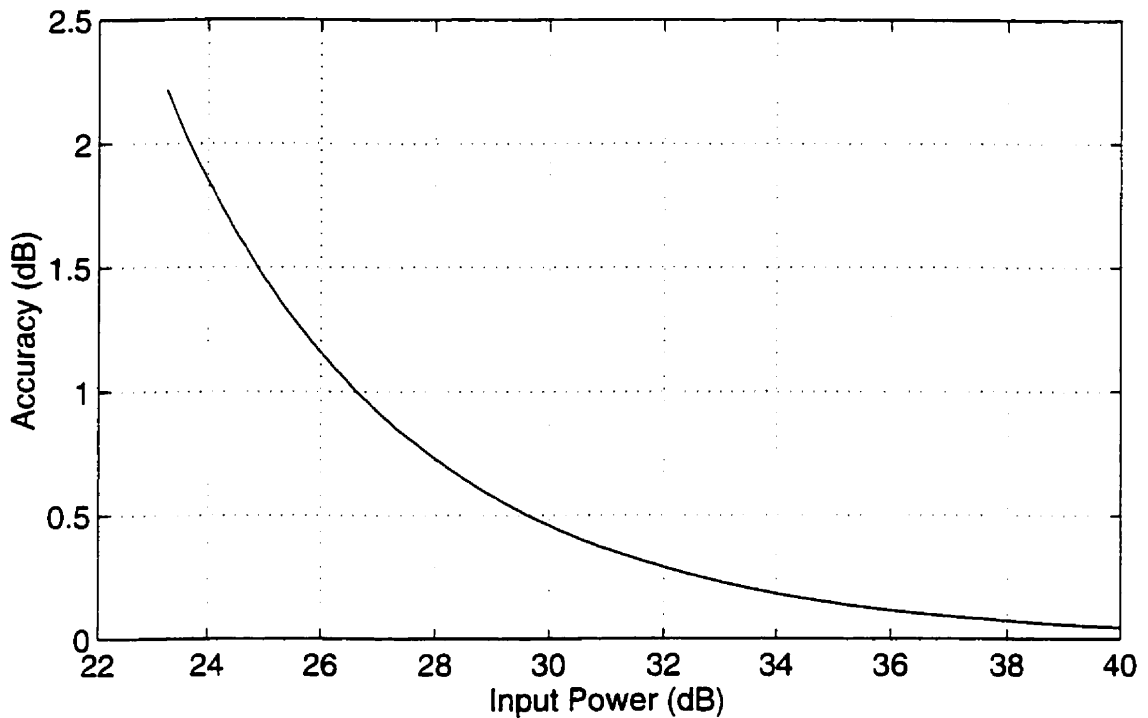


Figure 5.13 Effect of Noise on System Accuracy

6.0 Conclusion

Two projects, each involving prototype designs, have been evaluated. The first project, the Cylindrical Slot Antenna, has been designed to operate as a cellular, base station antenna. A prototype antenna was built to test the proposed Cylindrical Slot Antenna design. The prototype was evaluated through its radiation pattern, input impedance, return loss and normalized S21 parameter. The results from these evaluators are very favourable and demonstrate a good design concept.

The second project, the pattern diversity scheme, has been evaluated using a continuous wave, uplink test system. The relative diversity improvement of space and pattern diversity schemes has been evaluated through cumulative distribution curves. The measured relative diversity improvements compare closely to theory and, together with the measured accuracy of the system, validate the results acquired from the test system. The selective combining of space and pattern diversity test signals has demonstrated a slight diversity improvement compared to the selective combining of the space diversity signals.

From the results of this thesis, the Cylindrical Slot antenna could be used in conjunction with the pattern diversity scheme to improve the received signal in a multipath environment. These results, also, indicate that the antenna design requires some additional tuning to meet the specifications of cellular, base station antennas. This design provides an inexpensive, sturdy antenna which can be used in a unique pattern diversity configuration which provides an overall reliability improvement.

6.1 Cylindrical Slot Antenna

A prototype antenna was developed from the proposed antenna design. The physical dimensions of the prototype antenna had to be reduced from actual design dimensions, therefore, the antenna evaluators had to be frequency scaled to better represent the actual operation of the design antenna.

The radiation pattern, input impedance, return loss and S21 parameter of the prototype antenna have been evaluated. These evaluators demonstrate that the Cylindrical Slot Antenna is an excellent design concept for cellular base station antennas. Some additional tuning is required for the prototype performance to meet the desired specifications. There are many degrees of freedom in the tuning of the basic feed component. This latitude in design should easily yield an acceptable antenna performance.

6.1.1 Radiation Pattern

The horizontal, vertically polarized radiation pattern measurement, Figure 4.20, indicates the potential coverage area of the design antenna. The approximate, desired radiation pattern determined from the planar array is presented in Figures 4.5 and 4.6. In comparing the original horizontal, vertically polarized requirement and the measured result, as shown as Figure 4.21, the radiation pattern goals are shown to be acceptably satisfied. The front lobes of the two radiation patterns are very similar and the back lobe of the prototype antenna is greatly reduced as desired. The goal of an antenna is to radiate signal to the desired area. In the cellular system, a large back lobe may result in co-channel interference and is, therefore, detrimental to the system.

The horizontal radiation pattern varies very little throughout the extended bandwidth. This is very desirable, since the coverage area should not vary with a change of frequency within the operational bandwidth.

The horizontal, horizontally polarized radiation pattern of the prototype antenna was not evaluated due to size limitations of the anechoic chamber, but is assumed to be minimal due to the type of radiating elements used.

The vertical radiation patterns are not evaluated directly, but the vertical polarized radiation pattern is indirectly evaluated by the S21 probe measurements. The vertical, vertically polarized radiation pattern is very similar to the theoretical requirement except the side lobes of the simulated results are slight larger than desired. The power in these sidelobes could potentially interfere with other cell sites. The radiating elements within the array are coupling together and thus the fields measured of the inner and outer slots are slightly disimilar. Additional tuning of the feed network to compoensate for the coupling will reduce the power in the sidelobes. The vertical, horizontally polarized radiation pattern is assumed to be minimal due to the radiating elements used.

6.1.2 Input Impedance and Return Loss

The input impedance and return loss graphs of the prototype antenna are presented in Figure 4.22. The slot separation and slot length have been designed to operate at 1.275 GHz; while, the feed network, due to the parameters selected, was designed to operate at 1.156 GHz. With a -5 dB return loss reference value, an acceptable operational bandwidth is obtained, although, the industry standard limits the return loss reference value to -10 dB.

This requirement limits the acceptable input impedance and therefore reduces the undeliverable power reflected back to the source.

The prototype demonstrates a good design concept but does require additional tuning cycles to optimize the performance. I do believe, due to the many degrees of freedom in the feed network design, that with additional tuning, the -10 dB return loss reference bandwidth can be easily achieved for the cellular frequencies.

6.1.4 Final Observation and Future Work

The prototype antenna appears to be a good design concept. More tuning of the individual slots is required to optimize performance and fulfil all requirements. I do feel that the antenna can be tuned to achieve all requirements of cellular, base station antennas. The prototype is a very compact, sturdy and (due to the materials required and lower labour content) cost effective antenna.

To make the antenna even more unique and desirable, a variable vertical beam tilt feature should be included in this design. Due to the type of feed network, the vertical radiation pattern could be easily adjusted using a dielectric within the cylinder. The dielectric would effectively slow the wave down along the vertical basic feed joining components of the feed network. Slowing down of the wave would adjust the phase of the signal being fed to each slot and the vertical radiation pattern could be adjusted. A variable beam tilt allows more control over the radiation pattern and would make the antenna more directive and, therefore, more desirable to potential buyers.

Additional design work is required to make the antenna more weather resistant and environmentally suitable. The Cylindrical Slot design must withstand the hostile environment of typical base station antennas. This means that the antenna must be sturdy and rust resistant. It is, also, necessary that the antenna be protected from small animals living about the base station area. The antenna must be designed so that there are no entrances to the physical structure through which small animals could penetrate or gain access and, therefore, degrade the antenna performance.

6.2 Magic T Experiment

The measured cumulative distribution curves presented in Section 5.4.3 are used to evaluate the relative diversity improvement from space, pattern and space/pattern combination diversity schemes. The relative diversity improvement between different schemes is determined in a cumulative distribution graph by the difference in signal level of the abscissa for a set probability on the ordinate axis. The measured cumulative distributions are compared to the ideal Rayleigh cumulative distributions of selection combined branches in order to verify the validity of the experimental results. The measured results are then examined to rate the performance of the diversity scheme.

6.2.1 Ideal Cumulative Distribution Curves

The ideal curves for the selection combining of completely uncorrelated branch signals in a Rayleigh channel is presented in Figure 6.1. In this

theoretical case, the branch signal with the highest SNR is selected as the output and since SNR is difficult to measure, in the actual test performed on the Magic T, the branch with the largest signal plus noise is selected as the output. Therefore, the absolute values of the ideal and measured distributions cannot be compared to determine the validity of the results. Since the abscissa units are the same, dB, the relative diversity improvements of the measured and ideal distributions can be compared, which in turn indicates the relative validity of the measured results. An industry standard used in evaluating the diversity improvement from cumulative distribution curves, is to compare signal levels of the abscissa at a 1% fade margin.

From Figure 6.1, at the 1% fade margin, the diversity improvement attributed to the selection combining of two uncorrelated signals over the no diversity branch signal is theoretically approximately 10.5 dB. The increased relative improvement from an uncorrelated three branch system over an uncorrelated two branch system is theoretically approximately 3.6 dB.

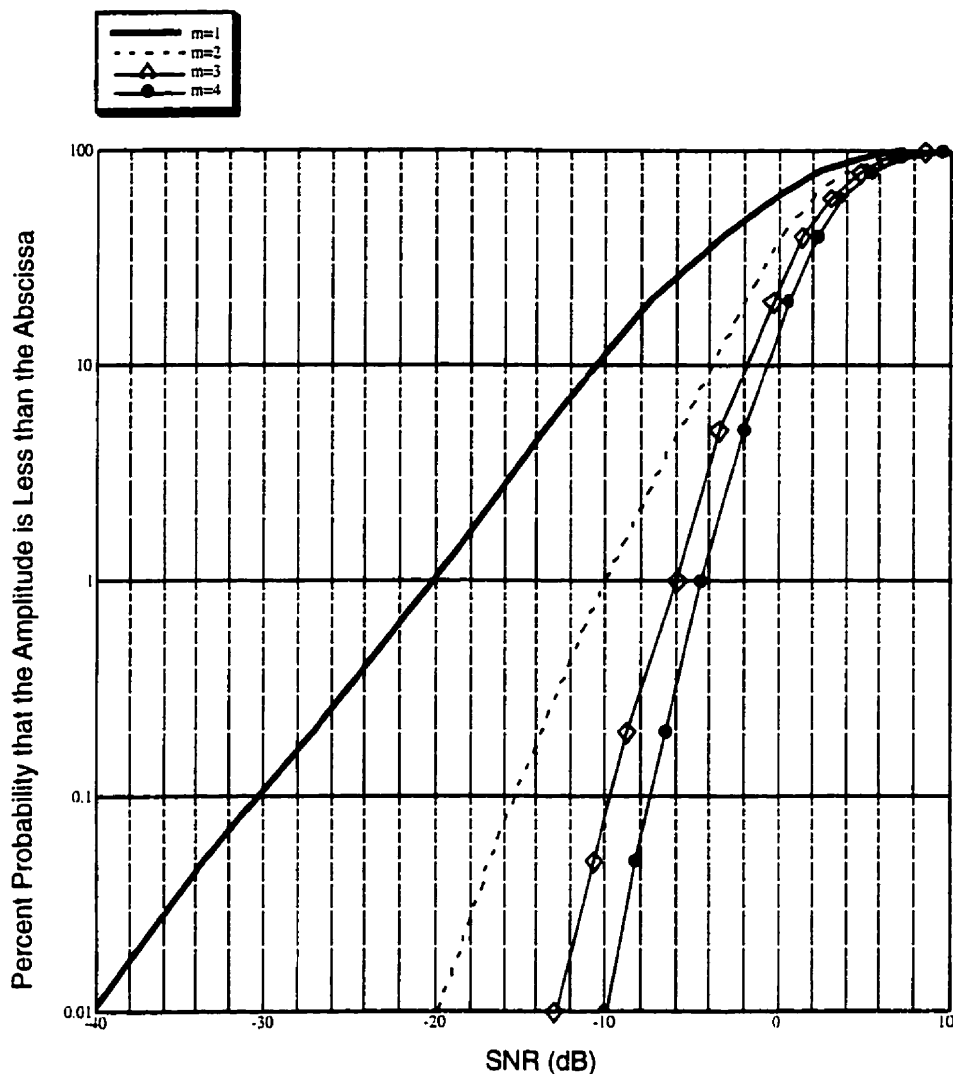


Figure 6.1 Ideal M Branch Selection Combining Curves [1]

In the ideal graph, Figure 6.1, the branch signals are completely uncorrelated. While Figure 6.1 indicates the trend of the relative diversity improvements due to the addition of uncorrelated branch signals, this graph is used as a rough estimate of the validity of the experimental results. Figure 6.2 is necessary to indicate the trend of two branch signals with varying envelope correlations because realistically received branch signals are not completely

uncorrelated. Figure 6.2 indicates that when the envelope correlation of the signals decreases from a value of one, equivalent to no diversity, the resulting value along the abscissa at a set probability also decreases. Therefore, as the correlation between two branch signals decreases, the diversity improvement increases. This trend can be generalized for all correlated branch signals in this system.

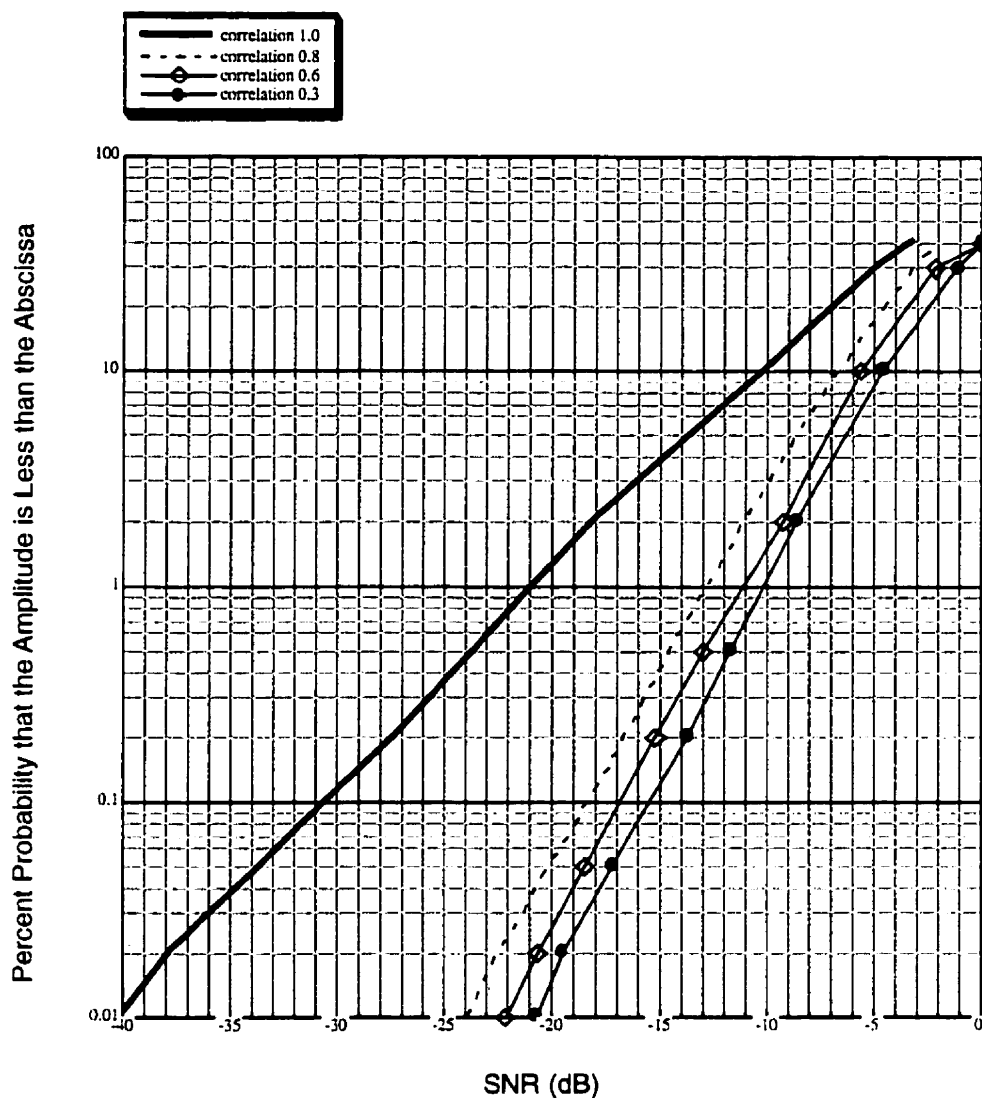


Figure 6.2 Two Branch Correlated Selection Combining [2]

6.2.2 Comparing Results and Ideal Curves

The results from the Magic T experiment are evaluated in stages; space diversity improvement, pattern diversity improvement, and space/pattern combination improvement.

6.2.2.1 Space Diversity

From the Figures 5.11 and 5.12, the results of the diversity improvement for the different diversity schemes can be evaluated. The diversity improvement of the space diversity scheme compared to no diversity is 9.06 dB at 5λ and 9.8 dB at 40λ . From Figure 6.1, the ideal diversity improvement is 10.5 dB. The measured distributions are very close to the ideal curves. Using Figure 6.2, these results indicate an envelope correlation of slightly less than 0.6 at 5λ and 0.3 at 40λ . These results indicate that the branch signals are reasonably uncorrelated and that the increased separation distance of the antennas provides a reduced correlation between signals. The correlation of space diversity base station antennas is determined by the radiation pattern, the separation distance and the incoming signal angle. But, generally, from observing Graphs 6.12a through 6.12c in Reference 6.3, the envelope correlation of antennas separated by 40λ is less than 5λ further validating the measured results.

6.2.2.2 Pattern Diversity

The results, shown in Figures 5.11 and 5.12, of the selection combining of the pattern diversity branch signals are very much the same as the selection combining of the space diversity branch signals.

Using the following deterministic approach [4], a rough insight into the validity of the experiment can be determined. In the experiment, two signals arrive at the base station antennas with rms amplitudes A_1 and A_2 and phases

θ_1 and θ_2 resulting in a phase separation θ . In the Magic T combiner, the signals are summed at the sum output resulting in a power output of

$$P_+ = A_1^2 + A_2^2 + 2A_1A_2\cos(\theta) \quad (6.1)$$

and are summed at the difference output resulting in a power output of

$$P_- = A_1^2 + A_2^2 - 2A_1A_2\cos(\theta). \quad (6.2)$$

In the selection combining of space diversity signals, the branch signal with the largest signal plus noise power is selected as the output. For simplicity, assume that the largest signal amplitude, either A_1 or A_2 , is selected for the output.

Letting $A_1 > A_2$, $0 \leq \theta \leq 360$ and the received branch noise power be σ^2 , the selection combining of the space diversity signals results in

$$\frac{A_1^2}{\sigma^2}. \quad (6.3)$$

In the selection combining of the branch signals from the Magic T, pattern diversity branch signals, the best phase case of these signals will be

$$P = (A_1 + A_2)^2 \quad (6.4)$$

when θ is ± 180 degrees and the worst phase case of these signals will be

$$P = A_1^2 + A_2^2 \quad (6.5)$$

when θ is ± 90 degrees. In the pattern diversity scheme, the noise floor is doubled due to the Magic T. Therefore, in the best overall case situation, when $A_2 = A_1$ and assuming independent noise powers, the selective combining of the pattern diversity signals results in

$$\frac{2A_1^2}{\sigma^2} \quad (6.6)$$

which is 3 dB better than the space diversity case. The worst case of the selection combining of the pattern diversity signals, when $A_2 = 0$, results in

$$\frac{A_1^2}{2\sigma^2} \quad (6.7)$$

which is 3 dB worst than the space diversity case.

Overall the space diversity and pattern diversity selective combining should average out and result in the same cumulative distribution. This is a very reasonable result since the pattern diversity signals originate from the space diversity signals and are similarly correlated with similar dynamic ranges. Therefore, the pattern diversity should not have an improvement or degradation of the diversity improvement compared to the selective combining of the space diversity branch signals.

6.2.2.3 Space and Pattern Combination Diversity

From Figures 5.11 and 5.12, the diversity improvement of the combination of space and pattern diversity signals over the lone space diversity signals can be evaluated. The diversity improvement of the combination space and pattern diversity scheme for both separations is 0.86 dB, indicating an independence relating to the separation of the antennas.

This system is now more than a two branch diversity scheme but since the space and pattern diversity signals are highly correlated, it is also not a true four branch diversity scheme. The system is more closely related to a three branch diversity scheme. The ideal gain of a three branch diversity system is given in Figure 6.1. The ideal diversity improvement of 3.6 dB over space diversity is much greater than the measured 0.86 dB gain indicated in Figures 5.11 and 5.12. This result indicates that the branch signals are quite highly correlated and, therefore, the diversity improvement is reduced. This is a reasonable result since the third and fourth branch signals are simply a special combination of the first two branch signals.

Assuming the same requirements as in the selective combining of pattern diversity signals, for selectively combined space and pattern diversity signals, the best case results in

$$\frac{2A_1^2}{\sigma^2} \quad (6.8)$$

which is the 3 dB better than the selection combining of the space diversity signals. The worst case of the selection combining of the space and pattern diversity signals is

$$\frac{A_1^2}{\sigma^2} \quad (6.9)$$

which is the same as the selection combining of space diversity signals.

Therefore, on average, there should be some improvement of the signal noted on the cumulative distribution graphs but relatively little.

6.2.3 Measured Curves

The graphs 5.11 and 5.12 appear to be typical cumulative distribution graphs. The lone signals from antenna 1 and 2 have fairly linear slopes running from a maximum fade of -35 dB to a minimum fade of +5 dB. The dynamic range of the fade is 40 dB compared to the maximum signal dynamic range of the system at 60 dB. The slope from the selective combining of all the branch signals has increased while the dynamic range has decreased to 22 dB, thus, indicating a reduced fade depth in the overall signal. The relative gain of the space diversity scheme over lone branch signals and the relative gain of the pattern diversity signals compared to the lone branch signals are very similar. This is expected, since the branch signals in each distribution have similar correlation properties and signal dynamic ranges. The selection combination of the space and pattern diversity branches have very similar slope and dynamic

range characteristics as the individual space and pattern diversity signals, but the curve is translated slightly to the right indicating a slight diversity improvement in the system.

6.2.4 Final Observation

The measured space diversity improvement compares very well with theory. These results give confidence in the overall test system used to evaluate the pattern diversity scheme. The initial objective is to improve the quality of the received signal in a multipath environment. The addition of the Magic T combiner into the space diversity system does indeed improve the reliability of the received signal in a multipath environment, but, unfortunately, not enough to warrant inclusion into existing systems. An important thrust in this project was to develop a valid test system. The measured results seem to indicate that the test set-up accurately measured diversity improvement in this particular situation.

References

Chapter One

- 1.1 L. Kinross, "Cellular Phone Services Remarkably Similar", Financial Post, Nov. 25, 1995, p 52.
- 1.2 J. Powell, "Changing The Way We Live and Work", Financial Post, Nov. 25, 1995, p 49.

Chapter Two

- 2.1 J.B. Andersen, T.S. Rappaport, and S. Yoshida, "Propagation Measurements and Models for Wireless Communications Channels", IEEE Communications Magazine, January 1995, pp 42-49.
- 2.2 W.C.Y. Lee, "Mobile Communications Engineering", New York: McGraw Hill, 1982, p 202.
- 2.3 W.C.Y. Lee, "Mobile Cellular Telecommunication Systems", New York, McGraw Hill, 1989, p 97.
- 2.4 W.C.Y. Lee, Mobile Cellular Telecommunications Systems, New York, McGraw Hill, 1989, pp 301- 302.
- 2.5 G.K. Chan, "Effects of Sectorization on the Spectrum Efficiency of Cellular Radio Systems", IEEE Transactions on Vehicular Technology, Vol. 41, No.3, August 1992, pp 217-225.
- 2.6 M. Fischetti, "The Cellular Phone Scare", IEEE Spectrum, New York, June 1993, pp 43 -47.
- 2.7 L.J. Levesque, "Three Way Diversity Antenna For Cellular Radio", M.Sc. Thesis, Dept. of Electrical and Computer Engineering, University of Calgary, 1994.
- 2.8 J.B. Andersen, T.S. Rappaport, and S. Yoshida, "Propagation Measurements and Models for Wireless Communications Channels", IEEE Communications Magazine, January 1995, pp 42-49.
- 2.9 R. Steele, J. Whitehead, and W.C. Wong, "System Aspects of Cellular Radio", IEEE Communications Magazine, January 1995, pp 80 - 86.
- 2.10 R. Johnston, ENEL 577 Transmission Media Notes, 1993.
- 2.11 D.Bogson, G.F. McClure, S.R. McCononghey, " Propagation Models", IEEE Transactions on Vehicular Technology, Vol 37, No. 1, February 1988, pp 20 - 25.

- 2.12 J.E. Padgett, C.G. Gunther, and T. Hattori, "Overview of Wireless Personal Communications", IEEE Communications Magazine, January 1995, pp 28 - 41.
- 2.13 W.C.Y. Lee, "Mobile Cellular Telecommunications Systems", New York, McGraw Hill, 1989.
- 2.14 R.H. Johnston, "A Survey of Diversity Antennas for Mobile and Handheld Radio", Proc TR Labs Wireless '93, pp 307- 318.
- 2.15 W.C.Y. Lee, "Mobile Communications Engineering", New York, McGraw Hill, 1982, p 275.
- 2.16 W.C.Y. Lee, "Mobile Communications Engineering", New York: McGraw Hill, 1982, pp 199-201.

Chapter Three

- 3.1 W. Hayt, Jr, "Engineering Electromagnetics", McGraw Hill, New York, 1989, Fifth Edition, p 433.
- 3.2 M. Douglas, "Dual Diversity Antennas For Hand-held Radio", M.Sc Thesis, Dept. of Electrical and Computer Engineering, University of Calgary, 1993, p 38.
- 3.3 R.H Johnston, J.G. McRory, L.P. Ager, "A New Antenna Efficiency Measurement Method", IEEE APS Int. Symposium, July 21-26, Baltimore, MD, USA, pp 176 - 179.
- 3.4 R. A. Serway, "Physics for Scientists and Engineers", Saunders Golden Sunburst Series, 3rd Edition, pp 1271 - 1273.
- 3.5 W. Hayt, Jr, "Engineering Electromagnetic", New York, McGraw Hill, 1989, Fifth Edition, pp 132-138.
- 3.6 R.H. Johnston, "Enel 575 Course Notes", Dept. of Electrical and Computer Engineering, University of Calgary, 1993, pp 68-70.
- 3.7 C. Balanis, "Antenna Theory, Analysis and Design", Harper & Row Publishers, New York, 1983, p 23.
- 3.8 W.H. Kummer and E.S. Gillespie, "Antenna Measurements - 1978", Proceedings of the IEEE, Vol 66, No. 4, April 1978, pp 483 - 507.
- 3.9 C. Balanis, "Antenna Theory, Analysis and Design", Harper & Row Publishers, New York, 1983, pp 711-712.

- 3.10 W.L. Stutzman and G.A. Thiele, "Antenna Theory and Design", John Wiley & Sons Inc., 1981, pp 216 - 220.
- 3.11 J. McRory, TRILabs Calgary, Personal Communications.
- 3.12 W. Hayt, Jr, "Engineering Electromagnetics", McGraw Hill, New York, 1989, Fifth Edition, p 398.
- 3.13 W. Hayt, Jr, "Engineering Electromagnetics", McGraw Hill, New York, 1989, Fifth Edition, p 336 - 344.
- 3.14 C. Balanis, "Antenna Theory", Harper & Row Publishers, New York, 1983, pp 148-154.
- 3.15 C. Balanis, "Antenna Theory", Harper & Row Publishers, New York, 1983, p 43.
- 3.16 C. Balanis, "Antenna Theory", Harper & Row Publishers, New York, 1983, p 29.
- 3.17 C. Balanis, "Antenna Theory", Harper & Row Publishers, New York, 1983, pp 63-65.
- 3.18 F. Fekri, University of Calgary & TRILabs, Personal Communications.
- 3.19 R. J. Davies, "In-building UHF Propagation Studies", M.Sc. Thesis, Dept. of Electrical and Computer Engineering, University of Calgary, 1989, pp 25 - 27.
- 3.20 R. J. Davies, AGT & TRILabs Calgary, Personal Communications.
- 3.21 G. McGibney, TRILabs Calgary, Personal Communications.
- 3.22 W.C.Y Lee, "Mobile Communications Engineering", New York, McGraw Hill, 1989, pp 287 - 288.
- 3.23 National Instruments," NB-DIO-32F User Manual", August 1992 Edition, August 1992, Part No. 320095-01.
- 3.24 R. J. Davies, "IRIS Development System", AGT Research and Development for TRILabs, TRILabs Calgary.
- 3.25 National Instruments," NB-A2100 User Manual", September 1991 Edition, Sept. 1991, Part No. 320252-01.
- 3.26 National Instruments," NB-DSP230X Series Interface Utilities User Manual", June 1991 Edition, June 1991, Part No. 320400-01.

- 3.27 W.H. Tranter & R.E. Ziemer," Principles of Communications Systems, Modulation and Noise, 2nd Edition, Houghton Mifflin, pp 562-568.
- 3.28 W.H. Tranter & R.E. Ziemer," Principles of Communications Systems, Modulation and Noise, 2nd Edition, Houghton Mifflin, p 570.
- 3.29 W.H. Tranter & R.E. Ziemer," Principles of Communications Systems, Modulation and Noise, 2nd Edition, Houghton Mifflin, pp 576 - 577.

Chapter Four

- 4.1 C. Balanis, "Antenna Theory Analysis and Design", Harper & Row Publishers, New York, 1983, pp 468 - 469.
- 4.2 R.E. Collin, "Antennas and Radiowave Propagation", McGraw Hill, New York, 1985, pp 55 - 75.
- 4.3 R.E. Collin, "Antennas and Radiowave Propagation", McGraw Hill, New York, 1985, pp 263 - 265.
- 4.4 J. McRory, TRILabs Calgary, Personal Communications.
- 4.5 R.H. Johnston, "Enel 575 Course Notes", Dept. of Electrical and Computer Engineering, University of Calgary, 1993, pp 29 - 34.

Chapter Five

- 5.1 R.H. Johnston, "Enel 575 Course Notes", Dept. of Electrical and Computer Engineering, University of Calgary, 1993, pp 65 - 73.
- 5.2 R.H. Johnston, "Enel 575 Course Notes", Dept. of Electrical and Computer Engineering, University of Calgary, 1993, pp 29 - 34.
- 5.3 L.J. Levesque, "Three Way Diversity Antenna For Cellular Radio", M.Sc Thesis, Dept. of Electrical and Computer Engineering, University of Calgary, 1994.
- 5.4 W.C.Y Lee, "Mobile Communications Engineering", New York, McGraw Hill, 1989, pp 103 - 106.
- 5.5 F. Fekri, University of Calgary & TRILabs, Personal Communications.
- 5.6 W.C.Y Lee, "Mobile Communications Engineering", New York, McGraw Hill, 1989, pp 55 - 57.
- 5.7 W.C.Y Lee, "Mobile Communications Engineering", New York, McGraw Hill, 1989, pp 64 - 65.

- 5.8 W.C.Y Lee, "Mobile Communications Engineering", New York, McGraw Hill, 1989, pp 72 - 73.
- 5.9 G. McGibney, "Phase Sensitive Reconstruction of Magnetic Resonance Images", M.Sc. Thesis, Dept. of Electrical and Computer Engineering, University of Calgary, 1991.
- 5.10 G. McGibney, TRILabs Calgary, Personal Communications.

Chapter Six

- 6.1 W.C. Jakes, "Microwave Mobile Communications", IEEE Press, New York, 1993, p 315.
- 6.2 W.C. Jakes, "Microwave Mobile Communications", IEEE Press, New York, 1993, p 326.
- 6.3 W.C.Y Lee, "Mobile Communications Engineering", New York, McGraw Hill, 1989, pp 199 - 201.
- 6.4 G. McGibney, TRILabs Calgary, Personal Communications.

Appendix A

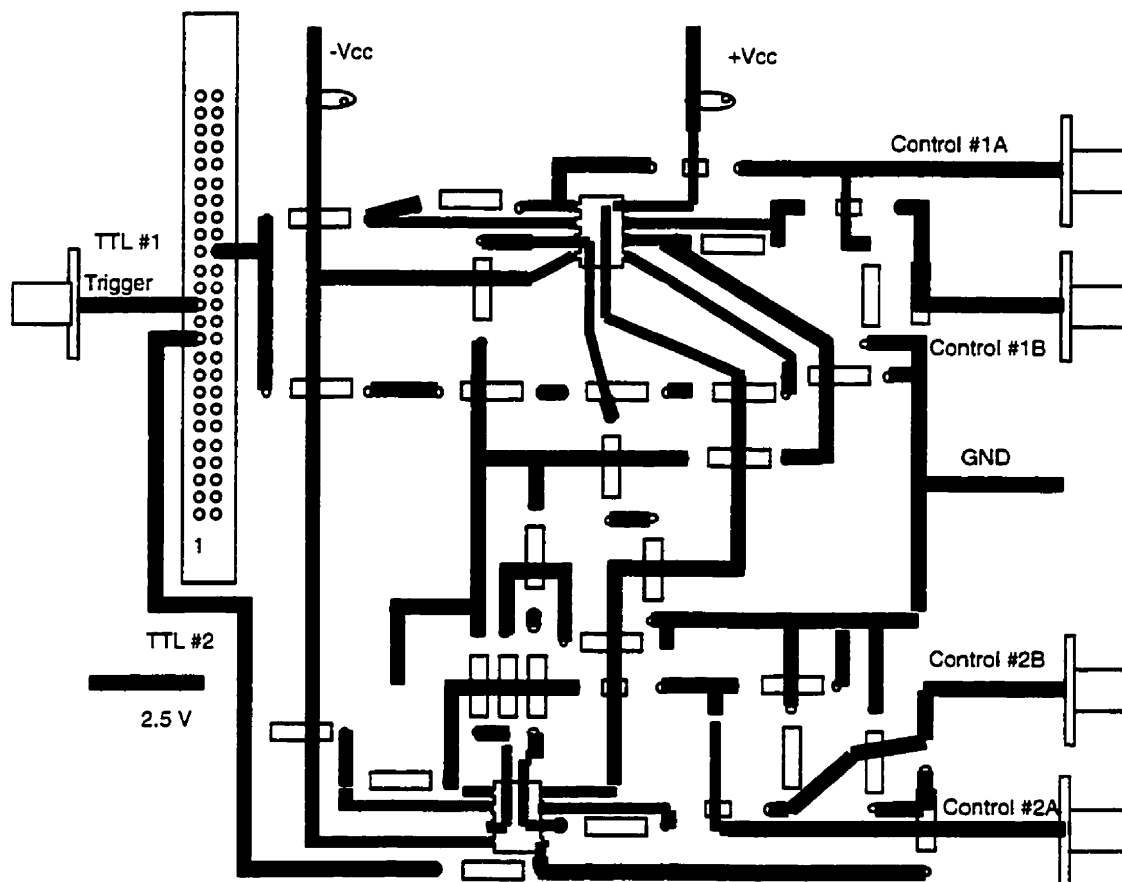


Figure A.1 Switch Control Layout

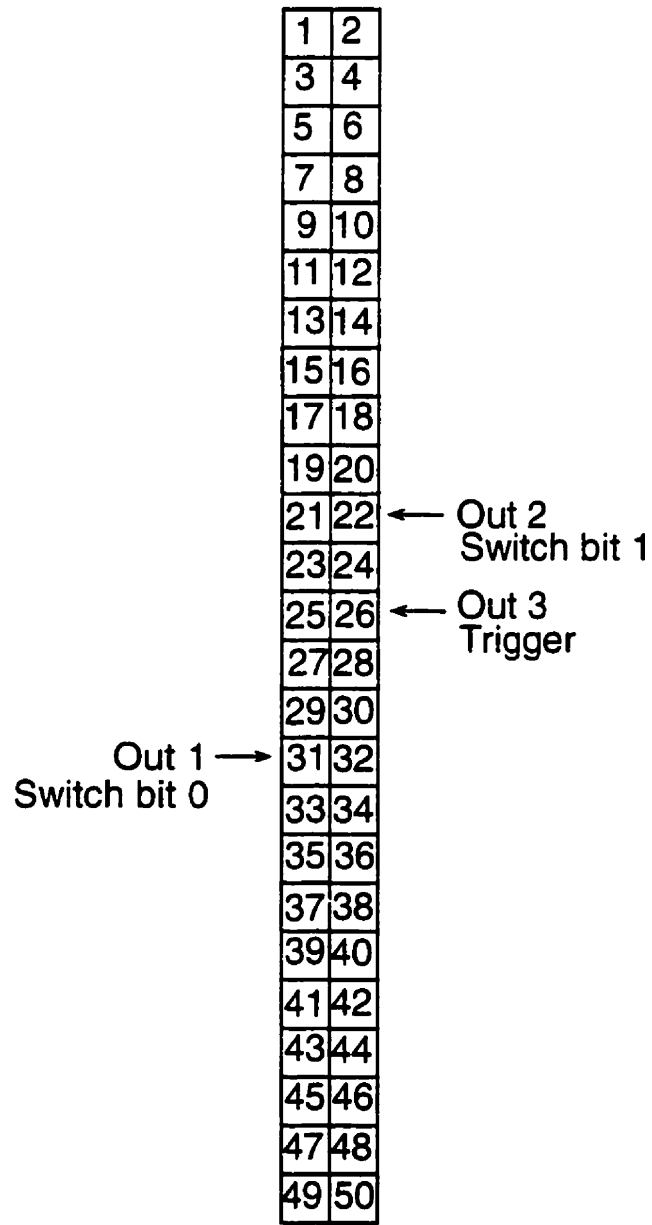


Figure A.2 I/O Computer Plug

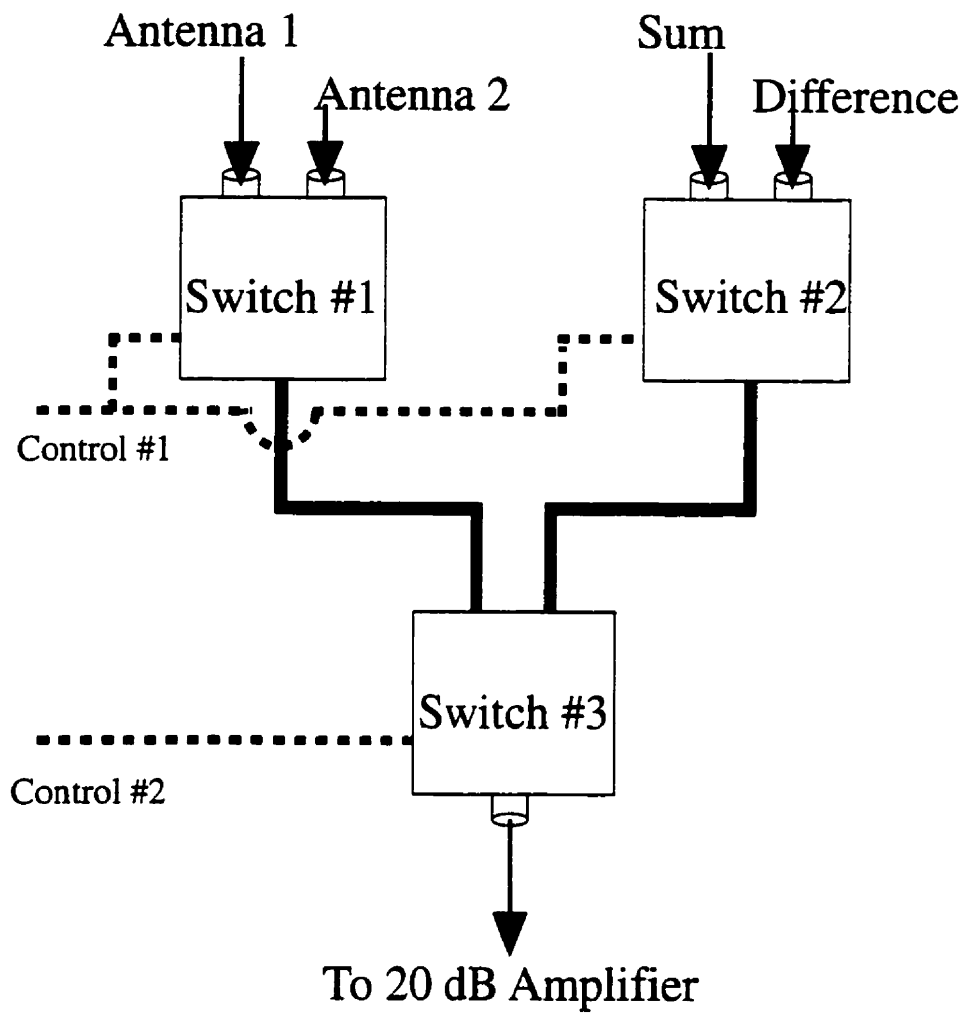
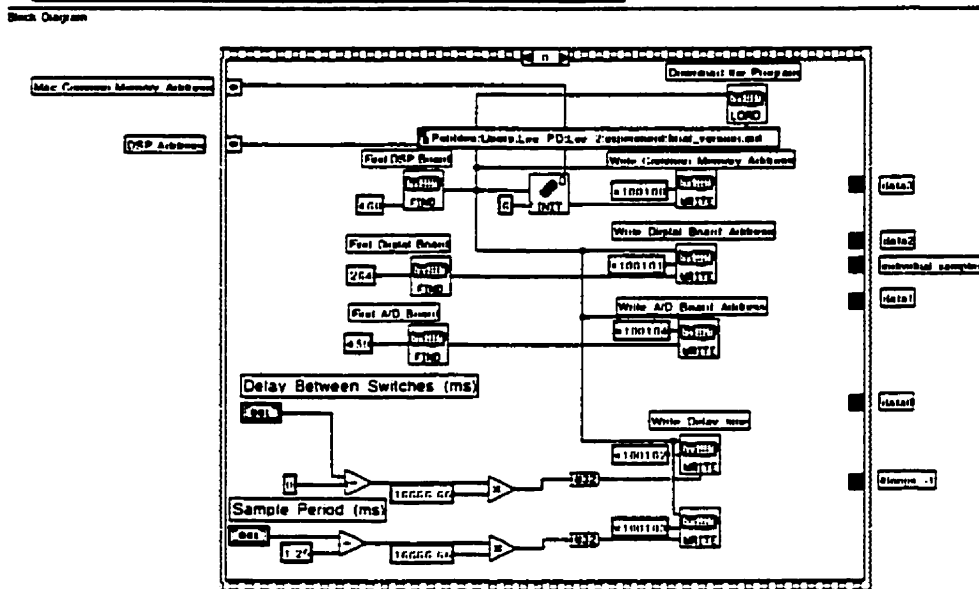
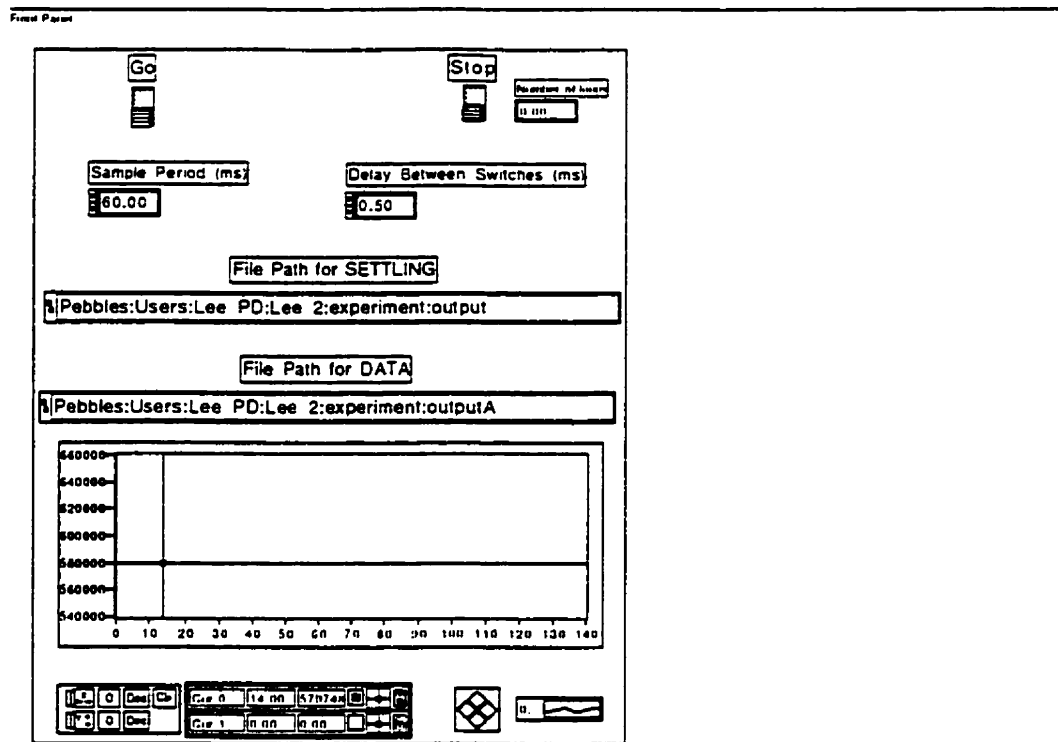
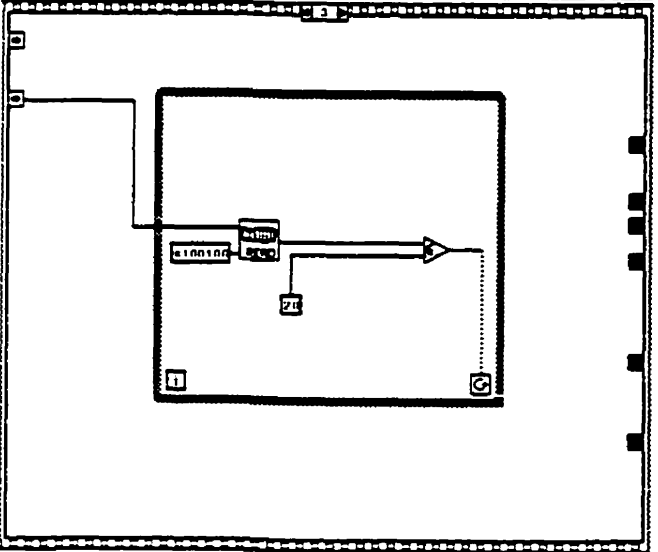
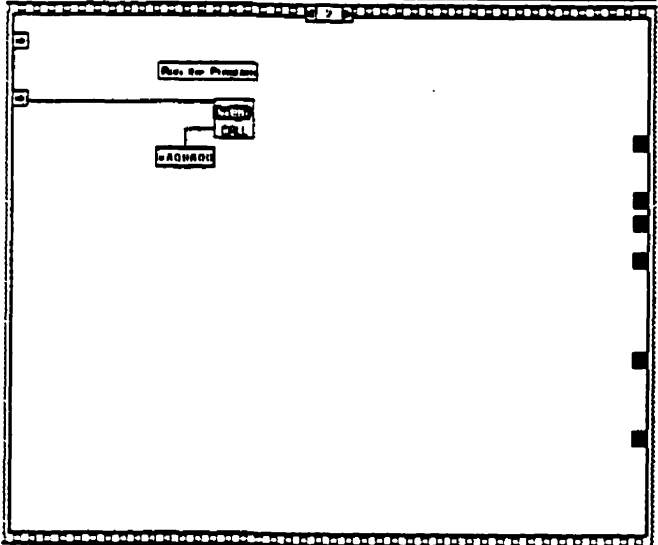
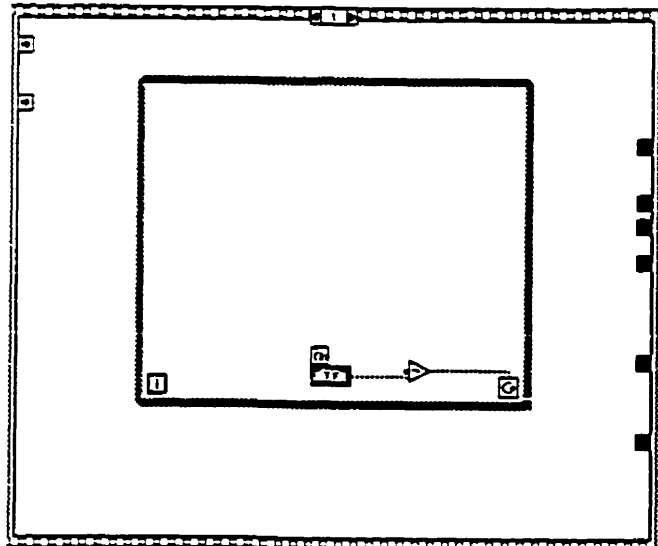


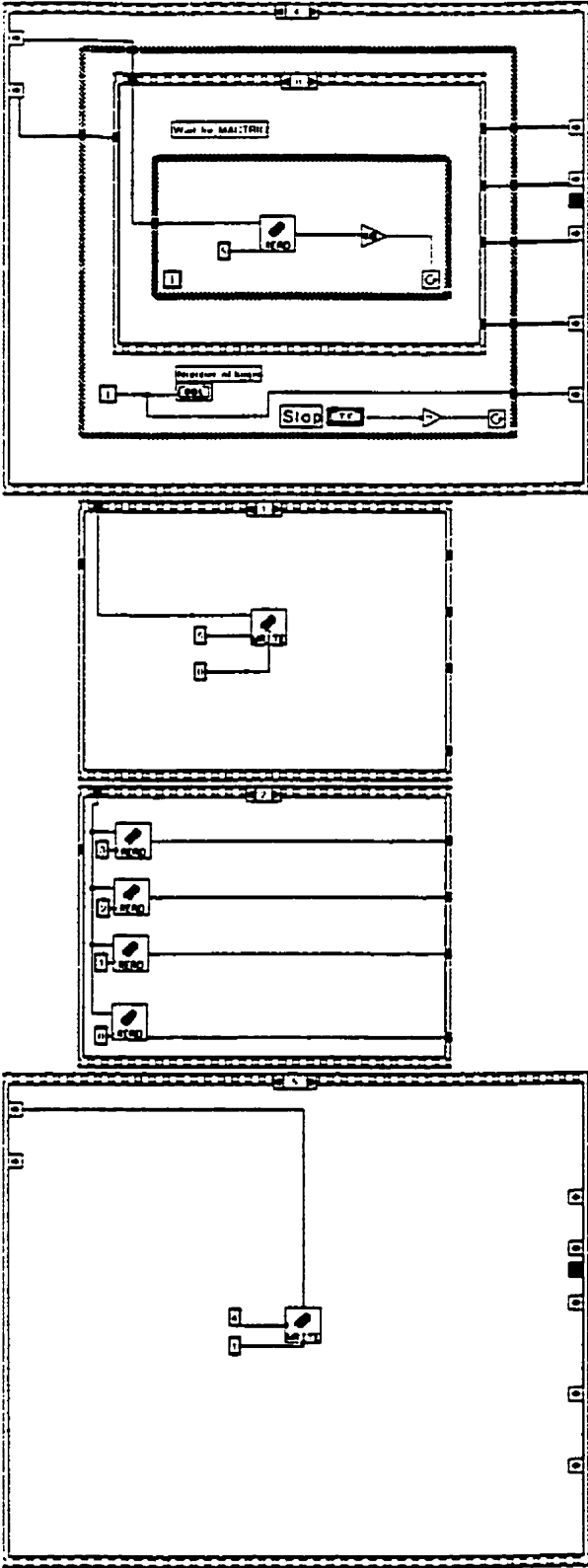
Figure A.3 4-to-1 Switch Configurations

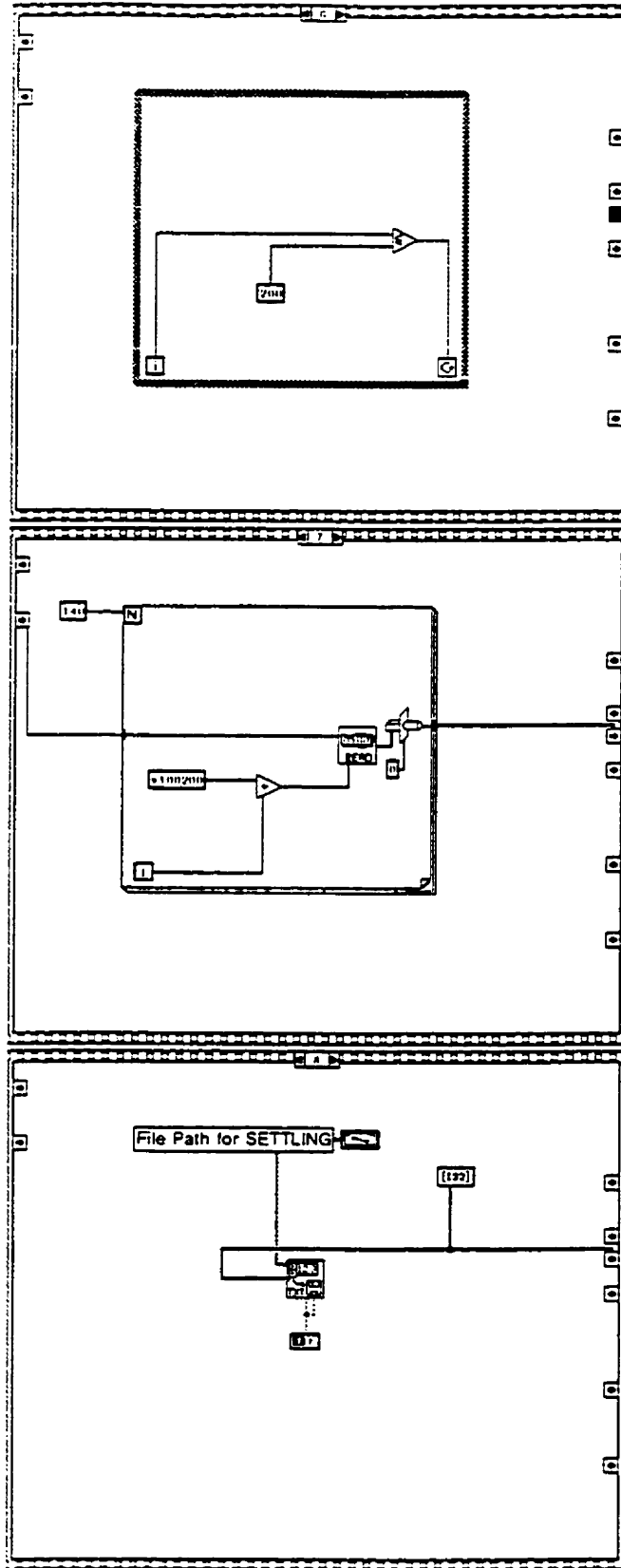
Appendix B

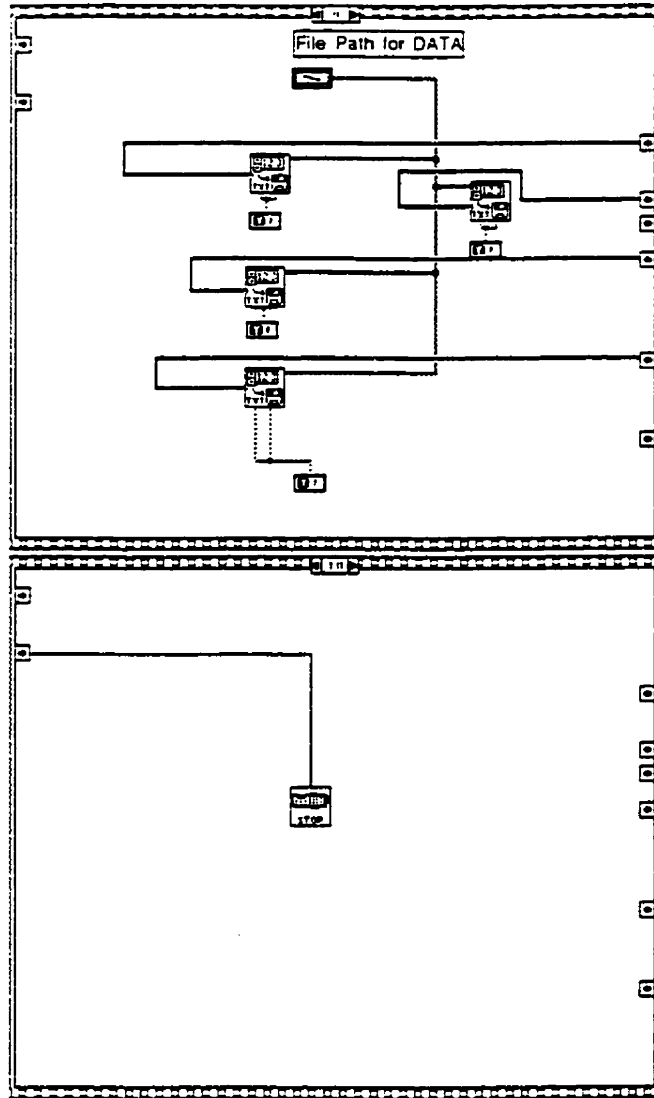
Labview Program name experiment.vi











- * file name final_version.asm
- * This program is to control the A/D board part of the magic T experiment
- * Using the ACH0 input and sampling at 48 kHz then storing the averaged sampled
- * values in 4 common memory locations to be read by the labview part of the program
- * The delay value must be 2 ms. 12 samples are averaged for each output value.
- * 6 pre and 6 post samples are for settling. With a 37 sample
- * wait time.

```

        .data

OFFCHIP      .word    100100H      ; contains address of common memory location See Labview
STACK        .word    0809BE0H    ; stack pointing to last 32 bits of block RAM
MACTRIG      .set     5           ; Flag to set high when measurement complete
DIOBASE      .set     1           ; base address of DIO board See Labview
ADBASE      .set     4           ; base address of A/D board See Labview
DELAY        .set     2           ; delay between switches (in 60ns steps) See Labview
PERIOD       .set     3           ; period of entire cycle (in 60ns steps) See Labview
SWITCH0      .word    0000000H    ; send to CFG2 to set switch to 0
SWITCH1      .word    1000000H
SWITCH2      .word    0010000H
SWITCH3      .word    1010000H
WARMUP       .set     6           ; a flag used to allow program to run 20 times
                                           ; before putting any measurements to file

CFG1         .word    00D00000H    ; address of CFG1 (zero offset from page register 1)
CFG2         .word    00D08000H    ; address of CFG2 (8000H words/20000H bytes offset)

START        .word    100200H

* main program
        .text
        .global MAIN

MAIN
addressed    LDP          800000H, DP      ; memory addresses 800000h to 80ffffh can be
                                           ; directly
        LDI          @STACK, SP
        LDI          @OFFCHIP, AR7; dual access memory addressed via AR7
        LDI          *AR7,AR6           ; put common memory location address in AR6

        ; calculate addresses of the two control registers

        LDI          *+AR7(DIOBASE), R0 ; get the top 10 bits for the page register
        LSH          -22, R0
        STI          R0, @805001H      ; page register 1 now points to the DIO board

        LDI          @CFG1, AR4        ; address of CFG1 in page 1
        LDI          @CFG2, AR5        ; address of CFG2 in page 1

        LDI          0, R0              ; load zero into common memory location 4
                                           ; (stop control)
        STI          R0, *+AR6(4)

        LDI          *+AR7(PERIOD), R6
        LDI          *+AR7(DELAY), R5
        SUBI         6, R5              ; tuning of period time
        SUBI         R5, R6             ; subtract the delay from period 4 times
        SUBI         R5, R6             ; should have been subtracted 6 times
        SUBI         R5, R6
        SUBI         R5, R6
        SUBI         R5, R6
        SUBI         14, R6            ; tuning of delay time

        LDI          0, R0              ; trigger off to CFG1
        STI          R0, *AR4
        LDI          @SWITCH0, R2      ; switch 0 to CFG2
        STI          R2, *AR5
        LDI          *+AR7(ADBASE), AR0 ; put the contents of 100104f into AR0 for the
analog_init routine
        .data

```

```

CARDBASE .word      0F00000h          ; base address of card in TMS memory space
STATREG   .word      0F08000h          ; status register
RTSIREG   .word      0F30000h          ; RTSI registers

```

```

.text

```

```

* ANALOG_INIT SETS UP A SERIAL LINK BETWEEN THE ANALOG I/O BOARD AND THE DSP
* BOARD. THE ANALOG BOARD WILL BE SET UP FOR A 48KHZ SAMPLING RATE, TWO CHANNELS.
* CALL ANALOG_INIT WITH THE BASE ADDRESS OF THE ANALOG I/O CARD IN REGISTER AR0

```

```

        LSH          -22, AR0
        STI          AR0, @805003H
        LDI          @CARDBASE, AR0

```

```

***** ANALOG I/O BOARD SETUP

```

```

* SET UP THE AtoD CONVERTERS

```

```

        ; set input configuration for 2-channel 48KHz sampling,
        ; DC coupling, the test input grounded (for now),
        ; and the digital circuits powered down (for now)
        LDI          2c08h, R0
        LSH          16, R0
        STI          R0, *AR0

```

```

        ; now power up the digital circuits to start the calibration

```

```

        LDI          0c08h, R0
        LSH          16, R0
        STI          R0, *AR0

```

```

        ; wait for the DCAL bit to go low to indicate the the calibration is done

```

```

WAIT_DCAL
        LDI          @STATREG, AR1
        LDI          *AR1, R0
        LSH          -16, R0
        TSTB        40h, R0
        BNZ         WAIT_DCAL

```

```

        ; now connect test inputs to the signal

```

```

        LDI          0808h, R0
        LSH          16, R0
        STI          R0, *AR0

```

```

        ; reset the FIFO

```

```

        STI          R0, *+AR0(4)

```

```

* SET UP THE DtoA CONVERTERS

```

```

        ; set up for 48kHz, both channels from serial link 0

```

```

        LDI          28h, R0
        LSH          16, R0
        STI          R0, *+AR0(1)

```

```

        ; reset the FIFO

```

```

        STI          R0, *+AR0(6)

```

```

* SET INTERRUPT AND DMA REGISTERS

```

```

        ; disable everything

```

```

        LDI          0, R0
        STI          R0, *+AR0(7)

```

```

* SET UP TRIGGER LINES

```

```

        ; disable everything

```

```

        LDI          0, R0
        LDI          @RTSIREG, AR1
        RPTS        55                                ; latch in 56 zeros
        STI          R0, *AR1
        STI          R0, *+AR1(1)                    ; strobe it in

```

```

* SET UP THE SERIAL LINK

```

```

; DtoA converters drive 0, AtoD converters drive 1
LDI          5, R0
LSH          16, R0
STI          R0, *+AR0(2)

```

***** DSP BOARD SETUP

```

.data
* RTSI configuration
SIDEA .word 0000090h
SIDEB .word 01057B9h
* Serial configuration
SERGLO1 .word 003c0000h ; initialize to 32 bit and reset
SERGLO2 .word 0c3c0000h ; remove reset
.text

* SET UP RTSI SWITCH 1 TO CONNECT THE RTSI BUS TO SERIAL PORT 0
LDI          @SIDEB, R0
LDI          27, RC ; need to shift in 28 bits
RPTB        LOOPB
LDI          R0, R1
AND          1, R1 ; get bit zero
LSH          1, R1 ; move it to bit one
STI          R1, @804004H ; store it in the RTSI switch
LOOPB LSH    -1, R0 ; move to next bit

LDI          @SIDEA, R0
LDI          27, RC ; need to shift in 28 bits
RPTB        LOOPA
LDI          R0, R1
AND          1, R1
LSH          1, R1
STI          R1, @804004H
LOOPA LSH    -1, R0

LDI          0, R0
STI          R0, @804005H ; strobe in the results

* SET UP THE SERIAL PORT CONFIGURATION
LDI          @SERGLO1, R0 ; Global register with reset
STI          R0, @8040H
LDI          0111H, R0 ; Port control registers
STI          R0, @8042H
STI          R0, @8043H
LDI          0, R0
STI          R0, @8044H ; Timer control register
STI          R0, @8046H ; Timer period register
STI          R0, @8045H ; Timer count register
LDI          @SERGLO2, R0 ; Global register without reset
STI          R0, @8040H

```

LOOP

```

LDI          *+AR7(WARMUP), R0
ADDI         1, R0
STI          R0, *+AR7(WARMUP) ; incrementing the warm up flag

LDI          @START, AR3 ;point to first memory location

```

```

LDI 0, R1
LDI 23, RC ; first 24 of 37 sample delay
RPTB WAIT_LOOPA ; experimentally determined

WAIT_INA
LDI @808040H, R0 ; serial port global register
TSTB 1, R0 ; has data come in?
BZ WAIT_INA ; if not then try again
LDI @80804CH, R0
LDI R0, R2 ; ACH0 in upper 16 bits
LSH 16, R2 ; while ACH1 in lower 16 bits
ASH -16, R2
ASH -16, R0
MPYI R0, R0 ; square I channel
MPYI R2, R2 ; square Q channel
ADDI R0, R2 ; add I and Q together
STI R2, *AR3++

WAIT_LOOPA
NOP ; 24 sample delay
LDI @SWITCH1, R0 ; memory location #1
STI R0, *AR5 ; switch to input #2
LDI 0, R1 ; 24 samples between switches
LDI 12, RC ; 13 sample delay required
RPTB WAIT_LOOPB ; for overall 37 sample delay

WAIT_INB
LDI @808040H, R0 ; serial port global register
TSTB 1, R0 ; has data come in?
BZ WAIT_INB ; if not then try again
LDI @80804CH, R0
LDI R0, R2 ; ACH0 in upper 16 bits
LSH 16, R2 ; while ACH1 in lower 16 bits
ASH -16, R2
ASH -16, R0
MPYI R0, R0 ; square I channel
MPYI R2, R2 ; square Q channel
ADDI R0, R2 ; add I and Q together
STI R2, *AR3++

WAIT_LOOPB
NOP ; 13 sample delay

WAIT_PRE_1
LDI 0, R1
LDI 5, RC ; 6 sample settling
RPTB PRE_SAMPLE_1 ;

PRE_SAMPLE_1
LDI @808040H, R0 ; serial port global register
TSTB 1, R0 ; has data come in?
BZ WAIT_PRE_1 ; if not then try again
LDI @80804CH, R0
LDI R0, R2 ; ACH0 in upper 16 bits
LSH 16, R2 ; while ACH1 in lower 16 bits
ASH -16, R2
ASH -16, R0
MPYI R0, R0 ; square I channel
MPYI R2, R2 ; square Q channel
ADDI R0, R2 ; add I and Q together
STI R2, *AR3++
NOP ; 6 sample settling

WAIT_1A
LDI 0, R1
LDI 4, RC ; 5/12 samples to be averaged
RPTB SAMPLE_1A ; switches

SAMPLE_1A
LDI @808040H, R0 ; serial port global register
TSTB 1, R0 ; has data come in?
BZ WAIT_1A ; if not then try again
LDI @80804CH, R0
LDI R0, R2 ; ACH0 in upper 16 bits
LSH 16, R2 ; while ACH1 in lower 16 bits
ASH -16, R2
ASH -16, R0
MPYI R0, R0 ; square I channel

```

```

MPYI R2, R2 ; square Q channel
ADDI R0, R2 ; add I and Q together
STI R2, *AR3++
SAMPLE_1A ADDI R2, R1 ; running average

LDI @SWITCH2, R0 ; common memory location
STI R0, *AR5 ; switch to the input #3
LDI 6, RC ; 7/12 samples to be averaged
RPTB SAMPLE_1B ; switches

LDI @808040H, R0 ; serial port global register
TSTB 1, R0 ; has data come in?
BZ WAIT_1B ; if not then try again
LDI @80804CH, R0
LSH R0, R2 ; ACH0 in upper 16 bits
ASH 16, R2 ; while ACH1 in lower 16 bits
ASH -16, R2
ASH -16, R0
MPYI R0, R0 ; square I channel
MPYI R2, R2 ; square Q channel
ADDI R0, R2 ; add I and Q together
STI R2, *AR3++
SAMPLE_1B ADDI R2, R1 ; 12 sample averaging
ASH -4, R1 ; divide by 16 for average
STI R1, *+AR6(0) ; store average value in
; first common memory location

LDI 0, R1
LDI 5, RC ; 6 sample settling
RPTB POST_SAMPLE_1

LDI @808040H, R0 ; serial port global register
TSTB 1, R0 ; has data come in?
BZ WAIT_POST_1 ; if not then try again
LDI @80804CH, R0
LSH R0, R2 ; ACH0 in upper 16 bits
ASH 16, R2 ; while ACH1 in lower 16 bits
ASH -16, R2
ASH -16, R0
MPYI R0, R0 ; square I channel
MPYI R2, R2 ; square Q channel
ADDI R0, R2 ; add I and Q together
STI R2, *AR3++
POST_SAMPLE_1 NOP ; 6 sample settling

LDI 0, R1
LDI 5, RC ; 6 sample settling
RPTB PRE_SAMPLE_2

LDI @808040H, R0 ; serial port global register
TSTB 1, R0 ; has data come in?
BZ WAIT_PRE_2 ; if not then try again
LDI @80804CH, R0
LSH R0, R2 ; ACH0 in upper 16 bits
ASH 16, R2 ; while ACH1 in lower 16 bits
ASH -16, R2
ASH -16, R0
MPYI R0, R0 ; square I channel
MPYI R2, R2 ; square Q channel
ADDI R0, R2 ; add I and Q together
STI R2, *AR3++
PRE_SAMPLE_2 NOP ; 6 sample settling

LDI 0, R1

```

```

LDI          4, RC          ; 5/12 samples to be averaged
RPTB        SAMPLE_2A      ; switches

WAIT_2A

LDI          @808040H, R0   ; serial port global register
TSTB        1, R0          ; has data come in?
BZ          WAIT_2A        ; if not then try again
LDI          @80804CH, R0
LDI          R0, R2        ; ACH0 in upper 16 bits
LSH          16, R2        ; while ACH1 in lower 16 bits
ASH          -16, R2
ASH          -16, R0
MPYI        R0, R0          ; square I channel
MPYI        R2, R2          ; square Q channel
ADDI        R0, R2          ; add I and Q together

SAMPLE_2A

STI          R2, *AR3++
ADDI        R2, R1          ; running average
LDI          @SWITCH3, R0   ; common memory location
STI          R0, *AR5        ; switch to the input #3
LDI          6, RC          ; 7/12 samples to be averaged
RPTB        SAMPLE_2B      ; switches

WAIT_2B

LDI          @808040H, R0   ; serial port global register
TSTB        1, R0          ; has data come in?
BZ          WAIT_2B        ; if not then try again
LDI          @80804CH, R0
LDI          R0, R2        ; ACH0 in upper 16 bits
LSH          16, R2        ; while ACH1 in lower 16 bits
ASH          -16, R2
ASH          -16, R0
MPYI        R0, R0          ; square I channel
MPYI        R2, R2          ; square Q channel
ADDI        R0, R2          ; add I and Q together

SAMPLE_2B

STI          R2, *AR3++
ADDI        R2, R1          ; 12 sample averaging
ASH          -4, R1          ; divide by 16 for average
STI          R1, *+AR6(1)   ; store average value in
                                ; second common memory location

LDI          0, R1
LDI          5, RC          ; 6 sample settling
RPTB        POST_SAMPLE_2

WAIT_POST_2

LDI          @808040H, R0   ; serial port global register
TSTB        1, R0          ; has data come in?
BZ          WAIT_POST_2    ; if not then try again
LDI          @80804CH, R0
LDI          R0, R2        ; ACH0 in upper 16 bits
LSH          16, R2        ; while ACH1 in lower 16 bits
ASH          -16, R2
ASH          -16, R0
MPYI        R0, R0          ; square I channel
MPYI        R2, R2          ; square Q channel
ADDI        R0, R2          ; add I and Q together

POST_SAMPLE_2

STI          R2, *AR3++
NOP          ; 6 sample settling

LDI          0, R1
LDI          5, RC          ; 6 sample settling
RPTB        PRE_SAMPLE_3

WAIT_PRE_3

LDI          @808040H, R0   ; serial port global register
TSTB        1, R0          ; has data come in?
BZ          WAIT_PRE_3    ; if not then try again
LDI          @80804CH, R0
LDI          R0, R2        ; ACH0 in upper 16 bits
LSH          16, R2        ; while ACH1 in lower 16 bits

```

```

        ASH          -16, R2
        ASH          -16, R0
        MPYI        R0, R0          ; square I channel
        MPYI        R2, R2          ; square Q channel
        ADDI        R0, R2          ; add I and Q together
PRE_SAMPLE_3 STI          R2, *AR3++
        NOP          ; 6 sample settling

        LDI        0, R1
        LDI        11, RC          ; 12 samples to be averaged
        RPTB      SAMPLE_3        ; switches

        LDI        @808040H, R0    ; serial port global register
        TSTB      1, R0          ; has data come in?
        BZ          WAIT_3        ; if not then try again
        LDI        @80804CH, R0
        LDI        R0, R2          ; ACH0 in upper 16 bits
        LSH        16, R2        ; while ACH1 in lower 16 bits
        ASH        -16, R2
        ASH        -16, R0
        MPYI        R0, R0          ; square I channel
        MPYI        R2, R2          ; square Q channel
        ADDI        R0, R2          ; add I and Q together
SAMPLE_3   STI          R2, *AR3++
        ADDI        R2, R1          ; 12 sample average
        ASH        -4, R1          ; divide by 16 for average
        STI        R1, *+AR6(2)    ; store average value in
        ; third common memory location

        LDI        0, R1
        LDI        5, RC          ; 6 sample settling
        RPTB      POST_SAMPLE_3   ;
WAIT_POST_3

        LDI        @808040H, R0    ; serial port global register
        TSTB      1, R0          ; has data come in?
        BZ          WAIT_POST_3   ; if not then try again
        LDI        @80804CH, R0
        LDI        R0, R2          ; ACH0 in upper 16 bits
        LSH        16, R2        ; while ACH1 in lower 16 bits
        ASH        -16, R2
        ASH        -16, R0
        MPYI        R0, R0          ; square I channel
        MPYI        R2, R2          ; square Q channel
        ADDI        R0, R2          ; add I and Q together
POST_SAMPLE_3 STI          R2, *AR3++
        NOP          ; 6 sample settling

        LDI        0, R1
        LDI        5, RC          ; 6 sample settling
        RPTB      PRE_SAMPLE_4    ;
WAIT_PRE_4

        LDI        @808040H, R0    ; serial port global register
        TSTB      1, R0          ; has data come in?
        BZ          WAIT_PRE_4    ; if not then try again
        LDI        @80804CH, R0
        LDI        R0, R2          ; ACH0 in upper 16 bits
        LSH        16, R2        ; while ACH1 in lower 16 bits
        ASH        -16, R2
        ASH        -16, R0
        MPYI        R0, R0          ; square I channel
        MPYI        R2, R2          ; square Q channel
        ADDI        R0, R2          ; add I and Q together
PRE_SAMPLE_4 STI          R2, *AR3++
        NOP          ; 6 sample settling

        LDI        0, R
        LDI        11, RC          ; 12 samples to be averaged
        RPTB      SAMPLE_4        ; switches
WAIT_4    LDI        @808040H, R0    ; serial port global register
        TSTB      1, R0          ; has data come in?

```

```

        BZ          WAIT_4          ; if not then try again
        LDI        @80804CH, R0
        LDI        R0, R2          ; ACH0 in upper 16 bits
        LSH        16, R2         ; while ACH1 in lower 16 bits
        ASH        -16, R2
        ASH        -16, R0
        MPYI       R0, R0          ; square I channel
        MPYI       R2, R2          ; square Q channel
        ADDI       R0, R2          ; add I and Q together
SAMPLE_4  STI
        ADDI       R2, *AR3++
        ADDI       R2, R1          ; 12 sample average
        ASH        -4, R1         ; divide by 16 for average
        STI        R1, *+AR6(3)   ; store average value in
        ; third common memory location
        LDI        0, R1
        LDI        5, RC          ; 6 sample settling
WAIT_POST_4 RPTB POST_SAMPLE_4
        LDI        @808040H, R0   ; serial port global register
        TSTB      1, R0          ; has data come in?
        BZ          WAIT_POST_4   ; if not then try again
        LDI        @80804CH, R0
        LDI        R0, R2          ; ACH0 in upper 16 bits
        LSH        16, R2         ; while ACH1 in lower 16 bits
        ASH        -16, R2
        ASH        -16, R0
        MPYI       R0, R0          ; square I channel
        MPYI       R2, R2          ; square Q channel
        ADDI       R0, R2          ; add I and Q together
POST_SAMPLE_4 STI
        R2, *AR3+
        NOP          ; 6 sample settling

        LDI        @SWITCH0, R0
        STI        R0, *AR5       ; return to switch 0
        LDI        1, R0         ; trigger the Mac
        STI        R0, *+AR6(5)

        LDI        0, R1
        LDI        11, RC        ; delay for accurate timing
        RPTB      WAIT_LOOPE     ; should have been 10 instead of 11
WAIT_INE  LDI        @808040H, R0 ; serial port global register
        TSTB      1, R0          ; has data come in?
        BZ          WAIT_INE     ; if not then try again
        LDI        @80804CH, R0
        LDI        R0, R2          ; ACH0 in upper 16 bits
        LSH        16, R2         ; while ACH1 in lower 16 bits
        ASH        -16, R2
        ASH        -16, R0
        MPYI       R0, R0          ; square I channel
        MPYI       R2, R2          ; square Q channel
        ADDI       R0, R2          ; add I and Q together
        STI        R2, *AR3++

```

Appendix C

| Instrument | Noise Figure | Gain |
|---------------|--------------|----------|
| Cavity Filter | 1.995 | 0.501187 |
| LNA | 1.41 | 100 |
| Broadband Amp | 3.16 | 1258 |
| Coax | 158 | 6.3e-3 |
| Splitter | 1.995 | 0.501187 |
| Combiner | 1.995 | 0.501187 |
| 4-to-1 Switch | 1.995 | 0.501187 |
| 4-to-1 Switch | 1.995 | 0.501187 |
| Amplifier | 2.138 | 100 |
| IRIS | 7.94 | |

Table C.1 Noise Figure and Gain Specifications

$$\begin{aligned}
 N.F = & 1.995 + \frac{1.41-1}{0.501187} + \frac{3.16-1}{.501187*100} + \frac{158-1}{.501187*100*1256} + \\
 & \frac{1.995-1}{.501187*100*1256*6.3e-3} + \frac{1.995-1}{.501187^2*100*1256*6.3e-3} + \\
 & \frac{1.995-1}{.501187^3*100*1256*6.3e-3} + \frac{1.995-1}{.501187^4*100*1256*6.3e-3} + \\
 & \frac{2.13-1}{.501187^5*100*1256*6.3e-3} + \frac{10-1}{.501187^5*100^2*1256*6.3e-3} + \\
 & \frac{7.94-1}{.501187^5*100^2*1256*6.3e-3}
 \end{aligned}$$

$$N.F = 2.94$$

$$N.F_{dB} = 10 * \log(N.F) = 4.68 \text{ dB}$$

Appendix D

```

% file name rad_plot.m
% This program converts the output file from the anechoic chamber set up
% to a radiation pattern polar plot

%clear all
%clg

% open the file

fid=fopen('FKFEED4.DAT');

% get the information

marker=0;
while(marker~=1)
    line=fgets(fid);
    line=upper(line);
    marker=findstr(line,'START:');
end

line(1:6)=[];
freq_start=sscanf(line,'%g')

marker=0;
while(marker~=1)
    line=fgets(fid);
    line=upper(line);
    marker=findstr(line,'STOP:');
end

line(1:6)=[];
freq_stop=sscanf(line,'%g')

marker=0;
while(marker~=1)
    line=fgets(fid);
    line=upper(line);
    marker=findstr(line,'POINTS:');
end

line(1:7)=[];
points=sscanf(line,'%g')

space=(freq_stop-freq_start)/(points-1);
freq_interest=input('What is the frequency of interest ? : [1275 MHz] ');
if isempty(freq_interest) freq_interest=1275; end
freq_interest=freq_interest*1e6;
point_interest=round(((freq_interest-freq_start)/space)+1);

% how many points to plot
number_incrments=input('How many measurements made ? [121] ');
if isempty(number_incrments) number_incrments=121; end

```

```

DEGREE=[];
MAG=[];

for cycles= 1:1:number_incraments

% get the data

    marker=0;
    while(marker~=1)
        line=fgets(fid);
        line=upper(line);
        marker=findstr(line,'BEGIN:');
    end
    line(1:7)=[];
    degree=sscanf(line,'%g')
    DEGREE=[DEGREE degree];

    number=2*point_interest;
    for picking_line=1:1:number
        line=fgets(fid);
    end

    ri_values=sscanf(line,'%g,%g');
    r_value=ri_values(1);
    i_value=ri_values(2);
    mag=((r_value^2)+(i_value^2)^.5;
    MAG=[MAG mag];

end
fclose(fid);

% normalize values

largest=max(MAG);
MAG_norm=MAG/largest;

DEG_rad=DEGREE*(pi/180);

% store values

DEG_rad=DEG_rad';
MAG_norm=MAG_norm';
output=[ DEG_rad MAG_norm];
output=output';
fid=fopen('fkfeed1275.dat','w')
fprintf(fid,'%g          %g\n',output);
fclose(fid);

% plot

polar(DEG_rad,MAG_norm,'k');
hold on
%polar(DEG_rad,MAG_norm,'k*');
hold off
grid

```

Appendix E

```

% file name extract_exp_output.m
% This program extracts the information from the fetched output file
% of the magic T experiment and graphs the square rooted output and
% again stores it to another file

clg
clear all

% open the data file and retrieve the data

fid=fopen('5l_jun8.txt');
output=fscanf(fid,'%g',[1 inf]);
fclose(fid);

% determine the matrices

columns=size(output,2);
x_axis=1:1:columns;

% perform the math

time=x_axis;
%log_output=10*log10(output);
output=output.^0.5;

% plot the desired section of log output versus time

%output_plot=log_output(1,1:columns);           % must be evenly dividable by 4
output_plot=output(1,1:columns);
time_plot=time(1,1:columns);
subplot(1,1,1),plot(time_plot,output_plot)
grid

% store output to file

time_plot= time_plot';
output_plot=output_plot';
list_output= [ time_plot output_plot];
list_output=list_output';

fid=fopen('run_5l_jun8.txt','w');
fprintf(fid,'%g  %g\n',list_output);
fclose(fid);

```

```

% file name output_extract_runs.m
% This program extracts the information from the extract_exp_output file
% of the magic T experiment and graphs the logged output that is required for
% the mean value program.

clc
clear all

% open the data file and retrieve the data

fid=fopen('run_5l_jun8.txt');
output=fscanf(fid,'%g          %g',[2 inf]);
fclose(fid);

% determine the matrices

column=size(output,2);

% plot the desired section of log output versus time

time=output(1,:);
notlog_output=output(2,:);

time_plot=time(1,:);
output_plot=notlog_output(1,:);

%subplot(2,1,1),plot(time_plot,output_plot,'*')
%grid

% separate the outputs into the respective switches

columns=size(output_plot,2);
period_time=columns/4;
shape_output=reshape(output_plot,period_time,4);

switch1=shape_output(:,1);
switch2=shape_output(:,2);
switch3=shape_output(:,3);
switch4=shape_output(:,4);

rows=size(switch2,1);
x_axis=1:1:rows;
time=(60e-3/60)*(x_axis');

switch_output1=[switch1 time];
switch_output2=[switch2 time];
switch_output3=[switch3 time];
switch_output4=[switch4 time];

```

```

switch_1=switch_output1';
switch_2=switch_output2';
switch_3=switch_output3';
switch_4=switch_output4';

%fid=fopen('switch1_5l_jun8.txt','w');
%fprintf(fid,'%g          %g\n',switch_1);
%fclose(fid);
%fid=fopen('switch2_5l_jun8.txt','w');
%fprintf(fid,'%g          %g\n',switch_2);
%fclose(fid);
%fid=fopen('switch3_5l_jun8.txt','w');
%fprintf(fid,'%g          %g\n',switch_3);
%fclose(fid);
%fid=fopen('switch4_5l_jun8.txt','w');
%fprintf(fid,'%g          %g\n',switch_4);
%fclose(fid);

subplot(2,2,1),plot(time,switch1,'k');
hold on
subplot(2,2,3),plot(time,switch3,'k');
subplot(2,2,2),plot(time,switch2,'k');
subplot(2,2,4),plot(time,switch4,'k');
hold off
grid

% file name mean_value.m
% This program opens a switch output file and has a central averaging
% window running through the data and determining the mean value.

clear all
clg

% open the switch output file

fid=fopen('switch1_40l_jun8.txt');
output=fscanf(fid,'%g          %g',[2 inf]);
fclose(fid);

columns=size(output,2);

% window length

window_term=input('Number of samples (1) or lambda length (2)? ');
if isempty(window_term) window_term=1; end

if window_term == 1

    number_samples=input('How many samples? [81] ');
    if isempty(number_samples) number_samples=81; end

```

```

else

    number_lambda=input('How many lambda ? [40] ');
    if isempty(number_lambda) number_lambda=40; end

    lambda=3e8/f;

    % sample twice every lambda

    number_samples=number_lambda*2;

end

integer_samples=fix(number_samples/2);
odd_or_even=number_samples-2*integer_samples;

if odd_or_even==0
    number_samples=number_samples+1;
end

% start at half the number of samples and end at half the number
% of samples before the end

switch=output(1,:);
time=output(2,:);

% determine mean

start_it=(number_samples+1)/2;
end_it=columns-start_it+1;
half_back=start_it;
half_forward=half_back-1;

sum=0;

for increment=1:1:number_samples

    sum=sum+switch(increment);
end

running_average=[];
running_average(start_it)=sum;

for increment=start_it+1:1:end_it

    beginning=switch(increment-half_back);
    ending=switch(increment+half_forward);
    sum=sum-beginning+ending;
    running_average(increment)=sum;
end

running_average=running_average/number_samples;

for fill=1:1:start_it-1
    running_average(fill)=switch(fill);
end

```

```

for fill=end_it+1:1:columns
    running_average(fill)=switch(fill);
end

% remove mean from statistics

short_term=switch./running_average;

log_running_average=10*log10(((running_average).^2)/2);
log_switch=10*log10((switch.^2)/2);
log_short_term=10*log10((short_term.^2)/2);

% store the short_term statistics

timer=time';
short_termer=short_term';

short_term_output=[timer short_termer];
short_term_output=short_term_output';

%fid=fopen('short_term_sw1_5l_jun8.txt','w');
%fprintf(fid,'%g          %g\n',short_term_output);
%fclose(fid);

%subplot(2,1,1),plot(time,log_switch);
%hold on
%subplot(2,1,1),plot(time,log_running_average,'k');
%subplot(2,1,2),plot(time,log_short_term);
%hold off

plot(time,log_short_term);

% file name selective_combining.m
% This program opens the four switch files and combines using the best
% signal strength then stores in another file

% open the files

fid=fopen('short_term_sw1_5l_jun8.txt');
output=fscanf(fid,'%g          %g',[2 inf]);
fclose(fid);

switch1=output(2,:);
time=output(1,:);
start_time=0*60*1000/60+1;
end_time=26*60*1000/60;

desired_switch1=switch1(start_time:end_time);
switch1=desired_switch1';
desired_time=time(start_time:end_time);

```

```

columns=size(desired_switch1,2);

fid=fopen('short_term_sw2_5l_jun8.txt');
output=fscanf(fid,'%g          %g',[2 inf]);
fclose(fid);

switch2=output(2,:);
desired_switch2=switch2(start_time:end_time);
switch2=desired_switch2';

fid=fopen('short_term_sw3_5l_jun8.txt');
output=fscanf(fid,'%g          %g',[2 inf]);
fclose(fid);

switch3=output(2,:);
desired_switch3=switch3(start_time:end_time);
switch3=desired_switch3';

fid=fopen('short_term_sw4_5l_jun8.txt');
output=fscanf(fid,'%g          %g',[2 inf]);
fclose(fid);

switch4=output(2,:);
desired_switch4=switch4(start_time:end_time);
switch4=desired_switch4';

%overall_matrix=[switch1 switch2];
%overall_matrix=[switch3 switch4];
overall_matrix=[switch1 switch2 switch3 switch4];
overall_matrix=overall_matrix';

best_signal=max(overall_matrix);
time=desired_time';
best_signal=best_signal';
best=[time best_signal];
best=best';

fid=fopen('best_signal_5l_jun8.txt','w');
fprintf(fid,'%g  %g\n',best);
fclose(fid);

plot(time,best_signal);

% file name cdf.m
% This program calculates the effective cumulative distribution of the
% input data

clear all
%clg

```

```

% open file

fid=fopen('best_signal_40l_jun8.txt');
output=fscanf(fid,'%g          %g',[2 inf]);
fclose(fid);

switch=output(2,:);
time=output(1,:);
columns=size(output,2);

start_time=10.*60*1000/60+1;
end_time=24*60*1000/60;

desired_switch=switch(start_time:end_time);
desired_time=time(start_time:end_time);
index=find(desired_switch>(10^(7/10)));
desired_switch(index)=ones(1,length(index)) ;
columns=size(desired_switch,2);

switch=desired_switch';
log_switch=10*log10((switch.^2)/2);

nb=10 % the number of bins

[n,x]=hist(log_switch,nb);

delta=abs(x(4)-x(3));

min_value=min(log_switch);
max_value=max(log_switch);

threshold_step=delta;
cum_value=[];

for cumulative=1:1:nb
    cumul=(n(1:cumulative));
    cum_value(cumulative)=sum(cumul);
    threshold(cumulative)=threshold_step*(cumulative-1)+min_value+delta;
end

cum_values=100-(cum_value./columns)*100;
cum_value=(cum_value./columns)*100;
reverse_cum_value=(1-cum_value)*100;
log_cum_value=10.^(cum_value);
%plot(threshold,cum_value);
%plot(threshold,signalgrabscissa)
%plot(threshold,reverse_cum_value);
semilogy(threshold,cum_value,'k- -');
grid

output=[threshold' cum_value'];

%fid=fopen('cdf_sw1_5l_jun8.txt','w');
%fprintf(fid,'%g          %g\n',output);
%fclose(fid);

```

```

% file name noise_mean.m
% This program determines the pdf of the experimental results

clear all
clg

% open the file

fid=fopen('switch1_5l_jun8.txt');
output=fscanf(fid,'%g          %g',[2 inf]);
fclose(fid);

switch=output(1,:);
time=output(2,:);
columns=size(output,2);
power_switch=((switch.^2)/2);
max_value=round(max(power_switch));

% select the data run

start_time=26*60*1000/60;
end_time=28.5*60*1000/60;

power_desired_switch=power_switch(start_time:end_time);
columns=size(power_desired_switch,2);
desired_time=time(start_time:end_time);
end_it=size(power_desired_switch,2);
for increment=1:1:end_it
    if power_desired_switch(increment) > 200
        power_desired_switch(increment)=150;
    end
end

% find the mean
average_value=(sum(power_desired_switch))/columns;
variance_value=sum((power_desired_switch-average_value).^2)/columns;
sigma=average_value./((pi/2)^.5);
sigma_noise=((2-pi/2)^.5)*sigma;
four_sigma_noise=round(4*sigma_noise);

%delta=(max_value-four_sigma_noise)/10000;
delta=(10000-four_sigma_noise)/1000;

%dynamic_range=[four_sigma_noise:delta:max_value];
dynamic_range=[four_sigma_noise:delta:10000];
log_dynamic_range=10*log10(dynamic_range);
base_linea=10*log10(dynamic_range+sigma_noise);
base_lineb=10*log10(dynamic_range-sigma_noise);
base_line=base_linea-base_lineb;
power_four_sigma_noise=round(10*log10(four_sigma_noise));
power_sigma_noise=10*log10(sigma_noise);
log_switch=10*log10(power_switch);
plot(log_dynamic_range,base_line)

```

Appendix F

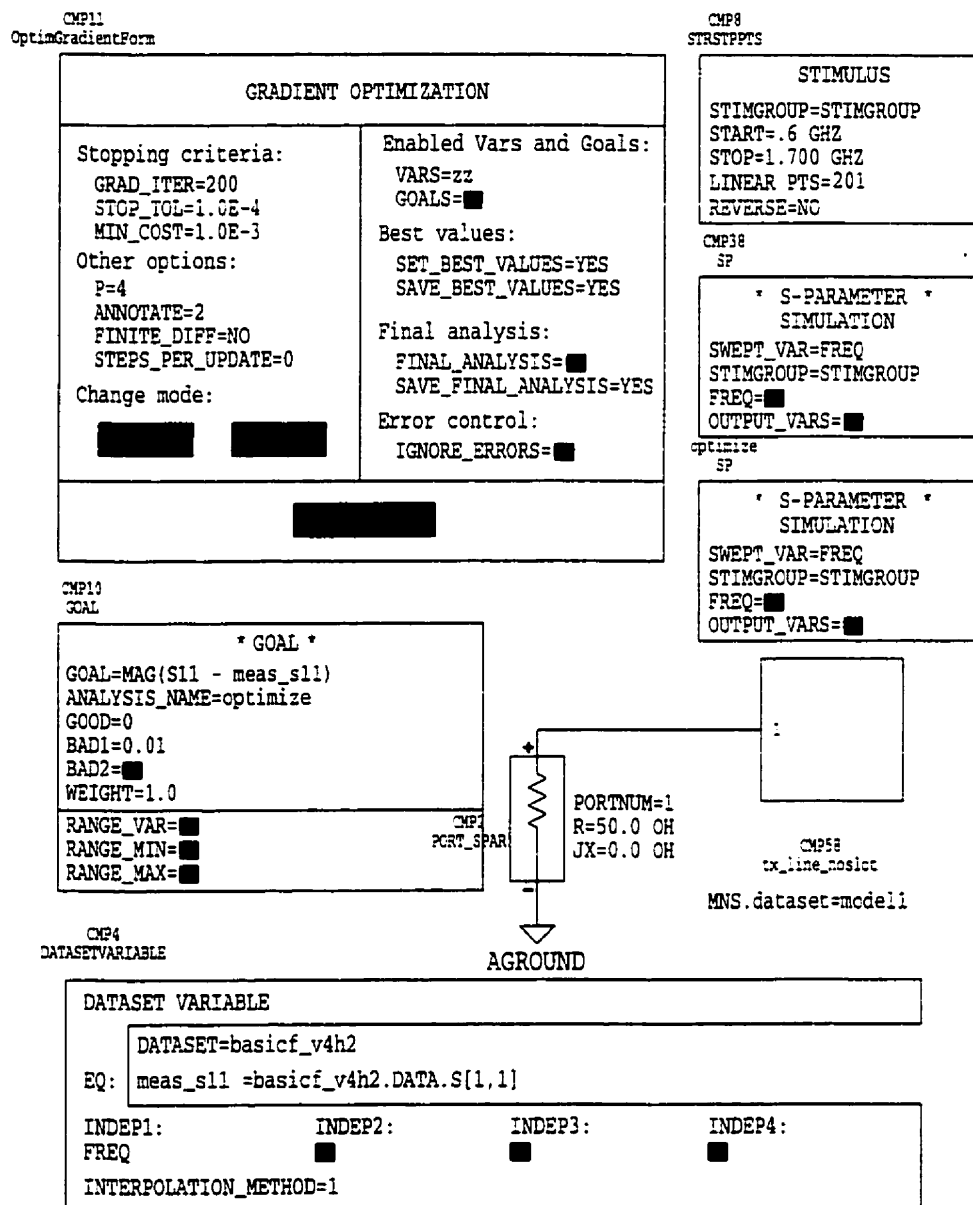


Figure F.1 MDS Test Set-up

Appendix G

```

% file name noise_mean.m
% This program determines the pdf of the experimental results

clear all
clg

% open the file

fid=fopen('switch1_5l_jun8.txt');
output=fscanf(fid,'%g          %g',[2 inf]);
fclose(fid);

switch=output(1,:);
time=output(2,:);
columns=size(output,2);
power_switch=((switch.^2)/2);
max_value=round(max(power_switch));

% select the data run

start_time=26*60*1000/60;
end_time=28.5*60*1000/60;

power_desired_switch=power_switch(start_time:end_time);
columns=size(power_desired_switch,2);
desired_time=time(start_time:end_time);

end_it=size(power_desired_switch,2);
for increment=1:1:end_it
    if power_desired_switch(increment) > 200
        power_desired_switch(increment)=150;
    end
end

% find the mean
average_value=(sum(power_desired_switch))/columns;
variance_value=sum((power_desired_switch-average_value).^2)/columns;
sigma=average_value./((pi/2)^.5);
sigma_noise=((2-pi/2)^.5)*sigma;
four_sigma_noise=round(4*sigma_noise);

%delta=(max_value-four_sigma_noise)/10000;
delta=(10000-four_sigma_noise)/1000;

%dynamic_range=[four_sigma_noise:delta:max_value];
dynamic_range=[four_sigma_noise:delta:10000];
log_dynamic_range=10*log10(dynamic_range);
base_linea=10*log10(dynamic_range+sigma_noise);
base_lineb=10*log10(dynamic_range-sigma_noise);
base_line=base_linea-base_lineb;
power_four_sigma_noise=round(10*log10(four_sigma_noise));
power_sigma_noise=10*log10(sigma_noise);
log_switch=10*log10(power_switch);
%subplot(2,1,1),plot(time,log_switch)
%subplot(2,1,2),plot(log_dynamic_range,base_line)
plot(log_dynamic_range,base_line)

```